Photo-Induced Electron Transfer Studies in Donor-Bridge-Acceptor Molecules

by

Subhasis Chakrabarti

BS, Presidency College, Calcutta University, India, 2000

MS, Indian Institute of Technology, Mumbai, India, 2002

Submitted to the Graduate Faculty of

Arts and Science in partial fulfillment

of the requirements for the degree of

Doctor of Philosophy

University of Pittsburgh

2008

UNIVERSITY OF PITTSBURGH

FACULTY OF ARTS AND SCIENCES

This dissertation was presented

by

Subhasis Chakrabarti

It was defended on

September 8, 2008

and approved by

Dr. David Pratt, Professor, Chemistry

Dr. Sunil Saxena, Professor, Chemistry

Dr. Hyung J. Kim, Professor, Chemistry

Dissertation Advisor: Dr. David H. Waldeck, Professor, Chemistry

PHOTO-INDUCED ELECTRON TRANSFER STUDIES IN DONOR-BRIDGE-ACCEPTOR MOLECULES

Subhasis Chakrabarti, PhD

University of Pittsburgh, 2008

Abstract

Electron transfer reactions through Donor-Bridge-Acceptor (DBA) molecules are important as they constitute a fundamental chemical process and are of intrinsic importance in biology, chemistry, and the emerging field of nanotechnology. Electron transfer reactions proceed generally in a few limiting regimes; nonadiabatic electron transfer, adiabatic electron transfer and solvent controlled electron transfer. This study is going to address two different regimes (nonadiabatic and solvent controlled) of electron transfer studies. In the nonadiabatic limit, we are going to explore how the electron tunneling kinetics of different donor-bridge-acceptor molecules depends on tunneling barrier. Different parameters like free energy, reorganization energy, and electronic coupling which govern the electron transfer were quantitatively evaluated and compared with theoretical models. In the solvent controlled limit we have shown that a change of electron transfer mechanism happens and the kinetics dominantly depends on solvent polarization response.

This study comprises of two different kinds of Donor-Bridge-acceptor molecules, one having a pendant group present in the cleft between the donor and acceptor hanging from the bridge and the other having no group present in the cleft. The electron transfer kinetics critically depend on the pendant unit present in the cavity between the donor and the acceptor moieties. The electronic character of the pendant unit can tune the electronic coupling between the donor

and the acceptor. If the cavity is empty then solvent molecule(s) can occupy the cavity and can influence the electron transfer rate between donor and acceptor. It has been shown that water molecules can change the electron transfer pathways in proteins. This study has experimentally shown that few water molecules can change the electron transfer rate significantly by forming a hydrogen bonded structure between them. This experimental finding supports the theoretical predictions that water molecules can be important in protein electron transfer.

Understanding the issues outlined in this work are important for understanding and controlling electron motion in supramolecular structures and the encounter complex of reactants. For example, the efficiency of electron tunneling through water molecules is essential to a mechanistic understanding of important biological processes, such as bioenergetics. Also, the influence of friction and its role in changing the reaction mechanism should enhance our understanding for how nuclear motions affect long range electron transfer.

TABLE OF CONTENTS

LIST OF TABLES

LIST OF FIGURES

LIST OF SCHEMES

ACKNOWLEDGEMENT

I would like to express my deep and sincere gratitude to my supervisor, Professor David H. Waldeck, Ph.D., Chair of the Department of Chemistry, University of Pittsburgh. His wide knowledge and his way of thinking towards a scientific problem had a great impact on my approach towards problem solving. His understanding, encouragements, and personal guidance have provided a good basis for the present thesis. His constant help and support from year 2001 (when I was a student in India) until today is something I can not express in words. I thank him for everything from the core of my heart.

I am deeply grateful to Professor David Pratt for providing me with his valuable comments and suggestions during my stay in Pittsburgh. He also introduced me to the field of Modern Quantum Mechanics when I took a course under him in my first year of graduate study.

I owe my most sincere gratitude to Professor Sunil Saxena for his help throughout this study. He also introduced me to the world of high resolution spectroscopy.

I thank Prof. Kim and Prof. Walker for their support and help.

I thank Professor Alex Star, who gave me the opportunity to work on my proposal under his guidance. I also thank Prof. Hutchison for his untiring help during my proposal.

I warmly thank Dr. Min Liu, for her detailed and constructive comments, for her help, and for her important support when I was a new graduate student and was learning about TCSPC and electron transfer theory.

During this work I have collaborated with many colleagues for whom I have great regard, and I wish to extend my warmest thanks to all those who have helped me with my work, especially Prof. Christian Schafmeister in the Department of Chemistry at the Temple University and Prof. M. Paddon-Row at the University of South Wales, Australia.

I owe my loving thanks to my fellow group members Lei Wang, Palwinder Kaur, Amit Paul, Angie Wu, Matt Kofke, Alex Clemens, and Dan Lamont for the lovely moments I had with them.

I like to thank my family and friends. Without their encouragement and understanding it would have been impossible for me to finish this work.

I warmly thank the expert staff in the Glass shop, the Electronic shop, and the Machine shop at University of Pittsburgh for their valuable advice and friendly help.

The financial support from NSF and University of Pittsburgh is gratefully acknowledged.

Pittsburgh, September 2008

Subhasis Chakrabarti

1.0 FIRST CHAPTER

1. Introduction

1.1 Prologue

Electron transfer reactions are one of the most fundamental prototype reactions in science and technology. The modern era of electron transfer reactions started after World War II with the study of self exchange reactions using isotopes. In 1950, Huang, Rhys and Kubo advanced a theory of non-radiative transitions of a localized electron from an electronically excited bound state to the ground electronic state in ionic crystals (in which the electron transfer is the dominating and central part).[1] Their pioneering work first quantitatively described the nuclear thermally averaged Franck-Condon (FC) vibrational overlap factor in a single frequency configurational diagram. Later in 1952, Willard Libby described the significance of nuclear reorganization in electron transfer reactions.[2] It was Marcus' landmark work, beginning from 1956, that built the foundation for much of what has been learned in the intervening decades about electron transfer and provided the quantitative description of the classical high temperature FC factor for outer sphere electron transfer.[3,4] In recent years, scientists have successfully used well-designed Donor-Bridge-Acceptor (DBA) molecules in order to address the important issues in electron transfer by systematically manipulating the molecular properties.[5,6,7]

1.2 Electron transfer theory

1.2.1 Origin and background

Electron transfer involves the movement of an electron from a donor molecule to an acceptor molecule. A simple example of electron transfer is the self exchange reaction.

$$Fe^{2+} + Fe^{3+} \leftrightarrow Fe^{3+} + Fe^{2+} \qquad \mathbf{1}$$

This simple example can be explained easily in terms of Marcus's classical two parabola model (two parabolas with same energy). In DBA molecules, the process of electron transfer is far more complex and we need to use the semiclassical electron transfer theory to describe the electron transfer process.

The semiclassical electron transfer theory model begins with Fermi's golden rule expression for the transition rate.

$$k = (2\pi/\hbar)\left|V\right|^2 FCWDS \qquad \mathbf{2}$$

where $\hbar = h/2\pi$; h = Planck's constant, $\left|V\right|$ is the electronic coupling matrix element and FCWDS is the Franck-Condon weighted density of states (thermally averaged vibrational Franck-Condon factor).[8,9] The FCWDS term includes the structural and environmental variables in the system. This equation satisfies the following conditions.

1. Electron transfer is described as a radiationless process.

2. The Born-Oppenheimer separability of electronic and nuclear motion applies, allowing for the description of the system in terms of diabatic potential surfaces.

3. The dynamics are described fully by microscopic ET rates which is basically the non-radiative decay rate of an initial state to the final quasi-degenerate state.

Electron transfer reactions are typically classified as occurring in one of two limits; the strong electronic coupling or adiabatic charge-transfer regime and the weak electronic coupling or nonadiabatic regime.[10] According to Equation 2, the electron transfer rate constant is proportional to the electronic coupling term $|V|^2$, where $|V|$ measures the

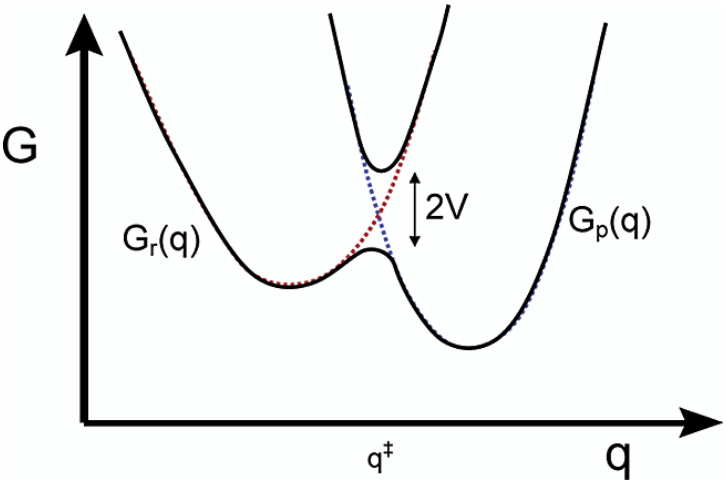

Figure 1.1 Diagram illustrating the two pictures (adiabatic and nonadiabatic) for the electron transfer. [This picture is taken from the reference Zimmt, M.B; Waldeck, D.H. *J. Phys. Chem. A*, **2003**, *107*, 3580.]

interaction between the donor and the acceptor electronic wavefunction. Figure 1.1 uses a simple one-dimensional reaction coordinate to illustrate how the electron transfer mechanism differs in these two regimes. The solid curve illustrates the adiabatic regime, in which a system's electronic state adiabatically follows the nuclear displacement, and the rate limiting step for the reaction is the evolution of the system along the nuclear coordinate and through the transition state. The dashed curve in the figure corresponds to the diabatic reactant and product electronic states. In the nonadiabatic limit, the system moves through the crossing point (transition state) many times before the electronic state switches from the diabatic

reactant surface to the diabatic product state. The rate determining factor depends on the probability of the quantum jump from the reactant electronic surface to the product electronic surface. In 1976, Jortner[10] used the Golden Rule formula (equation 1) and derived an expression for the FCWDS term that accounted for both quantum and classical nuclear degrees of freedom. In the general case, the term can be written as

$$FCWDS = \frac{\left[\sum_i \sum_f \exp(-E_i / kT) \left| < i \middle| f > \right|^2 \delta(E_i - E_f)\right]}{\left[\sum_i \exp(-E_i / kT)\right]} \qquad \textbf{3}$$

where E_i is the energy of the initial vibronic state i, E_f is the energy of the final vibronic states, and $< i \middle| f >$ is their overlap. The sums are performed over all initial vibronic states i and over all final vibronic states f. This expression represents a thermally averaged value for the Franck-Condon overlap factor between the initial and the final vibronic states. Frequently the systems are modeled as possessing two sets of vibronic states; one set is very low frequency ($\nu < kT/h$) and modeled classically and a second set that is higher frequency ($\nu >> kT/h$) and treated quantum mechanically. Contributions to the FCWDS from the classical degree of freedom are included through the outer sphere reorganization energy λ_0, whereas the quantum degrees of freedom are included through the product of effective harmonic modes i with quantum number n_i and frequencies ν_i. The change in reorganization energy of each quantum degree of freedom is given by λ_i. Detailed investigations of the vibrational dependence of the electron-transfer dynamics are few, but those available are consistent with the model.[11-12]

Figure 1.2 illustrates essential features of the generally accepted view of electron transfer reactions in the nonadiabatic/electron-tunneling limit. The electronic energy is

sketched as a function of the electron coordinate on the left and as a function of the nuclear coordinate on the right; each is approximated as an effective one-dimensional coordinate. In the reactant state

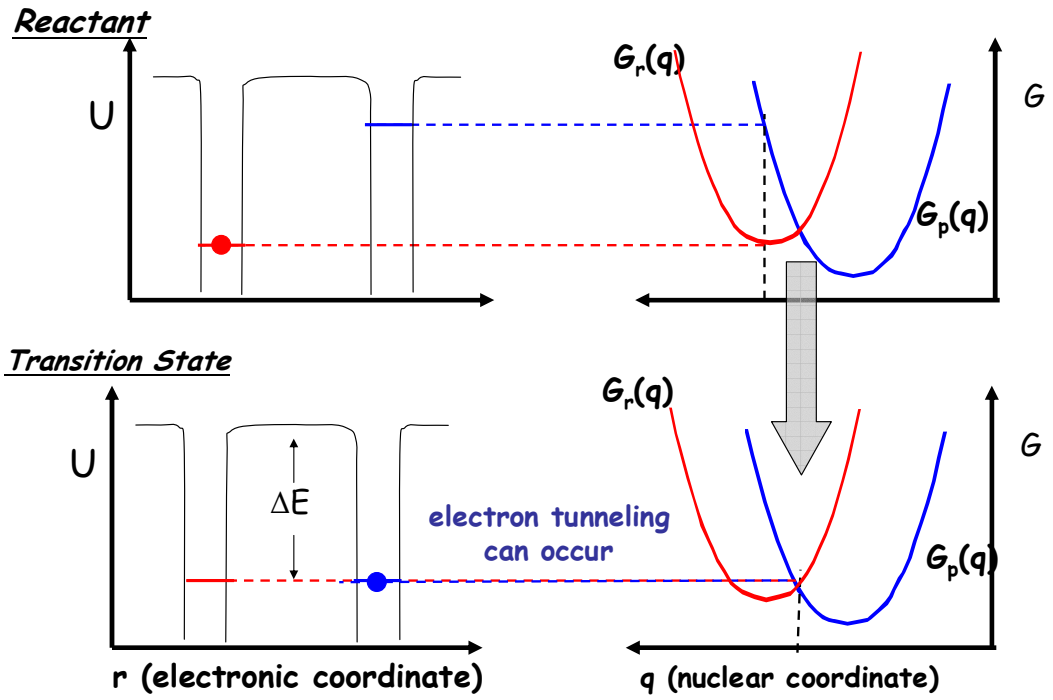

Figure 1.2 Energetics relevant electron transfer reactions are shown for the reactant state (top panel) and the transition state (bottom panel). Both electronic (r) and nuclear (q) coordinates (r, q) are involved in the reaction.

(top panel) the electronic energy of the reactant is lower than that of the product, and reaction does not occur. The bottom panel shows the case for the transition state, where the electronic energies are degenerate and the electron can tunnel along the electron coordinate (diagram on the left) between the reactant and product wells. This diagram underscores the fact that a

successful electron transfer reaction requires motion along the nuclear coordinate(s) to the transition state and motion along the electronic coordinate from the reactant to the product. If the electronic interaction between the product and reactant curves at the transition state is weak enough (pure nonadiabatic limit), the electron transfer rate is controlled by the electronic motion (tunneling from the reactant to product states). In this limit, the rate constant $k_{ET,NA}$ is given by equation 2. For the DBA molecules studied in this work, a semiclassical expression, with a single quantized nuclear mode, has been found to provide an adequate description of the rate constant. In the analysis a coarser representation of the quantized modes is used. With only one quantum mode, [13] the rate expression becomes

$$k_{et} = \frac{4\pi^2}{h}|V|^2 \frac{1}{\sqrt{4\lambda_0 \pi k_B T}} \sum_{n=0}^{\infty} \exp(-S)\left(\frac{S^n}{n!}\right).\exp\left[-\frac{(\Delta_r G + \lambda_0 + nh\nu)^2}{4\lambda_0 k_B T}\right] \qquad \mathbf{4}$$

where ν is the effective frequency for the quantized vibrational mode, $\Delta_r G$ is the reaction free energy, S is the Huang-Rhys factor $\lambda_i / h\nu$, and the λ_i is the total inner sphere reorganization energy for all of the relevant modes. The summand n refers to the product's vibrational quantum levels. For the systems studied below, the first few terms in the sum over product vibrational states provide an accurate evaluation of the rate constant, and equation 4 affords a reasonable description of the rate constant.

The electron transfer rate constant predicted by equation 4 is a strong function of the parameter set used, and an accurate determination of these parameters is necessary when drawing comparisons with experimental rate data. The quantities $h\nu$ and λ_i are typically evaluated using a combination of experimental charge-transfer spectra and ab-initio calculations. Usually, $\Delta_r G$ is estimated through experimental redox data and dielectric continuum corrections to the solvation energy. This approach is not appropriate for weakly

polar or non-polar solvents; however, in this study, $\Delta_r G$ is obtained in non-polar aromatic solvents from an analysis of the kinetic data using a two-state model (scheme 2).[14, 15] This two- state model assumes that equilibrium exists between the locally excited state and the charge-separated state and permits the evaluation of the forward and backward electron transfer rate constants. These data are used to calibrate a molecular-based solvation model that is able to reproduce experimental $\Delta_r G(T)$ values. The same model is used to predict the temperature dependence of λ_0. The electronic coupling $|V|$ and λ_0 (295K) are obtained by fitting the experimental rate constant data using the $\Delta_r G$ and $\frac{d\lambda_0}{dT}$ values from the model in conjunction with λ_i and ν values (taken from charge transfer spectra of similar molecule).

Scheme 1. Kinetic scheme for the forward and backward electron transfer.

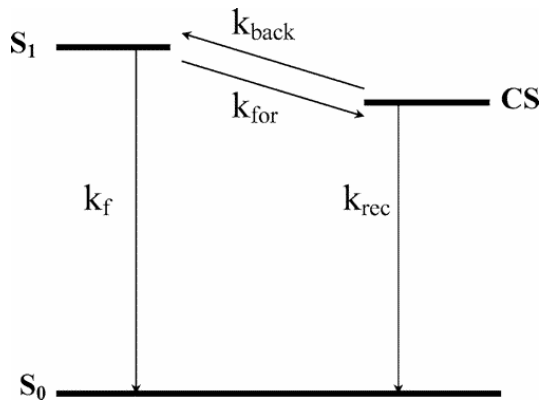

1.3 Reorganization energy and reaction free energy

The reorganization energy λ is a combination of two contributions ($\lambda = \lambda_V + \lambda_0$). λ_V (Internal reorganization energy) comes from the structural change of the reactant and the product state from their equilibrium configuration. So λ_V is related to the local changes of the geometry of

the reactant and the product state during electron transfer. In a single–mode semiclassical expression, the interaction with the solvent is modeled classically and the solute vibrations which are expressed as a single effective high-frequency mode are modeled quantum mechanically. Previous studies have shown that the internal reorganization energy λ_v and the effective mode frequency ν do not have a significant solvent dependence. For typical organic DBA systems (the molecules used for this study), one finds that the characteristic vibrational frequencies in the range of 1400-1600 cm^{-1} constitute a major fraction of the reorganization energy changes in the high frequency modes. This reflects the changes in the carbon-carbon bond lengths in these aromatic molecules during electron transfer. From charge transfer spectra (if available) and quantum chemistry calculations one can quantify the high frequency mode parameters. For systems in which charge transfer spectra are detected, free energy and reorganization parameters can be extracted from the spectral position and the line shape.[16] Using a single quantum mode expression for the charge transfer, the spectral shape is given by

$$I_{emission}(\nu') = \sum_j \frac{e^{-S} S^j}{j!} . \exp\left[-\frac{(jh\nu + \Delta G_{rec} + \lambda_0 + h\nu'_{fl})^2}{4\lambda_0 kT} \right] \qquad \mathbf{5}$$

Fitting the experimental charge transfer spectra to equation 5, we can compute the internal reorganization energy. The study described here have used the value of λ_i as 0.63 eV and the value for the vibrational frequency 1600 cm^{-1}.This value is related to the carbon-carbon bond stretching frequency.[17]

The outer sphere reorganization energy λ_0, also called the solvent reorganization energy, arises from the change in polarization and orientation of solvent molecules from reactant to product state. The solvent reorganization energy and the reaction free energies are computed by solvation characteristics; i.e., solute-solvent interaction energies. Two different

models can be used to treat the solute-solvent interactions; a dielectric continuum model and a molecular solvation model. The simple dielectric continuum model calculates solvation energies using a static dielectric constant ε_S and a high-frequency dielectric constant ε_∞.[18-20] The solute is treated as a spherical (or even ellipsoidal) cavity containing a point source. In the case of bimolecular reactions, the model includes two spherical cavities, each containing a point charge, whereas for intramolecular electron transfer reactions, it is more convenient to consider the solute as a cavity having a permanent dipole moment.

The solvent reorganization energy is given by equation 6 which is given below

$$\lambda_S = \frac{(\Delta\mu)^2}{a_0^{\,3}}\left(\frac{\varepsilon_S - 1}{2\varepsilon_S + 1} - \frac{\varepsilon_\infty - 1}{2\varepsilon_\infty + 1}\right) \qquad \mathbf{6}$$

and the reaction free energy from this model is computed as

$$\Delta_r G = \Delta_{vac} G - \frac{(\left|\overrightarrow{\mu_{CS}}\right|^2 - \left|\overrightarrow{\mu_{LE}}\right|^2)}{a_0^{\,3}}\left(\frac{\varepsilon_S - 1}{2\varepsilon_S + 1}\right) \qquad \mathbf{7}$$

in which $\overrightarrow{\mu_{LS}}$ is the dipole moment of the initially excited state, $\overrightarrow{\mu_{CS}}$ is the dipole moment of the charge-separated state, and a_0 is the cavity radius. The reaction free energy in a vacuum $\Delta_{vac} G$ provides a reference from which to include the solvation effect. $\Delta\mu$ is the magnitude of the dipole moment difference vector for the locally excited and the charge separated states, i.e., $\Delta\mu \equiv \left|\vec{\mu}_{CS} - \vec{\mu}_{LE}\right|$.

Matyushov has developed a solvation model that accounts for the discrete nature of the solute and solvent and incorporates electrostatic, induction, and dispersion interactions between the molecules comprising the fluid.[21] This treatment accurately computes the reaction free energies and reorganization energy for charge-transfer reactions. The solute is

modeled as a sphere with a state-dependent, point dipole moment m_i and polarizability $\alpha_{0,i}$. The solvent is treated as a polarizable sphere, with an electrostatic charge distribution that is axial and includes both a point dipole and a point quadrupole (Figure 1.3). The relative importance of the solvent's dipolar and quadrupolar contributions to the solvation energy can be expressed by the ratio $\left(< Q >^2 / |\mu|^2 \sigma^2\right)$. When this ratio is much larger than 1, quadrupole interactions dominate; when it is one or smaller, dipole contributions dominate. The quantity <Q> is defined as $< Q >= \left(2/3 \sum_i Q_{ii}^{\ 2} \right)^{1/2}$ and represents the effective axial moment for the traceless quadrupole tensor and σ is the effective hard-sphere diameter. It is evident from these simple considerations that quadrupolar interactions should dominate in the weakly polar aromatic solvents and should be insignificant in highly polar and non-aromatic solvents.

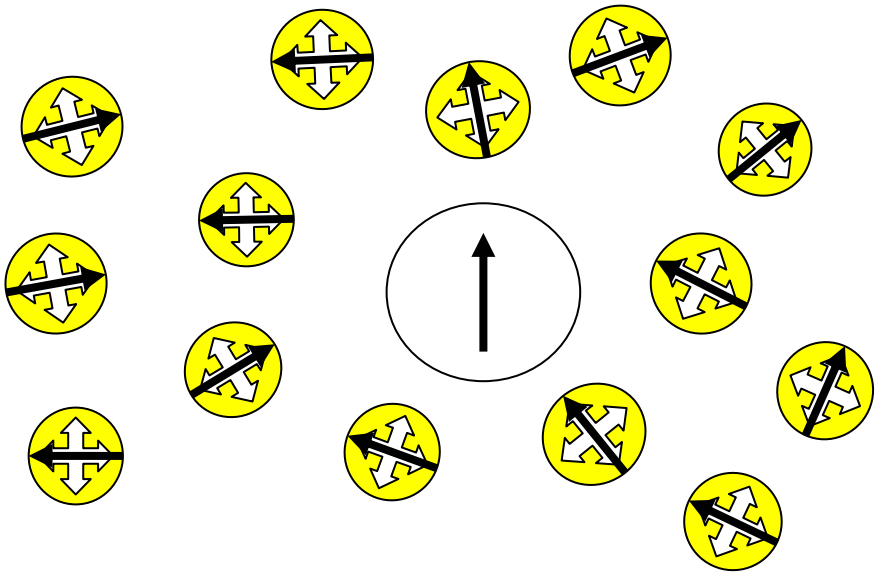

Figure 1.3 The multiple interactions between the solute and solvent molecules according to Matyushov model

In the molecular model, the reaction free energy $\Delta_r G$ is written as a sum of four terms,

$$\Delta_r G = \Delta_{vac} G + \Delta_{dq,i} G^{(1)} + \Delta_{disp} G + \Delta_i G^{(2)} \quad \textbf{8}$$

where $\Delta_{vac} G$ is the vacuum free energy, $\Delta_{dq,i} G^{(1)}$ contains first-order electrostatic and induction contributions, $\Delta_{disp} G$ contains dispersion terms, and $\Delta_i G^{(2)}$ contains second-order induction terms. Correspondingly, the outer-sphere reorganization energy λ_0 is written as a sum of three contributions,

$$\lambda_0 = \lambda_p + \lambda_{ind} + \lambda_{disp} \quad \textbf{9}$$

where λ_p includes contributions arising from the solvent dipole and quadrupole moments, λ_{ind} includes contributions from induction forces, and λ_{disp} includes contributions from dispersion forces. After parameterizations, the model is used to calculate the reorganization energy in order to calibrate the solvents and to predict the reaction free energies and the reorganization energies in more polar solvents.

1.4 Electronic coupling

The electron transfer rate constant (equation 4) is proportional to the square of the electronic coupling $|V|$ between the diabatic states at the curve crossing. In a one-electron approximation, $|V|$ is the resonance integral for electron delocalization over the donor and the acceptor. If no other atoms or molecules lie between the donor and the acceptor, the coupling magnitude depends on the overlap between the wavefunction of the donor and the acceptor and exhibits a sharp, exponential decrease with increasing separation. At separations greater than a couple of angstroms, simultaneous exchange interactions of the donor and the acceptor

with the intervening pendant group (non-bonded contact), or inclusion of the solvent molecule in the cleft, mediates the electronic coupling, generating larger interaction energies than the direct exchange interaction. In the U-shaped DBA molecules the electronic coupling is found to be solvent independent. The rotation and conformation of the intervening pendant group can also affect the magnitude of the electronic coupling.

Intervening molecules and ligands can mediate electronic interactions by a number of different mechanisms. A superexchange model proposed by McConnell [22] has received the most attention. According to this model, the initial and final diabatic states mix by virtue of their interactions with higher energy electronic configurations. For the case of identical mediating sites and only nearest neighbor interactions, the electronic coupling V is given by

$$V = (T^2/\Delta)(-t/\Delta)^{N-1} \qquad \textbf{10}$$

where T is the interaction energy between the donor (acceptor) and the terminal super-exchange orbital of the intervening structure. Δ is the energy difference between the diabatic transition state and the superexchange configurations involving the promoted electron, and t is the interaction energy between the N adjacent bridge sites. This perturbation treatment is valid if t and T are much less than Δ. The approximations of the McConnell model lead to the following predictions; (i) an exponential decrease of the donor-acceptor coupling magnitude with increasing separation/number of sites (N) of the intervening medium, i.e., $\ln|V| \propto (N-1)$; and (ii) the characteristic decay length for the interaction (the proportionality constant β) becomes small as (t/Δ) approaches one.[23] This model has been successfully used in order to explain solvent-mediated electron transfer. In our case, the electron transfer from donor to acceptor is mediated by the presence of a pendant group. So the interaction between all these molecules is important for understanding the electron transfer in these systems. The 't' term is

not important here as the electron tunnels through the non-covalent contacts (through space), not through the bridge. So the magnitude of the term t/Δ is very low. At the same time the value of N reduced to unity as there will be one pendant molecule between donor and acceptor and the size, rotation and the orientation of the pendant molecule plays an important role in the electronic coupling. Hence, for fixed donor-spacer-acceptor molecules, different pendant groups can modulate the electronic coupling.

1.5 Dynamic Solvent Effect

A solvent molecule can change the energetics of the electron transfer reaction either by interacting with the reactant and product or by actively participating in the reaction in a more dynamic way by exchanging energy and momentum with reacting species. This effect is known as a solvent dynamic effect. Dynamic solvent effects are mainly associated with the dielectric friction of the polar solvents. These dynamical features of polar interactions can play an important role in determining the electron transfer reaction rates. The molecular mechanism of dynamic solvation can be viewed as the reorientation of dipolar solvent molecules around the solute molecules due to the newly distributed charge of a solute. The more polar the solvent, the stronger is the coupling between the molecules. The polarization responses also depend on the intermolecular solvent interactions. Zusman[24] first considered this effect, which has since been studied by several other groups.[25-30]

One approach to study solvation dynamic effects are "continuum" models.[31-36] These models treat the solute as a point dipole in a spherical cavity that is immersed in solvent which is treated as a continuum, frequency-dependent dielectric. Simple continuum models

predict that the solvent has an exponential solvation response function, given by the following equation

$$S(t) = \exp(-t/\tau_L) \quad \textbf{11}$$

The dynamic solvation time is equal to the longitudinal relaxation time (τ_L) of the solvent

$$\tau_L = \tau_D \frac{\varepsilon_\infty}{\varepsilon_0} \quad \textbf{12}$$

where ε_0 is the static dielectric constant, ε_∞ is the high-frequency dielectric constant, and τ_D is the dielectric (or Debye) relaxation time.

In intramolecular electron transfer reactions, when the electron tunneling rate is much faster than the reorientation time of the solvent, then the solvent reorientation can become the rate limiting step of the reaction. In this case, the electron transfer rate is limited by the relaxation rate of the solvent and the reaction is a solvent-controlled electron transfer reaction. In contrast, when the solvent reorientation rate is much faster than the electron transfer rate, the relaxation time of solvent has no effect on the electron transfer and it is a nonadiabatic electron transfer reaction.

For non Debye solvents, which are characterized by more than one relaxation time scale, people have used the correlation time of the solvent relaxation which is defined as

$$\langle \tau \rangle = \int_0^\infty S(t)dt \quad \textbf{13}$$

This correlation time is a measure of the solvation time.

1.6 Summary

This thesis probes the electron transfer mechanism and kinetics in different DBA molecular systems in detail. Chapter 2 and 3 use different U-shaped Donor-Bridge-Acceptor molecules to illustrate how the electron transfer mechanism and kinetics depends on the nature of the pendant unit present in the "*line of sight"* between the donor and acceptor moieties (Figure 1.4). The experimental results are compared with the semiclassical equation and molecular solvation model. The results prove that the electronic coupling depends on the nature of the substituent groups on the phenyl ring present in the cavity. Electron

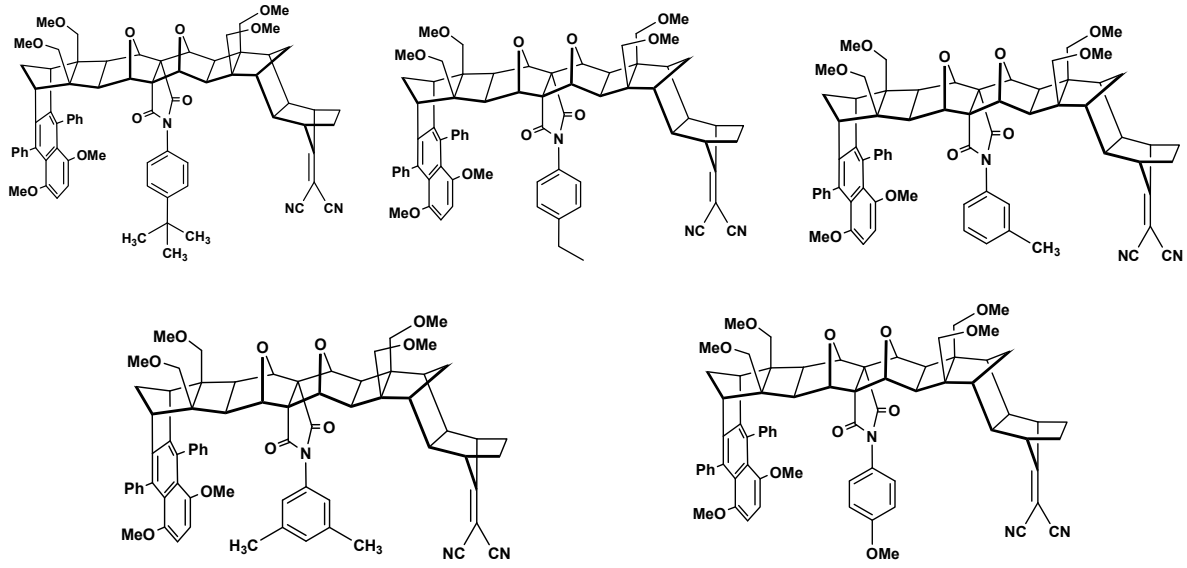

Figure 1.4 U-shaped Donor-Bridge-Acceptor molecules studied in chapter 2, 3 and 4

donating groups present in the aromatic ring do not change the electronic coupling values whereas the presence of electron withdrawing groups present in the ring can enhance the electronic coupling a lot and hence the electron transfer rate. Chapter 4 demonstrates that a switchover of electron transfer mechanism occur from a nonadiabatic electron transfer

towards an “adiabatic” electron transfer in highly viscous and slowly relaxing solvent NMP. The experimental results were analyzed in terms of different theoretical models to explain the dynamic solvent effect observed in our system.

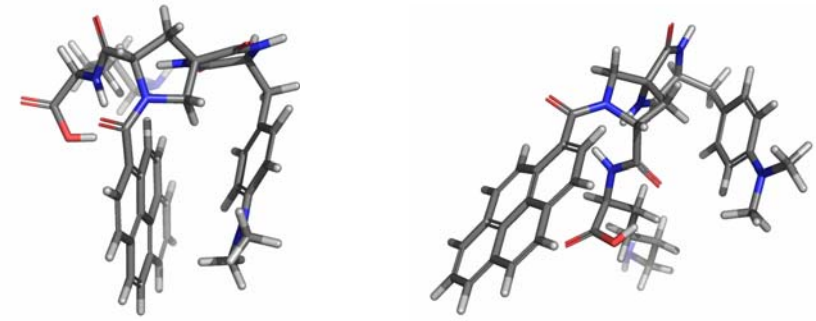

Figure 1.5 Model peptide systems studied in chapter 5 and 6

Chapters 5 and 6 study the effect of water molecules on electron transfer in different DBA systems (Figure 1.5). We are able to show experimentally that water molecules can influence significantly the electron transfer pathways in model peptide systems through the hydration layer formed between the donor and acceptor, which is not possible for aprotic solvents like DMSO. To further confirm our results we have performed solvent isotope and pH effect studies on electron transfer. Our experimental findings support the theoretical predictions of water effects on protein electron transfer.

Our study strongly supports the idea that the electron rate constant and outer-sphere reorganization energy depend on the nature of the pendant group in these DBA molecules. We have calculated the electronic coupling and outer-sphere reorganization energy in these compounds in different solvents. To study the electron transfer in low temperature is another part of these studies. The low temperature data indicates that in the two different temperature regimes the electron transfer mechanisms differ from each other. At higher temperature the

electronic tunneling mechanism dominates and at lower temperature the rate is limited by solvent dynamical effects. The last part of this thesis studies how water molecules affect the electron transfer kinetics. The results show that water molecules can greatly influence the electron transfer rate.

1.7 References

1. Bixon, M.; Jortner, J. *Adv. Chem. Phys*. **1999**, *106*, 35.

2. Libby, W. F. *J. Phys. Chem*. **1952**, *56*, 863.

3. Marcus, R. A. *J. Chem. Phys*. **1956**, *24*, 966.

4. (a) Zimmt, M. B.; Waldeck, D. H. *J. Phys. Chem. A*. **2003**, *107*, 3850.(b) Paddon- Row, M. N. *Acc. Chem. Res*. **1994**, *27*, 18. (c) Balzani, V., Ed. *Electron Transfer in Chemistry*, Vol. 3; Wiley-VCH: Weinhein, 2001. (d) Johnson, M. D.; Miller, J. R.; Green, N. S.; Closs, G. L. *J. Phys. Chem*. **1989**, *93*, 1173.

5. (a) Zeng, Y.; Zimmt, M. B. *J. Phys. Chem*. **1992**, *96*, 8395. (b) Oliver, A. M.; Paddon-Row, M. N.; Kroon, J.; Verhoeven, J. W. *Chem. Phys. Lett*. **1992**, *191*, 371.

6. Closs, G. L.; Miller, J. R. *Science* **1988**, *240*, 440.

7. Zener, C. *Proc. R. Lond. A*. **1932**, *137*, 969.

8. Landau, L. *Phys. Z. Sowj*. U. **1932**, *1*, 88.

9. (a) Zusman, L. D. *Z. Phys. Chem*. **1994**, *186*, 1. (b) Onuchic, J. N.; Beratan, D. N.; Hopfield, J. J. *J. Phys. Chem*. **1986**, *90*, 3707.

10. Jortner, J. *J. Chem. Phys*. **1976**, *64*, 4860.

11. (a) Kelly, A. M. J. Phys. Chem. A. 1999, 103, 6891. (b) Wang, C.; Mohney, B. K.; Williams, R.; Hupp, J. T.; Walker, G. C. *J. Am. Chem. Soc*. **1998**, *120*, 5848 (c) Markel, F.; Ferris, N. S.; Gould, I. R.; Myers, A. B. *J. Am. Chem. Soc*. **1992**, *114*, 6208.

12. Barbara, P. F.; Meyer, T. J.; Ratner, M. A. *J. Phys. Chem*. **1996**, *100,* 13148.

13. Gu, Y.; Kumar, K.; Lin, Z.; Read, I.; Zimmat, M. B.; Waldeck, D. *J. Photochem. Photobiol. A.* **1997**, *105*, 189.

14. Read, I.; Napper, A.; Kaplan, R.; Zimmat, M. B.; Waldeck, D.H. *J. Am. Chem. Soc.* **1999**, *121*, 10976.

15. (a) Marcus, R. A. J. Phys. Chem. 1989, 93, 3078. (b) Cortes, J.; Heitele, H.; Jortner, J. *J. Phys. Chem*. **1994**, *98*, 2527.

16. Napper, A. M.; Head, N. J.; Oliver, A. M.; Shephard, M. J.; Paddon-Row, M. N.; Read, I.; Waldeck, D. H. J. *Am. Chem. Soc.* **2002**, *124*, 10171,

17. Newton, M. D.; Basilevsky, M. V.; Rostov, I. V. *Chem. Phys*. **1998**, *232*, 201.

18. Sharp, K.; Honig, B. *Annu. Rev. Biophys. Chem*. **1990**, *19*, 301.

19. Sitkoff, D.; Sharp, K. A.; Honig, B. *J. Phys. Chem*. **1994**, *98*, 1978.

20. Brunschwig, B. S.; Ehrenson, S.; Suttin, N. *J. Phys. Chem*. **1986**, *90*, 3657.

21. Matyushov, D. V.; Voth, G. A. *J. Chem. Phys*. **1999**, *111*, 3630.

22. McConnell, H. M. *J. Chem. Phys*. **1961**, *35*, 508.

23. (a) Evenson, J. W.; Karplus, M. D. *Science*, **1993**, *262*, 1247. (b) Paddon-Row, M. N.; Shephard, M. J.; Jordan, K. D. *J. Am. Chem. Soc*. **1993**, *115*, 3312.

24. Zusman, L. D. *Chem. Phys.* 1980, *49*, 295.

25. Calef, D. F.; Wolynes, P. G. *J. Phys. Chem* 1983, *87*, 3387.

26. Sumi, H.; Marcus, R. A. *J. Chem. Phys* 1986, *84*, 4272.

27. Sumi., H.; Marcus, R. A. *J. Chem. Phys* 1986, *84*, 4894.

28. Rips, I.; Jortner, J. *Chem. Phys. Lett.* 1987, *133*, 411.

29. Marcus, R. A.; Sumi., H. *J. Electroanal. Chem.* 1986, *204*, 59.

30. Onuchic, J. N.; Beratan, D. N.; Hopfield, J. J. *J. Phys. Chem* 1986, *90*, 3707.

31. Loring, R. F.; Yan, Y. J.; Mukamel, S. *Chem. Phys. Lett.* 1987, *135*.

32. Castner, E. W.; Bagchi, B.; Fleming, G. R. *Chem. Phys. Lett.* 1988, *143*, 270.

33. Van der Zwan, G.; Hynes, J. T. *J. Phys. Chem* 1985, *89*, 4181.

34. Barchi, B.; Oxtoby, D. W.; Fleming, G. R. *Chem. Phys.* 1984, *86*, 257.

35. Yu, T. M. *Opt. Spectrosc. (USSR)* 1974, *36*, 283.

36. Maroncelli, M. *J. Molecular Liquids* 1993, *57*, 1.

37. Onsager, L. *Can. J. Chem*. **1977**, *55*, 1819.

2.0 CHAPTER TWO

Pendant Unit Effect on Electron Tunneling in U-Shaped Molecules

This work has been published as Liu, M.; Chakrabarti, S.; Waldeck, D. H.; Oliver, A. M.; Paddon-Row, M. N. Chem. Phys. 2006, 324, 72

The electron transfer reactions of three U-shaped donor-bridge-acceptor molecules with different pendant groups have been studied in different solvents as a function of temperature. The pendant group mediates the electronic coupling and varies the electron tunneling efficiency through nonbonded contacts with the donor and acceptor groups. Quantitative analysis of the temperature dependent rate data provides the electronic coupling. The influence of steric changes on the electronic coupling magnitudes is explored by structural variation of the pendant groups.

2.1 Introduction

Electron transfer reactions are one of the most fundamental reactions in chemistry and play important roles in biology and in the emerging field of molecular electronics. Electron transfer reactions are distinguished from other chemical reactions by their ability to proceed even when the reductant (electron donor) and oxidant (electron acceptor) are not in direct

contact, although they are in contact through some kind of intervening medium (e.g. hydrocarbon groups, protein segments). For example, photosynthesis reaction centers in plants use light driven electron transfer to produce a charge-separated state across a membrane. This electron transfer occurs by a sequence of electron transfer steps, each one proceeding by a super-exchange mechanism in which the donor – acceptor electronic coupling is mediated by the interaction of the donor and acceptor states with virtual ionic states of the intervening medium.

Over the past four decades, rigid, covalently linked donor-bridge-acceptor (DBA) molecules, in which the donor and acceptor chromophores are held at well-defined separations and orientations with respect to each other, have been successfully used to explore the dependence of electron transfer dynamics on a variety of factors,[1] including interchromophore distance[2] and orientation,[3] bridge configuration[4] and orbital symmetry.[5] These studies have revealed that the electronic interaction between the donor (reductant) group and the acceptor (oxidant) group is controlled by the covalent linkages in the molecules. Changes in the bonding patterns in the bridging group and their energetics may be used to manipulate the electronic coupling magnitude and hence the electron transfer rate.[6]

In the past ten years, electron transfer kinetics in highly curved DBA molecules[7], where the distances between two redox centers are significantly larger than the sum of their van der Waals' radius, has been used to investigate electron tunneling through nonbonded contacts. When the electron transfer is nonadiabatic, the tunneling probability is proportional to the electronic coupling squared, $|V|^2$. Previous work[8] shows that the placement and electronic properties of the pendant group in U-shaped DBA molecules can strongly affect the electron tunneling efficiency. Corresponding studies on C-shaped molecules which display

electron tunneling by way of solvent molecules located in the cleft are also available.[9,10] These studies show that the electron tunneling efficiency correlates with the electron affinity of the solvent molecules and their ability to fit in the cleft, i.e., steric constraints.

Scheme 1

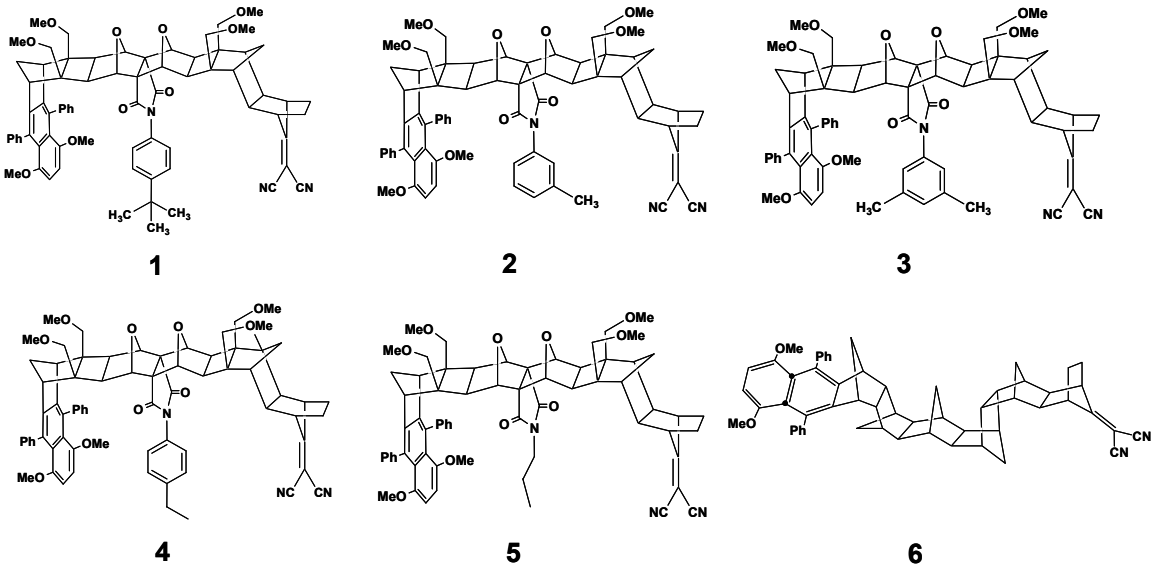

The current work studied electron transfer in three U-shaped molecules (**1**, **2** and **3**) and compared them to the previously studied compound **4** to explore how steric properties of the pendant group affect the electronic coupling. The U-shaped DBA molecules (**1** - **5**) have a highly curved and rigid bridge, which holds the donor and an acceptor groups at a fixed distance and orientation. A pendant group is covalently attached to the bridge and occupies the space between the donor and acceptor unit. Previous studies[8] explored how the electron transfer rate constants and electronic couplings vary amongst the compounds **4**, **5** and **6**. The results revealed that the coupling for **4** is 2.5 times larger than that for **5**.[8b] The electronic coupling is enhanced by an aromatic pendant group, compared to an alkyl group, in the "line-of-sight" between the donor and acceptor, because the virtual ionic states of the pendant aromatic ring in **4**, being mainly of π character, are energetically closer to the naphthalene

donor and dicyanovinyl acceptor states than are the virtual ionic σ states of the pendant alkyl group in **5**. The photoinduced electron transfer rate constant of **4** is 15 times faster than compound **6** in toluene.[8a] Compound **6** has a bridge, with the same number of bonds linking the donor and acceptor units as do **4** and **5**, but it is not U-shaped. Thus, the electronic coupling between the naphthalene and dicyanovinyl groups in **6** can only occur by way of a superexchange mechanism operating through the bridge and is weaker than the corresponding electronic coupling in **4** and **5** which takes place more directly, through superexchange involving the pendant group.

The schematic energy diagram in Figure 1 shows an effective one-dimensional nuclear reaction coordinate. Two possible electron transfer regimes are distinguished by the strength of the electronic coupling $|V|$, the interaction between the reactant and the product states at the curve crossing. When the electronic coupling is weak $|V| << k_BT$, the reaction is nonadiabatic (dashed curve in Figure 1) and the rate constant is proportional to $|V|^2$. In this regime, the system may move through the curve crossing region $q^{\ddagger}$ many times before the electronic state changes. The second regime is adiabatic electron transfer, where $|V| >> k_BT$ (solid curves in Figure 1). In this limit, the electronic state change evolves as the nuclear motion proceeds; i.e., the strong coupling mixes the donor and acceptor states and the reaction proceeds along a single electronic state.

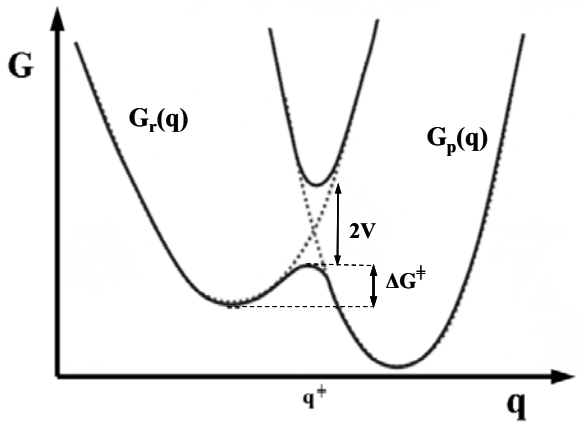

Figure 2.1 Diagram illustrating the adiabatic (the solid curves) - strong coupling - and nonadiabatic (the diabatic dashed curves) – weak coupling.

For the U-shaped molecules, the electronic coupling between the donor and acceptor moieties is weak enough that the electron transfer lies in the nonadiabatic limit. The semiclassical model for electron transfer in the nonadiabatic limit begins with a Fermi's Golden Rule expression for the transition rate; namely

$$k = (2\pi / \hbar)|V|^2 FCWDS \qquad \mathbf{1}$$

where $\hbar$ is Planck's constant divided by 2π, $|V|$ is the electronic coupling matrix element, and FCWDS is the Franck-Condon weighted density of states. The FCWDS term accounts for the probability that the system achieves a nuclear configuration in which the electronic state can change. The square of the coupling, $|V|^2$, measures the probability of changing from the reactant to product electronic state.

2.2 Modeling the Rate Constant

Previous work successfully applied the Golden Rule rate constant expression with a single effective quantum mode, and described k_{ET}[10] by the semiclassical rate equation.

$$k_{ET} = \frac{4\pi^2}{h} |V|^2 \frac{1}{\sqrt{4\lambda_o \pi k_B T}} \sum_{n=0}^{\infty} \exp(-S) \left(\frac{S^n}{n!} \right) \exp\left[- \frac{(\Delta_r G + \lambda_o + nh\nu)^2}{4\lambda_0 k_B T} \right] \quad \textbf{2}$$

where λ_0 is the solvent reorganization energy; $\Delta_r G$ is the reaction free energy; $S = \frac{\lambda_v}{h\nu}$ and λ_v is the internal reorganization energy. The $h\nu$ term refers to the average energy spacing of a single effective quantized mode frequency in the electron transfer reaction and is a characteristic of the solute. The sum is performed over the vibrational states of the effective quantum mode.

The quantities $h\nu$ and λ_v are determined primarily by the donor and acceptor groups and is not sensitive to their separation. Charge-transfer absorption and emission measurements of compound **7** in hexane, in conjunction with theoretical calculations[11] were used to quantify $h\nu$ and λ_v. This analysis provided a value of 1600 cm^{-1} for the single effective quantized mode and 0.63 eV for the solute reorganization energy λ_v. This effective frequency is comparable to typical carbon-carbon stretching frequencies in aromatic ring systems, such as the naphthalene, which primarily show stretching modes of ~ 1600 cm^{-1} upon formation of the cation.[8a] A lower frequency of 1088 cm^{-1}associated with out-of-plane bending of the dicyanovinyl group. A previous study[8a] showed that inclusion of this mode frequency affected the absolute magnitude of $|V|$ that is extracted from the data but did not affect the relative magnitude of $|V|$, for **4** and **5**. The internal reorganization energy is dominated by the dicyanovinyl acceptor which provides values in a range of 0.30 – 0.50 eV from the charge transfer emission experiment.[7b] The values of $h\nu$ and λ_v are consistent with those reported for charge transfer complexes of hexamethylbenzene with tetracyanoethylene in CCl_4 and cyclohexane.[13] In the current work, these two parameters are kept fixed in the fit of the rate constant to equation 2.

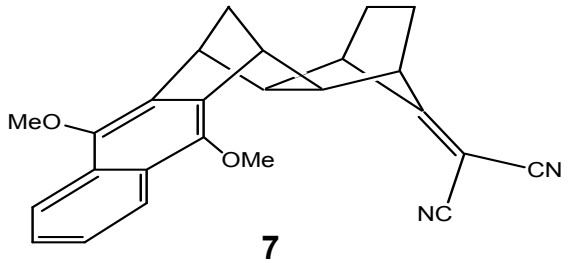

7

The values of the three remaining parameters contained in the semiclassical rate expression (Eqn 2), namely λ_0, $|V|$ and $\Delta_r G$, need to be determined. The solvent reorganization energy λ_0 and the reaction free energy $\Delta_r G$ are determined by calibration of Matyushov's molecular solvation model[14] with experimental $\Delta_r G$ data. The reaction free energy $\Delta_r G$ in weakly polar or non-polar solvents can be experimentally measured from an analysis of the equilibrium between the locally excited state and the charge-separated state. Previous reports[8a] parameterized the molecular solvation model for **4** in the solvents toluene and mesitylene and used it to predict the reaction free energy and the solvent reorganization energy in polar solvents. This model, parameterized in the same way, was used to fit the electron transfer reaction rate constant in the new U-shaped molecules, **1**, **2** and **3**.

The Matyushov solvation model accounts for the discrete nature of the solute and the solvent. The solute is treated as a sphere with a point dipole moment and polarizability. The solvent is modeled as a polarizable sphere with an electrostatic charge distribution that includes both a point dipole and a point quadrupole. The model incorporates the interactions between the solute and the solvent molecules and amongst the solvent molecules themselves, including the dipole-dipole interactions, the dipole-quadrupole interactions, the quadrupole-quadrupole interactions, the induction, and dispersion interactions. The molecular model properly describes the temperature dependence of the solvation[15], as compared to a continuum model, and is superior for analyzing these data.

The current work reports the electron transfer behavior of three new U-shaped molecules (**1** – **3**) with pendant groups having different steric properties, compared to compound **4**. Compound **4** has a *para* ethyl group on the phenyl ring, **1** has a *para t*-butyl unit, **2** has one methyl at a *meta* position of the phenyl ring; and **3** has two methyl groups, one at each *meta* position. The rate constant model described above is used to compare the electronic coupling in these U-shaped molecules. The similarity found for the electronic coupling in these dissimilar substitution patterns suggests that the average orientation of the phenyl ring, with respect to the donor and acceptor, is similar.

2. 3 Experimental

2.3.1 Time-Resolved Fluorescence Studies

Each sample was dissolved in the different solvents at a peak optical density of less than 0.2 in all of the experiments. The solvent acetonitrile (99.9% HPLC) was purchased from Burdick & Jackson without further purification. The solvents toluene, mesitylene and *p*-xylene were fractionally distilled two times using a vigreux column under vacuum after purchased from Aldrich. The purified fraction was used immediately in all the experiments. Each solution was freeze-pump-thawed a minimum of five cycles.

Each sample was excited at 326 nm by the frequency-doubled cavity-dumped output of a Coherent CR599-01 dye laser, using DCM (4-dicyanomethylene-2-methyl-6-p-dimethylamino-styryl-4H-Pyran) dye, which was pumped by a mode locked Coherent Antares Nd:YAG. The dye laser pulse train had a repetition rate of 300 kHz. Pulse energies were kept below 1 nJ, and the count rates were kept below 3 kHz to prevent a pile-up effect. All

fluorescence measurements were made at the magic angle, and data were collected until a standard maximum count of 10,000 was observed at one channel.

The time-resolved fluorescence kinetics for **1**, **2** and **3** and their donor-only analogues were carried out in different solvents as a function of temperature. The temperature ranged from 273 K to a high of 346 K. The experimental temperature was controlled by an ENDOCAL RTE-4 chiller and the temperature was measured using a Type-K thermocouple (Fisher-Scientific), accurate to within 0.1 ºC.

The instrument response function was measured using a sample of colloidal $BaSO_4$. The fluorescence decay curve was fit by a convolution and compare method using IBH-DAS6 analysis software. Independent experiments on individual donor only molecules at the measured temperatures, always a single exponential fluorescence decay, was used to determine the intrinsic fluorescence decay rate of the locally excited state. The DBA molecules **1** – **4** have a small amount of donor-only impurity. The measurement of the donor-only molecule's characteristics in each solvent and temperature allowed their contribution to be subtracted from the decay law of their DBA molecules**.** The decay law of **1** – **4** in acetonitrile was a single exponential function and in the weakly polar solvents toluene, mesitylene and *p*-xylene was a double exponential function. Fitting to the semiclassical equation (equation 2) was performed using Microsoft Excel 2003.

2.4 Results and Analysis

2.4.1 Steady-State Spectra:

The U-shaped molecules **1**, **2**, **3** and **4** have been studied in the polar solvent acetonitrile, the weakly polar solvent toluene, and the nonpolar solvents mesitylene and *p*-xylene. The spectra of the DBA molecules are the same as those of the donor only analogues, hence the spectroscopic properties of the donor units in these molecules dominate the spectral features. Figure 2 shows the absorption and emission spectra of these molecules in acetonitrile and mesitylene.

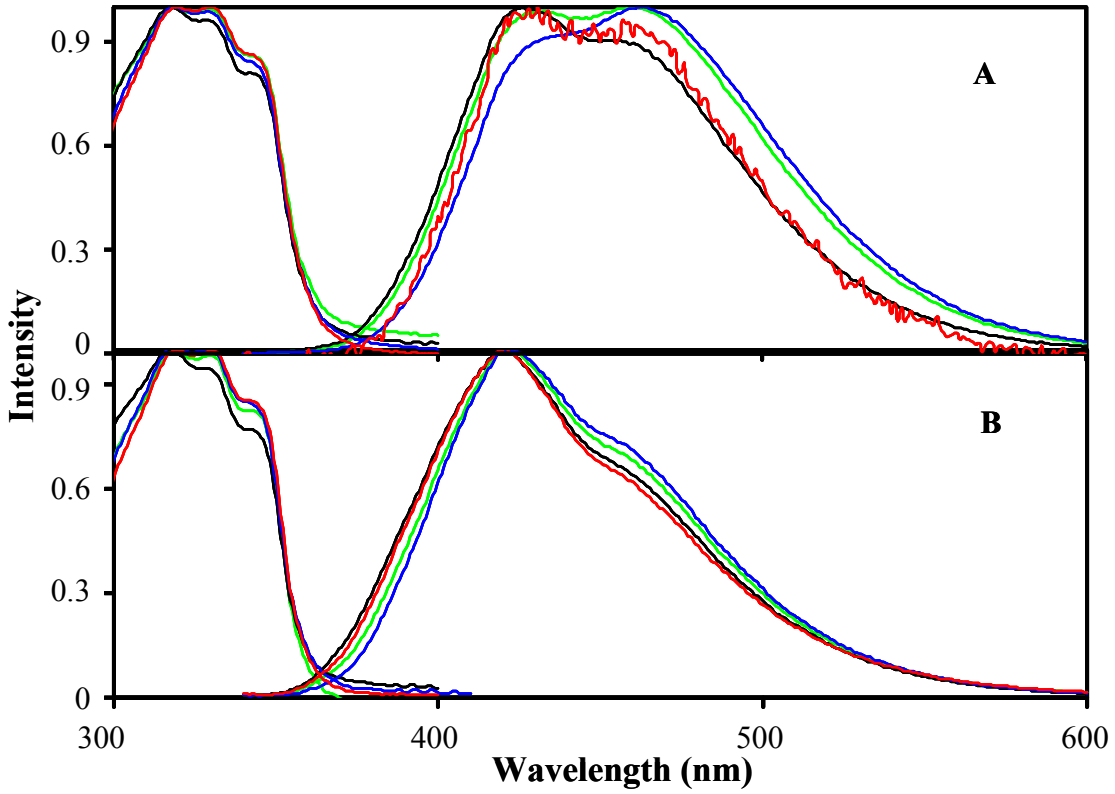

Figure 2.2 Absorption spectra (left) and emission spectra (right) of **1** (black), **2** (green), **3** (blue) and **4** (red) in acetonitrile (A) and mesitylene (B)

The donor unit of compounds **1** through **4** is the same, 1,4–dimethoxy-5,8-diphenylnaphthalene, and accounts for the similarity of the spectra in a given solvent. The naphthalene chromophore has two close lying excited electronic states, ^1L_a and ^1L_b in the Platt notation, that are accessed in the ultraviolet. The red shift of the donor spectrum and the loss of vibronic structure, as compared to naphthalene, are consistent with the methoxy group (and phenyl) substitution.[16] Although 1-substituted naphthalenes typically have the ^1L_b state below the ^1L_a state (transition is polarized along the short axis), high-resolution spectra of 1-aminonaphthalene in a jet expansion show a reversal of this ordering; i.e., the ^1L_a state is below the ^1L_b state.[17] This example underscores the sensitivity of the relative ordering of the ^1L_b and ^1L_a states to perturbations.

The variations in the spectral substructure must arise from changes in the excited state properties with changes in the solvent and the pendant group. The spectra in mesitylene solvent (Figure 2.2B) are shown because it is expected to perturb the chromophore the least of all the solvents and illustrate the spectral perturbations that arise from the changes in the pendant groups. Polar solvent molecules, such as acetonitrile (Figure 2.2A) interact with the solute to stabilize the excited ^1L_b state and this changes the relative intensity of the two peaks in the emission spectrum. Despite the change in intensity of these two emission peaks the fluorescence decay law does not change with emission wavelength; i.e., it is the same across the band.

Although the absorption spectra show different absorption bands, the fluorescence spectrum and lifetime do not depend on the excitation energy. It is understood that both electronic configurations involve π-π^* single electron excitations and the energy difference is small enough that the ^1L_a and ^1L_b states are strongly mixed. This claim is supported by the

identical emission spectra that were obtained at different excitation energies for each compound and by the fact that the lifetime of compound **4** does not change with the excitation energy from 296 nm to 359 nm.

2.4.2 Fluorescence Kinetics

In polar solvents, like acetonitrile, the fluorescence decay of the U-shaped molecules is single exponential with rate constant k_{obs}, and the electron transfer rate constant can be determined from $k_{ET} = k_{obs} - k_f$, where k_f is the fluorescence decay rate of the donor only molecule and k_{ET} is the electron transfer rate.

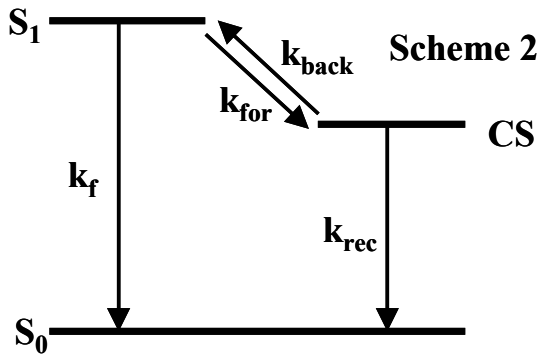

In toluene and nonpolar solvents, mesitylene and *p*-xylene, the fluorescence decay is double exponential. The biexponential kinetic arises because the free energy of the charge separated state is close to zero and equilibrium between the locally excited state (LE) and the charge separated state (CS) occurs[10] (see scheme 2). The double exponential kinetics can be analyzed to extract the reaction free energy, $\Delta_r G$, from the experiment. By writing the fluorescence intensity as

$$I(t) = [a_+ \exp(-k_+ t) + (1 - a_+)\exp(-k_- t)]I(0) \qquad \textbf{3}$$

the forward electron transfer rate constant is

$$k_{for} = a_{+}(k_{+} - k_{-}) + k_{+} - k_{f} \quad \textbf{4}$$

and the backward electron transfer rate constant is

$$k_{back} = k_{-} - k_{rec} - a_{+}(k_{+} - k_{-}) \quad \textbf{5}$$

The free energy difference between the locally excited state (LE) and the charge separated state (CS) is

$$\Delta_r G = -RT \ln\left(\frac{k_{for}}{k_{back}}\right) \quad \textbf{6}$$

The experimentally determined reaction free energy for all these U-shaped molecules as a function of temperature in toluene, mesitylene and *p*-xylene are used to calibrate the solute parameters in this model.[9]

2.4.3 Reaction Free Energy $\Delta_r G$

A number of solvent parameters (some of them are listed in Table 2.1) are required to analyze the molecular solvation model. The polarizability of toluene, mesitylene and acetonitrile were kept the same as used previously[8a] and the polarizability of *p*-xylene was obtained from literature.[18] The dipole moments and quadrupole moments of the different solvents were computed using Gaussian 2003 at the MP2/6-31 G level. Rather than use the quadrupole moment tensor, an effective axial moment $\langle Q \rangle = (\frac{2}{3}\sum_i Q_{ii}^{\,2})^{1/2}$ was evaluated.[19] The origin was defined as the center of mass of the molecule to calculate the quadrupole moment. The sizes (sigma) of the solvents and the Lennard-Jones energies were obtained from the literature.[20, 21]

Table 2.1 Solvent parameters used in the Molecular Solvation Model

Solvent	Polarizability ($Å^3$)	Quad Moment (D Å)	Dipole Moment (D)	Sigma (Å)	Lennard-Jones energy[d] (K)
Toluene	12.32	8.76	0.363	5.68	603
Mesitylene	16.14	8.58	0.0671	6.40	720
Acetonitrile	4.48	3.37	4.0664	4.24	405
p-Xylene	14.23	8.77	0.0542	6.04	725

The best fit of the experimental reaction free energies to the solvation model provides the solute parameters listed in Table 2.2. Details of the analysis are available elsewhere.[9] Because the bridge is so rigid and the size changes on the pendant group are small compared to the overall molecular size, the radius of solute was kept constant at 7.66 Å for the different molecules. The solute's ground and excited state dipole moments were kept the same as the previous calculation[8a], 5.75 D for the ground state and 28.64 D for the charge-separated state. The polarizabilities of **1** – **4** were adjusted slightly to account for changes in the pendant group.[22] The polarizability of **4** is 128 $Å^3$; the same as previously.[8a] The ΔG_{vac} value was chosen independently for the four solutes and treated as an adjustable parameter when fitting the experimental free energy to the molecular solvation model. The best fit provides similar ΔG_{vac} values for these solutes, see Table 2.2.

Table 2.2 Solute parameters used in the Molecular Solvation Model

System	Radius[a](Å)	$\Delta\gamma^a$ ($Å^3$)	μ_{ex} (D)	μ_{gs} (D)	Polarizability[25] ($Å^3$)	$\Delta G_{vac}{}^a$ (eV)
1	7.66	5.29	28.64	5.75	133	0.19
2					128	0.18
3					130	0.17
4					128	0.18

[a.] obtained from the best fit of the molecular solvation model

Figure 2.3 plots the reaction free energy of **1**, **2**, **3** and **4** in mesitylene as a function of temperature. The model fits the experimental data well in each case where the Gibbs energy change could be measured experimentally. The reaction free energy for these U-shaped molecules in mesitylene changes systematically with temperature from -0.10 to -0.05 eV (see Figure 2.3). Similar behavior was observed in toluene and *p*-xylene.

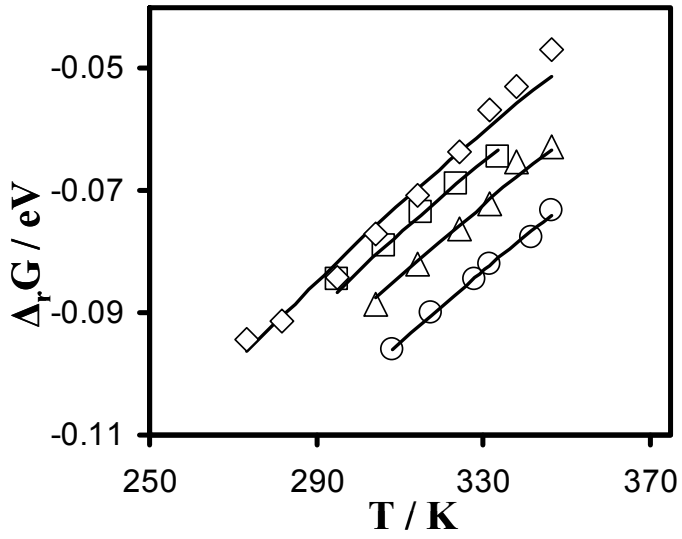

Figure 2.3 The experimental $\Delta_r G$ values are plotted for **1** (diamond), **2** (triangle), **3** (circle) and **4** (square) in mesitylene. The lines show the $\Delta_r G$ values predicted from the molecular model with the solvent parameters given in Table 2.1

After parameterization, the reaction free energies of these molecules in acetonitrile were predicted. Table 2.3 compares the free energies of these compounds at 295 K in different solvents. The free energy becomes more negative as the solvent becomes more polar. Mesitylene and *p*-xylene (which have no dipole moment) have the most positive $\Delta_r G$. Toluene has a small dipole moment and the $\Delta_r G$ becomes more negative, whereas the strongly polar acetonitrile has the most negative reaction free energy.

Table 2.3 Best fit of $\Delta_r G$ (295 K) values for U-shaped molecules

System	$\Delta_r G$, eV (295 K)			
	Toluene	Mesitylene	*p*-xylene	Acetonitrile
1	-0.11	-0.082	-0.087	-0.55
2	-0.12	-0.094	-0.099	-0.55
3	-0.13	-0.10	-0.11	-0.57
4	-0.12	-0.087	-0.092	-0.55

For molecules **1** – **4** in weakly polar and nonpolar solvents, $\Delta_r G$ becomes more negative as the size of the phenyl ring's substituent increases; in the more polar acetonitrile the variation of $\Delta_r G$ with the pendant group is not apparent. Although the molecular model provides a means for estimating $\Delta_r G$ as a function of temperature, it contains significant simplifying assumptions; for example, it treats the solute as a sphere containing a point dipole moment and polarizability. In comparing the model with the experimental $\Delta_r G$ for compounds **1** – **4** in mesitylene (see Figure 3), the $\Delta_r G$ difference in **1** varies from -8.4% to 2.1%; **2** varies from -3.7% to 1.2%; **3** varies from -0.89% to 1.3%; and **4** varies from -2.5% ~2.1%. Although this finding suggests some slight systematic error in the model fitting, the overall agreement is excellent. A previous analysis reported a $\Delta_r G$ of -0.52 eV for **4** in acetonitrile, whereas the current value is -0.55 eV (see Table 2.3), a 5% deviation. Although the fit of the molecular model to the $\Delta_r G$ data depends on three adjustable solute parameters, the ability to fit a range of different solvents and use very similar solute parameters for compounds **1** to **4** indicates that the molecular model provides a reliable and consistent description of the reaction free energy.

2.4.4 Kinetic Analysis

With the reaction free energy obtained from the model and the internal reorganization energy parameters from the previous studies, [8a] it is possible to fit the temperature dependent rate constant data to equation 2 and extract the electronic coupling $|V|$ and the solvent reorganization energy λ_0. $|V|$ is treated as a temperature independent quantity. The solvent reorganization energy has a temperature dependence because the solvation is temperature dependent. The temperature dependence of the solvent reorganization energy was predicted from the molecular solvation model and the best fit was used to extract the solvent reorganization energy at 295 K.

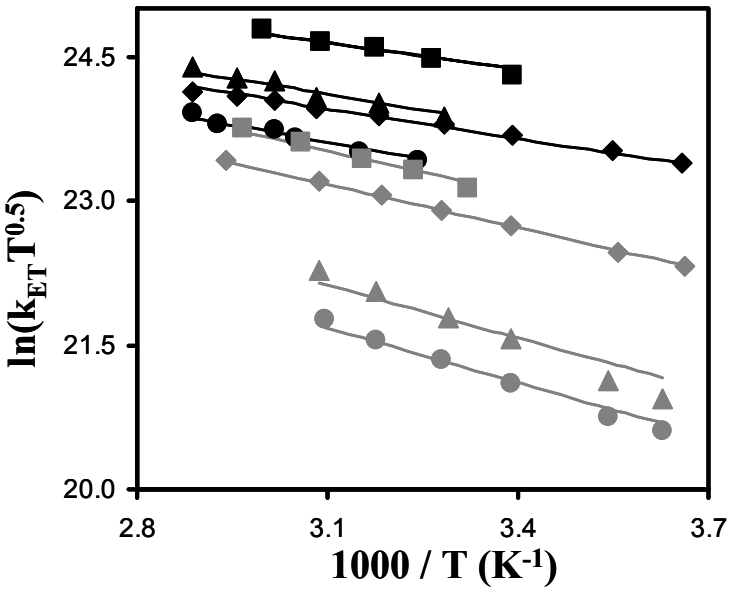

Figure 2.4 Experimental rate constant data are plotted versus 1/T, for **1** (diamond), **2** (triangle), **3** (circle) and **4** (square) in mesitylene (black) and acetonitrile (gray). The lines represent the best fits to equation 2

The fit of the temperature dependent rate constant data to equation 2 (see Figure 2.4) was used to determine the electronic coupling $|V|$ and λ_0 (295 K), listed in Table 2.4. Figure 2.4 shows fits of the experimental rate constant to the model for these four molecules in mesitylene and acetonitrile. The rate data in toluene and *p*-xylene behave similarly. Table 2.4 lists the solvent reorganization energies, λ_0, at 295 K and electronic couplings $|V|$ that are obtained for the four solutes by fitting to the temperature dependent rate constant expression, equation 2.

Table 2.4 Best fit of $|V|$ and λ_0 (295 K) values for U-shaped molecules

System	$\lvert V\rvert$, cm^{-1}	λ_0, eV (295 K)			
		Toluene	Mesitylene	*p*-xylene	Acetonitrile
1	139	0.75	0.71	0.72	1.53
2	147	0.78	0.73	0.75	1.67
3	130	0.85	0.77	0.80	1.72
4	147	0.70	0.66	0.67	1.50

The reorganization energies in weakly polar and nonpolar solvents at 295 K lie in the range of 0.66 to 0.85 eV; in acetonitrile they are considerably higher within 1.50 to 1.72 eV. In these analyses, the solvent reorganization λ_0 is modeled as temperature dependent and an adjustable λ_0 offset is used to fit the data. From the molecular model prediction, λ_0 is associated with both solvent rotational degrees of freedom, which increase slightly with increasing temperature, and solvent translational degrees of freedom, which decrease with increasing temperature.[23] For compounds **1** – **4** in mesitylene from 273 K to 346 K, the net decrease in λ_0 is 10% to 13% of the adjustable λ_0 offset. The previous molecular model fitting of λ_0 (295) for **4**[8a] reported a value of 0.69 eV in mesitylene and 1.50 eV in acetonitrile, which

are consistent with the current fit (Table 2. 4). The values of λ_0 for compounds **1** – **3** are close to those found for **4**, as expected.

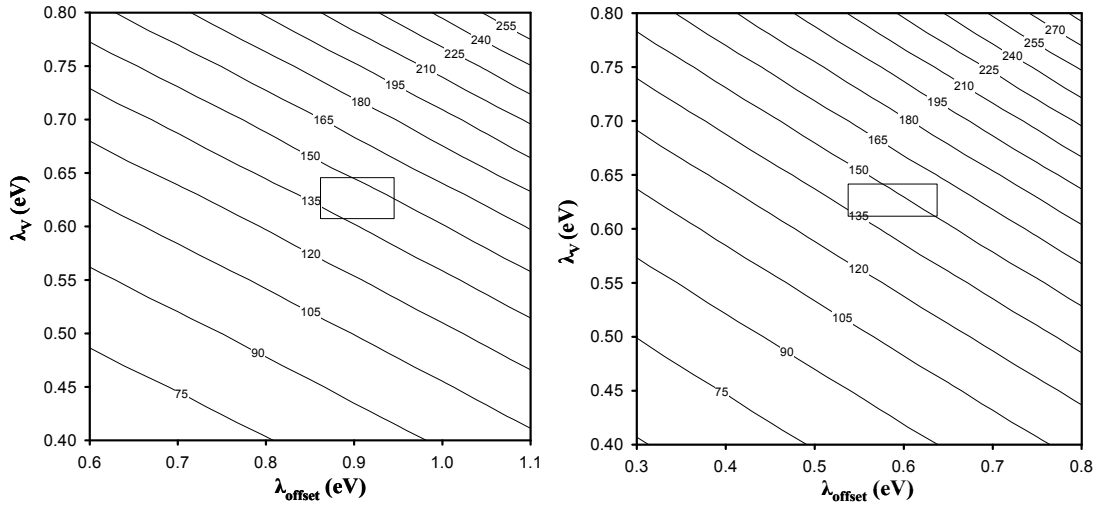

Figure 2.5 Contours of constant |V| are shown for **4** in acetonitrile (panel A) and mesitylene (panel B). The rectangular region contains parameter values for which the χ^2 parameter in the fit is ≤ 3 times its optimal value. Outside of this region the fits to the rate data visibly deviate

Table 2.4 lists the values of $|V|$ for **1** – **4** obtained from the best fit to equation 2. Compound **1** with a *t*-butyl substituent on the phenyl ring gives a |V| of 139 cm^{-1}; **2** has one methyl group and a |V| of 147 cm^{-1}; **3** has two methyl substituents and a somewhat lower |V| of 130 cm^{-1}. In comparison with a |V| value of 168 cm^{-1}, for **4** reported previously[8a], a 13% smaller value of 147 cm^{-1} was obtained from the current fit. The disparity of the electronic coupling from the different fits is within expected errors in the analysis. Although the steric properties of the pendant group in these U-shaped molecules may change the phenyl ring geometry, the values of the electronic couplings are similar.

Although $|V|$ is treated as independent of the solvent, it strongly relies on the value of the parameters λ_0, λ_v, $\Delta_r G$ and $d\lambda_0/dt$ in the fit. Figure 2.5 illustrates how the best fit value

of the electronic coupling changes with the magnitude of the internal reorganization energy and the outer sphere reorganization energy used in the analysis. The contours represent different values of the electronic coupling. The boxed region in each case identifies the range for λ_v and λ_{offset} over which the χ^2 changes by a factor of three.

2.5 Theoretical Calculations

Structural features of the U-shaped systems were investigated by carrying out geometry optimizations of the ground states of **1** - **3** at the B3LYP/6-31G(d) level of theory, which has been demonstrated previously to be acceptable for these types of systems.[12] Complete geometry optimizations were carried out with no imposed constraints using Gaussian 03.[24] Each system was found to have two stable conformations differing in the orientation of the naphthalene methoxy groups. The lowest energy conformation for each system, exemplified by **1a** (Figure 2.6), has both methoxy groups lying in the plane of the naphthalene ring, whereas in the other conformation, exemplified by **1b**, one of the methoxy groups is twisted out of the plane of the naphthalene ring. Unsurprisingly, conformation **b** in each system is 8 - 9 kJ/mol less stable than conformation **a,** and therefore is expected not to play a significant role in the electron transfer dynamics. In any case, apart from the differences in methoxy group orientation, conformations **a** and **b** have very similar structural features, particularly with respect to interchromophore separation and pendant group twisting about the N-C (phenyl) bond. Two additional conformations were located for each of **2a** and **2b**, distinguished by the different direction of twisting of the pendant 3-methylphenyl ring about the N-C (phenyl) bond. In one conformation, the 3-methyl side of the pendant group is twisted towards the naphthalene ring whereas in the other conformation, it is twisted towards

the dicyanovinyl group. The former conformation is slightly more stable than the latter, by about 1.5 kJ/mol.

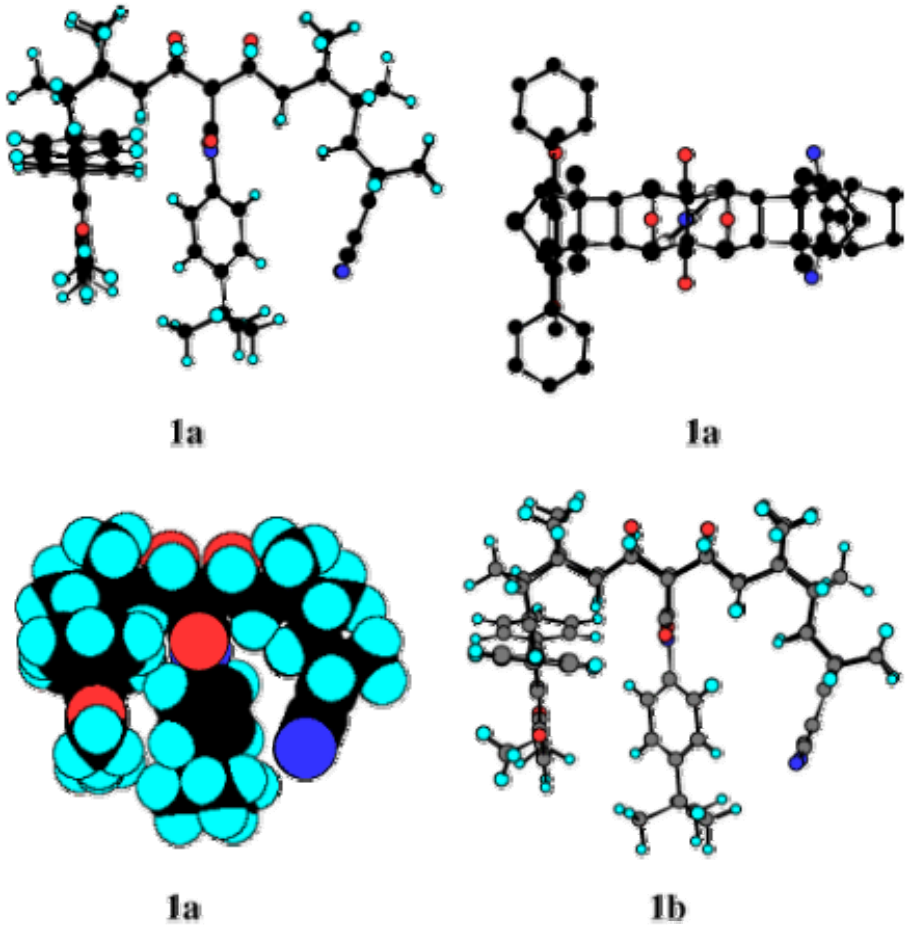

Figure 2.6 B3LYP/6-31G(d) optimized geometries of two conformations of **1**, namely **1a** (more stable), in which both OMe groups of the 1,4-dimethoxy-5,8-diphenylnaphthalene ring approximately lie in the plane of the naphthalene and **1b** (less stable), in which one of the methoxy groups is twisted out of the naphthalene plane. A plane view of **1a** is shown (minus all H atoms and the *tert*-butyl group for clarity) which depicts the degree of twisting of the N-*tert*-butylphenyl pendant group about the N-C (phenyl) bond. A space-filling depiction of **1a** is also shown (using standard van der Waals atomic radii)

The following discussion of geometries refers to the lowest energy conformation for each system. The space-filling depiction of **1a** is representative of all three molecules and shows that the pendant group is fairly close to both the donor and acceptor moieties. Another important geometric parameter, which is linked to the distances between the pendant and donor and acceptor groups, is the torsional (twist) angle about the C-N bond connecting the pendant group to the succinimide ring. The twist angle is equal to 0^o when the planes of the pendant aromatic ring and succinimydyl ring coincide and it is equal to 90^o when the two planes are orthogonal to each other. The twist angle and closest distances between the donor, pendant and acceptor groups for the lowest energy conformation of each molecule are given in Table 2.5. The pendant group in **8** is the unsubstituted phenyl group (i.e. **8** is **1** with *tert*-butyl replaced by H).

Table 2.5 Twist angles (degrees) and closest distances (Å) between the pendant group and acceptor and donor groups and the closest distance between the donor and acceptor

Molecule	Twist[a]	*r*(dcv-ar)[b]	*r*(nap-ar)[c]	*r*(dcv-napd)[b]
1	44	3.8	4.0	9.4
2	40	3.8	4.2	9.6
3	32	4.5	4.2	9.9
4[e]	47	3.8	3.9	9.4
8[f]	48	3.8	3.9	9.5

[a] Torsional angle about the N-C(aromatic pendant group) bond. [b] Closest distance between the dicyanovinyl and the aromatic pendant groups. [c] Closest distance between the naphthalene and the aromatic pendant groups. [d] Closest distance between the dicyanovinyl and thenaphthalene groups. [e] The pendant group has a methyl substituent rather than the ethyl substituent of 4. [f]phenyl (C_6H_5)

In none of the stable molecular conformations are the pendant and succinimide rings coplanar, a consequence of steric repulsions between the two *ortho* C-H hydrogens of the pendant aromatic ring with the carbonyl groups of the succinimide ring which are present in the coplanar conformation. The twist angle decreases along the series **1** > **2** > **3** and this trend reflects the increasing steric bulk at the *meta* positions of the pendant aromatic ring, by the presence of methyl substituents. Reducing the magnitude of the twist angle therefore reduces destabilizing steric interactions of the pendant group with the acceptor and donor groups. This increasing steric interaction along the series **3** > **2** > **1** is also probably responsible for the slight increases in the closest distances between the various groups along the series **1** < **2** < **3** (Table 2.5). The placement of a *tert*-butyl group (or an ethyl group **4**) at the *para* position of the pendant aromatic ring has little effect on the molecular geometry (*cf.* **1** and **8**). This is understandable because the *para* substituent is remote (> 4 Å) from the donor and acceptor groups.

It is difficult to predict the trend in the strengths of the electronic coupling term in the series of U-shaped systems because it seems to depend, not only on the closest distances between the pendant group and the donor and acceptor groups, but also on the type of overlap between the π orbitals of the pendant group with those of the donor and acceptor. Thus, model calculations reported previously[8c] suggested that the coupling is stronger when the plane of the pendant ring is parallel to those of the donor and acceptor (twist angle = 0^o) than when it is perpendicular to those planes (twist angle = 90^o). In the former case, the overlap of the π orbitals is of σ-type whereas for the latter case, it is a mixture of σ- and π-types. The data shown in Table 5 indicate that as the twist angle *decreases* along the series **1** > **2** > **3**, the closest distances between the pendant ring and the donor and acceptor groups *increase*

slightly. Thus, the electronic coupling term may well be approximately constant along the series.

2.6 Discussion

The electron transfer rate constants in compounds **1** through **3** behave similarly to changes in temperature and solvent as does **4**. The electron transfer rate constants in these molecules are not the same; e.g., at 298 K **4** is ten times faster than **3** in acetonitrile and three times faster in mesitylene. The differences in the electron transfer rate constants arise from changes in the energetics rather than changes in the couplings. The difference in the electron transfer energetics is apparent from Figure 2.3 and Table 2.3 which shows the experimentally determined reaction free energy for the four solutes in mesitylene. Because the only change between the compounds is alkylation of the pendant phenyl ring, these energetic differences likely arise from changes in the pendant polarizability and the extent of Coulomb stabilization of the charge separated state.

A fit of the rate constant data as a function of temperature to Equation 2 was used to extract values for the solvent reorganization energy and the electronic couplings (see Table 2.4). The reorganization energies in the aromatic solvents range from 0.66 eV to 0.85 eV, whereas those in acetonitrile range from 1.5 eV to 1.7 eV. The reorganization energy for **1**, **2**, and **3** are similar in size to those reported previously for **4**. The magnitudes of the reorganization energies reported here are larger than those reported for analogous systems containing a methoxyanthracene donor and a diacetylvinyl acceptor[9], however this difference can be attributed to differences in size of the donor and acceptor moieties and distortion of the dicyanovinyl acceptor group in the charge separated state. In particular, the distortion of the

dicyanovinyl group may contribute up to 0.5 eV [25] in reorganization energy. The trend in solvent reorganization energy correlates with the changes in solvent polarity. The variations in the reorganization energy between solutes are consistent for the different solvent systems; however, they are small enough compared to the expected error that they are not interpreted here.

In the nonadiabatic picture the electron transfer rate constant is directly proportional to the electronic coupling squared $|V|^2$, which gives the probability for electron tunneling from the locally excited state to the charge separated state. For the four solutes studied here (**1** through **4**), the electronic couplings are all very similar, ranging from 130 cm^{-1} to 150 cm^{-1}. This observation is consistent with electron affinities of alkyl benzenes that does not vary much with substitution pattern.[26] Previous work demonstrated that the electronic coupling in systems of this type occurs by electron mediated superexchange.[27,28] The similar |V| values are consistent with the computational studies and may reflect a compensation between a decrease of the electronic coupling as the phenyl ring twists away from 0° and an increase of the electronic coupling as the donor and acceptor groups distance decreases with the phenyl twist (*vide supra*).

Studies of electron tunneling through nonbonded contacts in related compounds, containing a dimethoxyanthracene donor and a diacetylvinyl acceptor separated by a 7 angstrom gap found a significant variation of the electronic coupling with the substitution pattern and steric bulk of the molecule in the gap between the donor and acceptor group.[9,10] In those studies the alkylated phenyl moiety was a solvent molecule and not tethered to the bridge, hence the change in electronic coupling could reflect either intrinsic changes arising from electronic state differences of the alkylbenzene or geometric changes arising from steric

constraints. The current studies show that placement of the aromatic moiety in the cleft gives electronic couplings that do not vary significantly with alkylation and supports the conclusions made in reference 9 that the electronic coupling variation results from steric constraints rather than intrinsic electronic differences.

The small changes in the electronic coupling magnitudes for the different systems studied here bears on studies of **4** in the slowly relaxing solvent N-methylacetamide. One study[8c] reported that **4** and **5** have different electron transfer rates at high temperatures, arising from differences in the electronic coupling, but have similar rates at low temperature. The possibility that phenyl ring rotation in **4** can conformationally gate the electron transfer in that system was proposed as a possible explanation. The small variation of the electronic coupling with the amount of alkyl substitution and the related geometric changes of the pendant group in the cleft suggest that modulation of the electron tunneling probability by changes in the phenyl ring geometry is not the cause of that behavior.

2.7 Conclusion

The electron transfer in U-shaped molecules containing a pendant group in the line of sight between an electron donor and an electron acceptor was studied. In each case the pendant group was an alkylsubstituted phenyl and had the aromatic moiety in the same location, although twisted at different average angles. The electronic coupling in these systems does not vary significantly.

2.8 Acknowledgement

We acknowledge the support from the Australian Research Council and we thank the U.S. National Science Foundation (CHE-0111435) for support. The UNSW group gratefully acknowledges support from the Australian Partnership for Advanced Computing (APAC) and the Australian Centre for Advanced Computing and Communications (ac3) for allocation of computing time.

2.9 Appendix

Table 2.6 Fluorescence decay of DBA molecules in toluene

System	Toluene							
	T(K)	Donor τ (ps)	A1%	τ_1 (ps)	τ_2 (ps)	k_{for} (s^{-1})	k_{back} (s^{-1})	$\Delta_r G$ (eV)
Compound 4	295.0	4203	99.0	399	25515	2.24×10^{9}	2.59×10^{7}	-1.13×10^{-1}
	305.6	3980	98.5	355	39882	2.52×10^{9}	4.63×10^{7}	-1.05×10^{-1}
	314.7	3814	98.0	324	41885	2.77×10^{9}	6.58×10^{7}	-1.01×10^{-1}
	323.9	3663	97.0	279	42236	3.21×10^{9}	1.15×10^{7}	-9.30×10^{-2}
	336.6	3479	95.8	264	38555	3.35×10^{9}	1.70×10^{7}	-8.64×10^{-2}
Compound 1	295.0	3610	99.2	642	18894	1.27×10^{9}	1.45×10^{7}	-1.14×10^{-1}
	304.6	3449	98.9	595	25233	1.37×10^{9}	2.13×10^{7}	-1.09×10^{-1}
	314.0	3262	98.3	541	36867	1.51×10^{9}	3.76×10^{7}	-9.99×10^{-2}
	324.3	3115	97.6	506	35573	1.61×10^{9}	5.51×10^{7}	-9.43×10^{-2}
	338.1	2914	95.8	425	32979	1.91×10^{9}	1.13×10^{7}	-8.25×10^{-2}
Compound 2	295.0	4352	99.2	706	20376	1.18×10^{9}	1.22×10^{7}	-1.16×10^{-1}
	304.4	4181	99.0	634	17595	1.32×10^{9}	1.69×10^{7}	-1.14×10^{-1}
	313.6	3995	98.8	565	35721	1.50×10^{9}	2.50×10^{7}	-1.11×10^{-1}
	324.4	3809	98.0	484	51482	1.77×10^{9}	4.59×10^{7}	-1.02×10^{-1}
	338.0	3602	96.8	436	52504	1.94×10^{9}	8.27×10^{7}	-9.20×10^{-2}
Compound 3	295.0	5452	94.7	1214	1764	6.26×10^{8}	5.32×10^{6}	-1.21×10^{-1}
	304.4	5216	98.1	1127	5836	6.81×10^{8}	1.43×10^{6}	-1.01×10^{-1}
	313.6	4981	99.2	1044	46604	7.50×10^{8}	9.42×10^{6}	-1.18×10^{-1}
	324.4	4720	99.0	928	38192	8.56×10^{8}	1.28×10^{7}	-1.18×10^{-1}
	338.1	4407	98.4	820	45718	9.73×10^{8}	2.31×10^{7}	-1.09×10^{-1}

Table 2.7 Fluorescence decay of DBA molecules in mesitylene

System	Mesitylene							
	T(K)	Donor τ (ps)	A1%	τ_1 (ps)	τ_2 (ps)	k_{for} (s^{-1})	k_{back} (s^{-1})	$\Delta_r G$ (eV)
Compound 4	295.0	3474	97.2	407	28211	2.10×10^{9}	7.59×10^{7}	-8.44×10^{-2}
	306.3	3294	96.1	349	28426	2.45×10^{9}	1.23×10^{8}	-7.90×10^{-2}
	314.9	3174	94.8	316	28059	2.69×10^{9}	1.78×10^{8}	-7.36×10^{-2}
	323.7	3063	93.5	296	27106	2.84×10^{9}	2.40×10^{8}	-6.89×10^{-2}
	333.7	2950	91.8	260	25142	3.19×10^{9}	3.39×10^{8}	-6.45×10^{-2}
Compound 1	273.3	4392	98.8	897	42871	8.74×10^{8}	1.59×10^{7}	-9.44×10^{-2}
	281.7	4139	98.5	809	37068	9.76×10^{8}	2.26×10^{7}	-9.15×10^{-2}
	294.9	3792	97.6	702	43591	1.13×10^{9}	4.11×10^{7}	-8.42×10^{-2}
	304.4	3588	96.5	639	41463	1.23×10^{9}	6.56×10^{7}	-7.70×10^{-2}
	314.3	3407	95.2	584	36678	1.34×10^{9}	9.79×10^{7}	-7.08×10^{-2}
	324.3	3241	93.3	543	31378	1.41×10^{9}	1.46×10^{8}	-6.35×10^{-2}
	331.5	3120	91.1	498	26001	1.51×10^{9}	2.08×10^{8}	-5.67×10^{-2}
	338.1	3020	89.6	473	22567	1.57×10^{9}	2.56×10^{8}	-5.28×10^{-2}
	346.3	2921	86.9	443	18316	1.63×10^{9}	3.39×10^{7}	-4.69×10^{-2}
Compound 2	304.5	3928	97.6	616	47992	1.33×10^{9}	4.56×10^{7}	-8.85×10^{-2}
	314.6	3739	96.5	541	46466	1.52×10^{9}	7.38×10^{7}	-8.20×10^{-2}
	324.8	3951	95.4	513	41172	1.58×10^{9}	1.03×10^{8}	-7.63×10^{-2}
	331.5	3462	94.2	437	36195	1.87×10^{9}	1.50×10^{8}	-7.21×10^{-2}
	339.4	3342	92.4	423	31387	1.89×10^{9}	2.03×10^{8}	-6.52×10^{-2}
	346.3	3266	91.2	379	27944	2.10×10^{9}	2.57×10^{8}	-6.28×10^{-2}
Compound 3	308.3	4873	98.2	936	54290	8.45×10^{8}	2.29×10^{7}	-9.59×10^{-2}
	317.4	4624	97.5	869	49846	9.07×10^{8}	3.38×10^{7}	-9.00×10^{-2}
	327.8	4354	96.6	762	46523	1.04×10^{9}	5.22×10^{7}	-8.45×10^{-2}
	331.5	4258	96.1	707	47701	1.13×10^{9}	6.39×10^{7}	-8.20×10^{-2}
	341.5	4025	95.2	672	41206	1.17×10^{9}	8.36×10^{7}	-7.77×10^{-2}
	346.3	3958	94.1	606	38478	1.30×10^{9}	1.12×10^{8}	-7.33×10^{-2}

Table 2.8 Fluorescence decay of DBA molecules in p-Xylene

System	*p*-Xylene							
	T(K)	Donor τ (ps)	A1%	τ_1 (ps)	τ_2 (ps)	k_{for} (s^{-1})	k_{back} (s^{-1})	$\Delta_r G$ (eV)
Compound 4	295.0	4051	97.9	418	48039	2.10×10^{9}	5.53×10^{7}	-9.24×10^{-2}
	305.1	3834	97.0	364	46308	2.40×10^{9}	8.94×10^{7}	-8.66×10^{-2}
	314.6	3641	96.1	339	44762	2.56×10^{9}	1.26×10^{8}	-8.18×10^{-2}
	323.1	3488	94.9	306	41869	2.82×10^{9}	1.80×10^{8}	-7.66×10^{-2}
	333.6	3317	93.4	265	36500	3.23×10^{9}	2.69×10^{8}	-7.14×10^{-2}
Compound 1	295.0	3851	97.8	722	82187	1.10×10^{9}	3.72×10^{7}	-8.60×10^{-2}
	305.3	3672	96.8	666	69655	1.18×10^{9}	5.77×10^{7}	-7.95×10^{-2}
	313.6	3496	95.5	611	59909	1.28×10^{9}	8.73×10^{7}	-7.26×10^{-2}
	323.5	3329	94.0	565	46653	1.37×10^{9}	1.27×10^{8}	-6.62×10^{-2}
	335.0	3128	91.7	512	34368	1.48×10^{9}	1.92×10^{8}	-5.89×10^{-2}
Compound 2	295.0	4217	98.7	763	38878	1.06×10^{9}	1.95×10^{7}	-1.02×10^{-1}
	305.3	4011	98.0	653	52550	1.25×10^{9}	3.50×10^{7}	-9.42×10^{-2}
	313.1	3860	97.3	578	59762	1.43×10^{9}	5.34×10^{7}	-8.87×10^{-2}
	323.7	3675	96.3	508	57896	1.62×10^{9}	8.37×10^{7}	-8.27×10^{-2}
	334.4	3497	94.6	448	49157	1.83×10^{9}	1.36×10^{8}	-7.49×10^{-2}
Compound 3	295.0	5377	98.9	1299	5377	5.77×10^{8}	6.57×10^{6}	-1.14×10^{-1}
	305.1	5072	98.9	1120	50337	6.86×10^{8}	1.18×10^{7}	-1.07×10^{-1}
	315.3	4824	98.5	1006	57091	7.72×10^{8}	1.85×10^{7}	-1.01×10^{-1}
	323.3	4585	97.8	898	64473	8.72×10^{8}	2.92×10^{7}	-9.47×10^{-2}
	333.9	4326	97.0	789	62787	9.99×10^{8}	4.58×10^{7}	-8.87×10^{-2}

Table 2.9 Fluorescence decay of DBA molecules in acetonitrile

System	Acetonitrile			
	T(K)	Donor τ (ps)	τ_1 (ps)	k_{ET} (s^{-1})
Compound 4	301	11375	1382	6.36×10^8
	309	11102	1172	7.63×10^8
	317	10472	1069	8.40×10^8
	327	9897	918	9.88×10^8
	337	9389	806	1.13×10^9
Compound 1	273	10900	2575	2.97×10^8
	281	10492	2286	3.42×10^8
	295	10478	1879	4.37×10^8
	305	10049	1662	5.02×10^8
	314	8985	1446	5.80×10^8
	324	9089	1295	6.62×10^8
	340	8401	1085	8.02×10^8
Compound 2	276	12828	6542	7.49×10^7
	282	12335	5858	8.96×10^7
	295	11432	4501	1.35×10^8
	304	11071	3893	1.67×10^8
	315	10448	3225	2.14×10^8
	324	10098	2775	2.61×10^8
Compound 3	276	14211	8040	5.40×10^7
	282	13952	7498	6.17×10^7
	295	13488	6265	8.55×10^7
	305	13218	5487	1.07×10^8
	315	12929	4848	1.29×10^8
	323	12757	4245	1.57×10^8
	338	12370	3467	2.08×10^8

2.10 References

1. a) Closs, G. L.; Miller, J. R. *Science*. **1988**, *240*, 440. b) Paddon-Row, M. N. *Acc. Chem. Res.* **1994**, *27*, 18. c) Barbara, P. F.; Meyer. T. J.; Ratner, M. A. *J. Phys. Chem.* **1996**, *100*, 13148. d) Paddon-Row; M. N. "*Electron Transfer In Chemistry"*; Balzani, V., Ed.; Wiley- VCH: Weinheim, **2001**; Vol. 3, Part 2, Chapter 1; p.179.
2. a) Hush, N. S.; Paddon-Row, M. N.; Cotsaris, E.; Oevering, H.; Verhoeven, J. W.; Heppener, M. *Chem. Phys. Lett.* **1985**, *117*, 8. b) Penfield, K. W.; Miller, J. R.; Paddon-Row, M. N.; Cotsaris, E.; Oliver, a. M.; Hush, N. S. *J. Am. Chem. Soc.***1987**, *109*, 5061. c) Pispisa, B.; Venanzi, M.; Palleschi, A. *J. Chem. Soc. Far. Trans.***1994**, *90*, 435. d) Closs, G. L.; Calcaterra, L. T.; Green, N. J.; Penfield, K. W.; Miller, J. R. *J. Phys. Chem.***1986**, *90*, 3673. e) Leland, B. A.; Joran, A. D.; Felker, P. M.; Hopfield, J. J.; Zewail, A. H.; Dervan, P. B. *J. Phys. Chem.***1985**, *89*, 5571.
3. a) Helms, A.; Heiler, D.; McClendon, G. *J. Am. Chem. Soc.* **1991,** *113*, 4325. b) Sakata, Y.; Tsue, H.; O'Neil, M. P.; Wiederrecht, G. P.; Wasielewski, M. R. *J. Am. Chem. Soc.* **1994**, *116*, 6904. c) Guldi, D. M.; Luo, C.; Prato, M.; Troisi, A.; Zerbetto, F.; Scheloske, M.; Dietel, M.; Bauer, W.; Hirsch, A. *J. Am. Chem. Soc.* **2001**, *123*, 9166.
4. a) Kroon, J.; Oliver, A. M.; Paddon-Row, M. N.; Verhoeven, J. W. *Rec, Trav. Chim. Pays-Ba*. **1988**, *107*, 509. b) Oliver, A. M.; Craig, D. C.; Paddon-Row, M. N.; Kroon, J.; Verhoeven, J.W. *Chem. Phys. Lett.* **1988**, *150*. c) Lawson, J. M.; Craig, D. C.; Paddon-Row, M. N.; Kroon, J.; Verhoeven, J. W. *Chem. Phys. Lett.* **1989**, *164*, 120.
5. a) Zeng, Y.; Zimmt, M. B. *J. Am. Chem. Soc.* **1991**, *113*, 5107. b) Oliver, A. M.; Paddon-Row, M. N.; Kroon, J.; Verhoeven, J. W. *Chem. Phys. Lett.* **1992**, *191*, 371.

6. Paddon-Row, M. N., Shephard, M. H. *J. Am. Chem. Soc*. **1997**, *119*, 5355.

7. a) Kumar, K.; Lin, Z.; Waldeck, D. H.; Zimmt, M. B. *J. Am. Chem. Soc.* **1996**,*118*, 243. b) Kumar, K,; Kurnikov, I.; Beratan, D.N.; Waldeck, D. H.; Zimmt, M. B. *J. Phys. Chem. A*. **1998**, *102*, 5529. c) Lokan, N. R.; Craig, D. C.; Paddon-Row, M. N. *Synlett*. 1999, 397. d) Lokan, N. R.; Paddon-Row, M. N.; Koeberg, M.; Verhoeven, J. W. *J. Am. Chem. Soc.* **2000**, *122*, 5075. e) Jolliffe, K. A.; Bell, T. D. M.; Ghiggino, K. P.; Langford, S. J.; Paddon-Row, M. N. *Angew. Chem. Int. Ed.* **1998**, 37, 915. f) Bell, T. D. M.; Jolliffe, K. A.; Ghiggino, K. P.; Oliver, A. M.; Shephard, M. J.; Langford, S. J.; Paddon-Row, M. N. *J. Am. Chem. Soc.* **2000**, *122*, 10661. g) Bell, T. D. M.; Ghiggino, K. P.; Jolliffe, K. A.; Ranasinge, M. G.; Langford, S. J.; Shephard, M. J.; Paddon-Row, M. N. *J. Phys. Chem. A*. **2002**, *106*, 10079. h) Smith, T. A.; Lokan, N.; Cabral, N.; Davies, S. R.; Paddon-Row, M. N.; Ghiggino, K. P. *J. Photochem. Photobiol. A: Chem.* **2002**, *149*, 55.

8. a) Napper, A. M.; Head, N. J.; Oliver, A. M.; Shephard, M. J.; Paddon-Row, M. N.; Read, I.; Waldeck, D. H. *J. Am. Chem. Soc*. **2002**, *124*, 10171. b) Napper, A. M.; Read, I.; Waldeck, D. H.; Head, A. N.; Oliver, A. M.; Paddon-Row, M. N. *J. Am. Chem. Soc.* **2000**, *122*, 5220. c) Liu, M.; Waldeck, D. H.; Oliver, A. M.; Head, N. J.; Paddon-Row, M. N. *J.Am.Chem.Soc.* **2004**, *126*, 10778.

9. Read, I.; Napper, A.; Kaplan, R.; Zimmt, M. B.; Waldeck, D. H. *J. Am. Chem. Soc.* **1999**, *121*, 10976.

10. Zimmt, M. B.; Waldeck, D. H. *J. Phys. Chem. A*. **2003**, *107*, 3580.

11. a) Oevering, H.; Verhoeven, J. W.; Paddon-Row, M. N.; Warman, J. M. *Tetrahedron*. **1989**, *45*, 4751. b) Oevering, H.; Paddon-Row, M. N.; Heppener, H.; Oliver, A. M.; Cotsaris, E.; Verhoeven, J. W.; Hush, N. S. *J. Am. Chem. Soc.* **1987**, *109*, 3258.

12. Wong, M. W. *Chem. Phys. Lett.* **1996**, *256,* 391.

13. Kulinowski, K.; Gould, I. R.; Myers, A. B. *J. Phys. Chem.* **1995**, *99*, 9017.

14. Matyushov, V.; Voth, G. A. *J. Chem. Phys.* **1999**, *111*, 3630.

15. Vath, P.; Zimmt, M. B.; Matyushov, D. V.; Voth, G. A. *J. Phys. Chem. B.* **1999**, *103*, 9130.

16. Birks, J. B. *Photophysics of Aromatic Molecules* (Wiley, NY, **1970**).

17. Berden, G.; Meerts, W. L.; Plusquellic, D. F.; Fujita, I.; Pratt, D. W. *J. Chem. Phys.* **1996**, *104*, 3935.

18. Martin, B.; Geneck, P.; Clark, T. *International Journal of Quantum Chemistry*. **2000**, *77*, 473.

19. Gray, C. G.; Gubbins, K. E. *Theory of Molecular Fluids, Vol. 1*; Clarendon Press: Oxford, **1984**

20. Ben-Amotz, D.; Willis, K. G. *J. Phys. Chem.* **1993**, *97*, 7736.

21. Matyushov, D. V.; Schmid, R. *J. Chem. Phys.* **1996**, *104*, 8627.

22. The pendant's polarizability was estimated from Ma, B.; Lii, J. H.; Allinger, N. L. *J. Comput. Chem.* **2000**, *21*, 813. The perpendicular polarizability, 5.7 $Å^3$ was used for the propyl group; the polarizability perpendicular to the phenyl axis was taken to be 7.4 $Å^3$; the average polarizability of toluene (12.30 $Å^3$), 2-methylpropene (8.29 $Å^3$), methane (2.56 $Å^3$) were used to approximate the polarizability of compound **1** – **3**. The change of the polarizability matches with the increasing size of the pendant groups in compound **1- 4**. This similar calculation predicts a shift in the reaction free energy amongst compound **1- 4**.

23. a) Matyushov, D. V. *Chem. Phys.* **1993**, *174*, 199. b) Matyushov, D. V. *Mol. Phys.* **1993**, *79*, 795.

24. Gaussian 03, Revision A.1, Frisch, M. J.; Trucks, G. W.; Schlegel, H. B.; Scuseria, G.E.; Robb, M. A,; Cheeseman, J. R.; Montgomery, Jr., J. A.; Vreven, T.; Kudin, K. N.; Burant, J. C.; Millam, J. M.; Iyengar, S. S.; Tomasi, J.; Barone, V.; Mennucci, B.; Cossi, M.; Scalmani, G.; Rega, N.; Petersson, G. A.; Nakatsuji, H.; Hada, M.; Ehara, M.;Toyota, K; Fukuda, R.; Hasegawa, J.; Ishida, M.; Nakajima, T.; Honda, Y.; Kitao, O.; Nakai, H.; Klene, M.; Li, X.; Knox, J. E.; Hratchian, H. P.; Cross, J. B.; Adamo, C.; Jaramillo, J.; Gomperts, R.; Stratmann, R. E.; Yazyev, O.; Austin, A. J.; Cammi, R.; Pomelli, C.; Ochterski, J. W.; Ayala, P. Y.; Morokuma, K.; Voth, G. A.; Salvador, P.; Dannenberg, J. J.; Zakrzewski, V. G.; Dapprich, S.; Daniels, A. D.; Strain, M. C.; Farkas, O.; Malick, D. K.; Rabuck, A. D.; Raghavachari, K.; Foresman, J. B.; Ortiz, J. V.; Cui, Q.; Baboul, A. G.; Clifford, S.; Cioslowski, J.; Stefanov, B. B.; Liu, G.; Liashenko, A.; Piskorz, P.; Komaromi, I.; Martin, R. L.; Fox, D. J.; Keith, T.; Al-Laham, M. A.; Peng, C. Y.; Nanayakkara, A.; Challacombe, M.; Gill, P. M. W.; Johnson, B.; Chen, W.; Wong, M. W.; Gonzalez, C.; Pople, J. A. Gaussian, Inc., Pittsburgh PA, 2003

25. Rothenfluh, D. F.; Paddon-Row, M. N. *J. Chem. Soc. Perkin Trans.* **1996**, *2*, 639.

26. Jordan, K. D.; Michejda, J. A.; Burrow, P. D. *J. Am. Chem. Soc.* **1976**, *98*, 1295.

27. a) Napper, A. M.; Read, I.; Kaplan, R.; Zimmt, M. B.; Waldeck, D. H. *J. Phys. Chem. A*. **2002**, *106*, 5288.b) Kaplan, R.; Napper, A. M.; Waldeck, D. H.; Zimmt, M. B. *J. Phys. Chem. A*. **2002**, *106*, 1917.

28. Koeberg, M.; de Groot, M.; Verhoeven, J. W.; Lokan, N. R.; Shephard, M. J.; Paddon-Row, M. N. *J. Phys. Chem. A*. **2001**, *105*, 3417. b) Goes, M. de Groot, M.; Koeberg, M.; Verhoeven, J. W.; Lokan, N. R.; Shephard, M. J.; Paddon-Row, M. N. *J. Phys. Chem. A*. **2002**, *106* , 2129.

3.0 CHAPTER THREE

Competing Electron Transfer Pathways in Hydrocarbon Frameworks: Short-Circuiting Through-Bond Coupling by Non-Bonded Contacts in Rigid U-Shaped Norbornylogous Systems Containing a Cavity-Bound Aromatic Pendant Group

This work has been published as S. Chakrabarti, D. H. Waldeck, A. M. Oliver, and M. Paddon-Row J. Am. Chem. Soc. 2007, 129, 3247-3256

This work explores electron transfer through non-bonded contacts in two U-shaped DBA molecules **1DBA** and **2DBA** by measuring electron transfer rates in organic solvents of different polarities. These molecules have identical U-shaped norbornylogous frameworks, twelve bonds in length and with diphenyldimethoxynaphthalene (**DPMN**) donor and dicyanovinyl (**DCV**) acceptor groups fused at the ends. The U-shaped cavity of each molecule contains an aromatic pendant group of different electronic character, namely *p*-ethylphenyl, in **1DBA**, and *p*-methoxyphenyl, in **2DBA**. Electronic coupling matrix elements, Gibbs free energy, and reorganization energy were calculated from experimental photophysical data for these compounds, and the experimental results were compared with computational values.

The magnitude of the electronic coupling for photoinduced charge separation, $|V_{CS}|$, in **1DBA** and **2DBA** were found to be 147 and 274 cm^{-1}, respectively, and suggests that the origin of this difference lies in the electronic nature of the pendant aromatic group and charge separation occurs by tunneling through the pendant group, rather than through the bridge. **2DBA**, but not **1DBA**, displayed charge transfer (CT) fluorescence in nonpolar and weakly polar solvents and this observation enabled the electronic coupling for charge recombination, $|V_{CR}|$, in **2DBA** to be made, the magnitude of which is ~ 500 cm^{-1}, significantly larger than that for charge separation. This difference is explained by changes in the geometry of the molecule in the relevant states; because of electrostatic effects, the donor and acceptor chromophores are about 1Å closer to the pendant group in the charge-separated state than in the locally excited state. Consequently the through-pendant-group electronic coupling is stronger in the charge-separated state – which controls the CT fluorescence process – than in the locally excited state – which controls the charge separation process. The magnitude of $|V_{CR}|$ for **2DBA** is almost two orders of magnitude greater than that in **DMN-12-DCV**, having the same length bridge as for the former molecule, but lacking a pendant group. This result unequivocally demonstrates the operation of the through-pendant-group mechanism of electron transfer in the pendant-containing U-shaped systems of the type **1DBA** and **2DBA**.

3.1 Introduction

Electron transfer reactions are a fundamental reaction type and are of intrinsic importance in biology, chemistry and the emerging field of nanoscience.[1] Donor-Bridge-Acceptor (DBA) molecules allow systematic manipulation of the molecular properties[2,3,4] and provide an avenue to address important fundamental issues in electron transfer. For example,

the U-shaped DBA molecules (in Scheme 1) hold the donor and the acceptor units at a fixed distance and conformation by a rigid hydrocarbon bridge and allow one to study the electron tunneling over a 5 to 10 angstrom distance scale. Placement of a pendant group in the cleft changes the electronic tunneling probability (electronic coupling magnitude) between the donor and acceptor, thereby changing the electron transfer rate. Previous work has shown that using an aromatic group as a pendant unit increases the electron tunneling probability, as compared to an aliphatic pendant,[5] but that different alkyl substituted phenyl groups have similar electronic couplings.[6]

The current work investigates the photoinduced electron transfer kinetics and charge-transfer emission spectra of the U-shaped DBA molecule **2DBA**, bearing a *p*-methoxyphenyl pendant group in different aromatic solvents, and compares it with the previously studied molecule **1DBA**, having an ethyl substituted phenyl group (Scheme 1). This allows us to explore how the electronic nature of the pendant group affects the electronic coupling. The molecules **1DBA** and **2DBA** have the same 1,4 diphenyl-5,8-dimethoxynaphthalene (**DPMN**) donor unit and 1,1-dicyanovinyl (**DCV**) acceptor unit connected through a highly curved bridge unit which holds the donor and the acceptor moieties at a particular distance and orientation. A pendant group is covalently attached to the bridge and occupies the space between the donor and the acceptor. It has been shown that the electron tunnels from the donor to the acceptor unit through the " *line-of-sight* " noncovalent linkage between the donor and the acceptor.[7] It has been established that the electron transfer mechanism in **1DBA** is non-adiabatic at high temperature and in solvents with rapid solvation responses. In this mechanistic limit, the electron tunneling probability is proportional to the square of the electronic coupling, $|V|^2$.

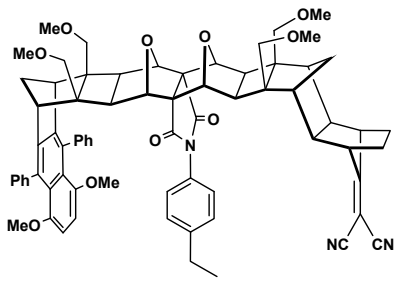

1DBA

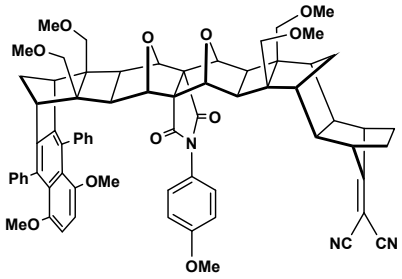

2DBA

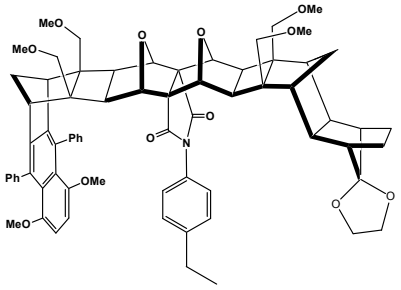

1DB

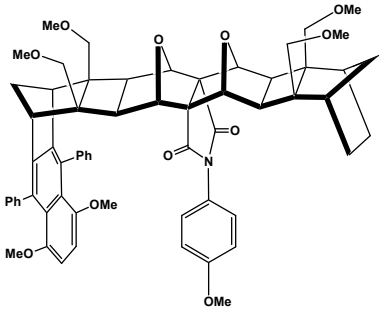

2DB

Scheme 1

The schematic energy diagram in Figure 3.1 shows an effective one-dimensional nuclear reaction coordinate. Two possible electron transfer regimes are distinguished by the strength of the electronic coupling $|V|$, the interaction between the reactant and the product states at the curve crossing. When the electronic coupling is weak $|V| << k_BT$, the reaction is nonadiabatic (dashed curve going through the dashed line at the curve crossing point in Figure 1) and the rate constant is proportional to $|V|^2$. In this regime, the system may move through the curve crossing region many times before the electronic state changes. The second regime is adiabatic electron transfer, where $|V| >> k_BT$ (dashed curves going through the solid line at the curve crossing point in Figure 1). In this limit, the electronic state change evolves as the nuclear motion proceeds; i.e., the strong coupling mixes the donor and acceptor states and the reaction proceeds along a single electronic state. A third regime is friction controlled electron transfer, in which the electronic coupling is weak but the polarization response of the solvent

is slow enough that nearly every passage through the crossing region results in a change of electronic state.

For the U-shaped molecules **1DBA**, the electronic coupling between the donor and acceptor moieties is weak enough that the electron transfer lies in the nonadiabatic limit. The semiclassical model for electron transfer in or near the nonadiabatic limit begins with a Fermi's Golden Rule expression for the transition rate; namely

$$k_{ET} = (2\pi / \hbar)\left|V\right|^2 FCWDS \qquad \textbf{1}$$

where $\hbar$ is Planck's constant divided by 2π, $\left|V\right|$ is the electronic coupling matrix element, and FCWDS is the Franck-Condon weighted density of states. The FCWDS term accounts for the probability that the system achieves a nuclear configuration in which the electronic state can change. The square of the coupling, $\left|V\right|^2$, is proportional to the probability of changing from the reactant state to the product state.

Previous work successfully applied the Golden Rule rate constant expression to **1DBA** with a single effective quantum mode,

$$k_{ET} = \frac{4\pi^2}{h} |V|^2 \frac{1}{\sqrt{4\lambda_o \pi k_B T}} \sum_{n=0}^{\infty} \exp(-S)\left(\frac{S^n}{n!}\right)\exp\left[-\frac{\left(\Delta_r G + \lambda_o + nh\nu\right)^2}{4\lambda_0 k_B T}\right] \qquad \textbf{2}$$

where λ_o is the solvent reorganization energy; $\Delta_r G$ is the reaction free energy; $S = \frac{\lambda_v}{h\nu}$ and λ_v is the internal reorganization energy. The $h\nu$ term is the average energy spacing of a single effective quantized mode frequency in the electron transfer reaction and is a characteristic of the donor and acceptor groups. The sum is performed over the vibrational states of the effective quantum mode.

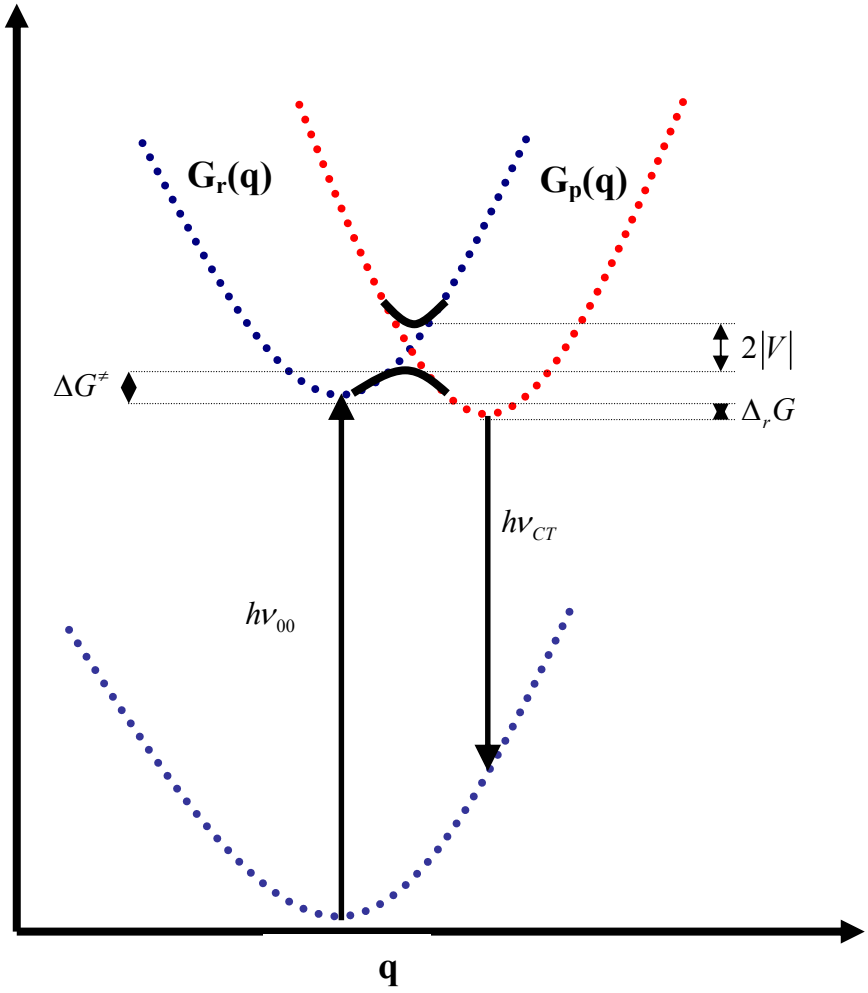

Figure 3.1 Diagram illustrating the adiabatic (proceeding along the solid line at the curve crossing point)-strong coupling and non-adiabatic (proceeding along the diabatic dashed line at the curve cross point)-weak coupling.

The quantities $h\nu$ and λ_v are determined primarily by the donor and acceptor groups and are insensitive to their separation distance. A previous analysis of charge transfer absorption and emission spectra in hexane solution for a DBA compound with the same donor and acceptor groups provides a reasonable estimate of these two parameters.[8] This analysis uses a value of 1600 cm^{-1} for the single effective quantized mode and 0.63 eV for the internal

reorganization energy λ_v . This effective frequency is comparable to typical carbon-carbon stretching frequencies in aromatic ring systems, such as the naphthalene. A detailed analysis of how this choice affects the $|V|$ extracted from the data and the impact of introducing a lower frequency mode, such as 1088 cm^{-1} for out-of-plane bending of the dicyanovinyl group, on the absolute magnitude of $|V|$ has been reported.[9]

In previous work, the three remaining parameters contained in the semiclassical rate expression (Equation 2), namely λ_0, $|V|$ and $\Delta_r G$, were determined by measuring the temperature dependence of k_{ET} and using Matyushov's molecular solvation model.[10,11] The reaction Gibbs energy $\Delta_r G$ of **1DBA** in toluene, mesitylene and *p*-xylene were experimentally measured from an analysis of the equilibrium between the locally excited state and the charge-separated state, and they were used to calibrate the molecular solvation model.[6,12] The solvation model, parameterized in this way, was also used to fit the photoinduced electron transfer reaction rate constant in **1DBA**. This rate constant model is used to analyze the photo-induced electron transfer behavior of **2DBA** and **1DBA** in different aromatic solvents and obtain the electronic coupling for charge separation ($|V_{CS}|$) in these two compounds. In marked contrast to **1DBA,** compound **2DBA** displayed charge transfer emission bands in nonpolar solvents, thereby providing the opportunity to determine the Gibbs energy, reorganization energy and the electronic coupling for charge recombination process ($|V_{CR}|$) in **2DBA**. The results obtained from the charge transfer emission band analysis are compared to the results obtained from the temperature dependent rate analysis and molecular solvation model analysis. These analyses show that the magnitude of the electronic coupling for charge separation; $|V_{CS}|$ for **2DBA** is greater than that for **1DBA**. We

also found that the strength of the electronic coupling for charge recombination; $|V_{CR}|$ from the charge-separated state to the ground state in **2DBA** is greater than that for charge separation, $|V_{CS}|$, for the same molecule. This finding may be attributed to differences in molecular geometry in the charge separated and ground state of these molecules.

3.2 Experimental

3.2.1 Steady-State and Time-Resolved Fluorescence Studies

Each sample was dissolved in the solvent at a concentration that gave a peak optical density of less than 0.2 at 330 nm. The solvent acetonitrile (99.9% HPLC) was purchased from Burdick & Jackson and used without further purification. The solvents toluene, mesitylene and *p*-xylene were fractionally distilled two times using a vigreux column under vacuum after being purchased from Aldrich. The purified fraction was used immediately in all the experiments. Nonpolar solvent methylcyclohexane (MCH) was purchased from Aldrich and was used without purification. Each solution was freeze-pump-thawed a minimum of five cycles.

Each sample was excited at 330 nm by the frequency-doubled cavity-dumped output of a Coherent CR599-01 dye laser, using DCM (4-dicyanomethylene-2-methyl-6-p-dimethylamino-styryl-4H-Pyran) dye, which was pumped by a mode locked Vanguard 2000-HM532 Nd:YAG laser purchased from Spectra-Physics. The dye laser pulse train had a repetition rate of 300 kHz. Pulse energies were kept below 1 nJ, and the count rates were kept below 3 kHz to prevent pile up effects. All fluorescence measurements were made at the magic angle, and data were collected until a standard maximum count of 10,000 was observed at the peak channel.

The steady-state and time-resolved fluorescence kinetics for **1DBA** and **2DBA** and their donor only analogues (compound **1DB** and **2DB**) were carried out in different solvents as a function of temperature (O.D ~ 0.10). The temperature ranged from 273 K to a high of 346 K. The experimental temperature was controlled by an ENDOCAL RTE-4 chiller and the temperature was measured using a Type-K thermocouple (Fisher-Scientific), accurate to within 0.1 ºC.

The instrument response function was measured using a sample of colloidal $BaSO_4$. The fluorescence decay curve was fit by a convolution and compare method using IBH-DAS6 analysis software. Independent experiments on individual donor only molecules at the measured temperatures, always a single exponential fluorescence decay, was used to determine the intrinsic fluorescence decay rate of the locally excited state. The DBA molecules, **1DBA** and **2DBA** have a small amount of donor only impurity. The measurement of the donor only molecule's fluorescence decay characteristic for each solvent and temperature allowed their contribution to be subtracted from the decay law of the DBA molecules**.** The decay law of **1DBA** in acetonitrile was a single exponential function, but in the weakly polar and nonpolar solvents toluene, mesitylene and *p*-xylene it was a double exponential function. The decay law for **2DBA** was single exponential in acetonitrile, and was nearly single exponential in the weakly polar and nonpolar solvents; i.e. the fit to a double exponential was superior but the dominant component exceeded 99% in all cases.

Fitting of the charge transfer emission spectra and rate constant to the semiclassical equation (Equation 2) was performed using Microsoft Excel 2003. In fits to a molecular solvation model the electronic coupling was treated as an adjustable parameter for each solute molecule and the reorganization energy at 295K was treated as an adjustable parameter for

each solvent type. The internal reorganization parameters were obtained from the charge transfer spectra of the similar compound [6] and were kept fixed since the solute has the same donor and acceptor group. The reaction Gibbs energy for **1DBA** was obtained from the experimental data except in the polar solvent acetonitrile. The experimental $\Delta_r G$ data were used to parameterize the molecular solvation model and predict the $\Delta_r G$ for **1DBA** in acetonitrile and the $\Delta_r G$ for **2DBA**. The charge transfer emission spectral analysis of **2DBA** was also used to determine the Gibbs energy, electronic coupling and the reorganization energy in different aromatic solvents.

3.3 Results

3.3.1 Emission Spectroscopy:

Figure 3.2 shows the steady-state emission spectra of **1DBA** and **2DBA** recorded in the polar solvent acetonitrile, the weakly polar solvent toluene, and the nonpolar solvents mesitylene and p-xylene. The spectral features of the DBA molecules, **1DBA** and **2DBA,** are dominated by the 1,4-dimethoxy-5,8-diphenylnaphthalene donor unit with two dominant transition bands in the UV region assigned to $^1A \rightarrow {}^1L_b$, and the $^1A \rightarrow {}^1L_a$ transitions.[6] For **1DBA** the steady-state emission spectra in weakly polar and nonpolar solvents are very similar (panel A), whereas the polar solvent Acetonitrile changes the relative intensity of the two peaks and shifts them to the red. A similar emission spectrum was observed for **2DBA** in acetonitrile.

For **2DBA** the steady state spectra in weakly polar and nonpolar solvents display three peaks (panel B) rather than the two peaks observed for **1DBA** (panel A). The locally excited (LE) emission bands for **2DBA** have the same position as those for

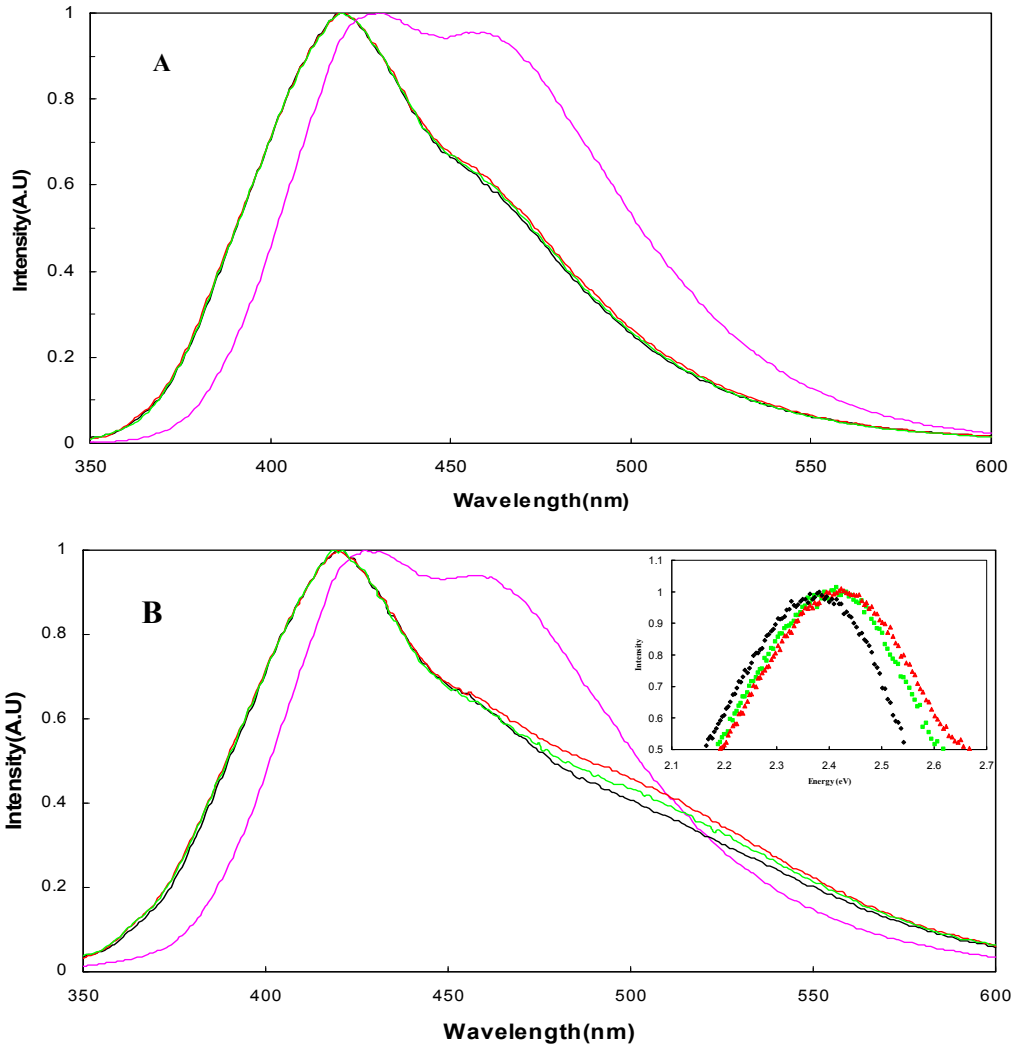

Figure 3.2 Steady-state emission spectra of compound **2DBA** (panel B) and compound **1DBA** (panel A) in acetonitrile (pink), toluene (black), mesitylene (red) and p-xylene (green). The inset of panel B shows the difference spectra of **2DBA** and **2DB**.

1DBA in all these solvents, but a new spectral band is evident to the red. This weak red band shifts further to the red with increasing solvent polarity (see the inset of panel B, which shows the difference of the spectra for **2DBA** and **2DB** in the different solvents). This emission band is not observed for **2DBA** in the most polar solvent acetonitrile. These

properties indicate that this emission is a charge-transfer ($CS \rightarrow S_0$) emission band.[12,13] Difference spectra of **2DBA** and **2DB** in different solvents are shown in the inset of figure 3.2 (also see Fig. 3.3) and were used to calculate values of $\bar{\nu}_{max}$. The solvent parameters and the resulting $\bar{\nu}_{max}$ values are listed in Table 3.1.

We have analyzed the solvent dependence of the CT fluorescence maximum of compound **2DBA** in terms of the well-known Lippert-Mataga relation (equation 3).[14,15] The frequency of the CT emission band's maximum intensity is given by

$$\bar{\nu}_{max} = \left[\frac{-2\Delta\vec{\mu}^2}{hca^3}\right]\Delta f + \bar{\nu}^0_{max} \qquad \textbf{3}$$

where $\Delta f = \left[(\varepsilon - 1)/(2\varepsilon + 1)\right] - \left[(n^2 - 1)/(4n^2 + 2)\right]$, $\bar{\nu}_{max}$ is in cm^{-1}; $\bar{\nu}^0_{max}$ is the emission maximum for $\Delta f = 0$, a is the effective radius of a spherical cavity that the donor-acceptor molecule occupies in the solvent, $\Delta\vec{\mu} = \left|\vec{\mu}_{CS} - \vec{\mu}_{S_0}\right|$ is the difference in dipole moments of the charge separated state and the ground state, h is the Planck constant, c is the velocity of light in vacuum, ε is the solvent dielectric constant; and n is the refractive index of the solvent. This result also incorporates the polarizability of the solute, which was taken equal to $\frac{1}{3}a^3$. The solvent parameter, Δf, depends on the static dielectric constant (ε_S) and refractive index (n) of the solvent, and it increases with increasing solvent polarity (see Table 3.1 and also Fig.3.3). The Δf parameter quantifies the solvent's ability to produce a macroscopic polarization in response to the newly formed charge distribution of the charge separated state. Figure 3.3 shows a Lippert-Mataga plot for **2DBA** in the four solvents, where

Table 3.1 Charge Transfer (CT) Emission Maxima ($\bar{\nu}_{max}$) of 2DBA in different solvents at 295 K and Solvent Parameters, *n*, ε_S (295K) and Δf for each solvent

Solvent	n [a]	ε_S [b]	Δf	$\bar{\nu}_{max}$ (cm^{-1})
Toluene	1.494	2.378	0.13	19157
Mesitylene	1.496	2.271	0.12	19267
p-Xylene	1.493	2.265	0.11	19417
MCH	1.423	2.000	0.10	19457

[a,b] Zimmt. M. B; Waldeck, D. H. *J. Phys. Chem. A* **2003**, *107*, 3580.

$\bar{\nu}_{max}$ of the charge transfer band decreases as a function of increasing polarity, or Δf. A reasonable linear fit to the data provides a slope of -10500 cm^{-1}. To estimate $\Delta\vec{\mu}$ from this slope and Equation 3, a cavity radius, *a*, of 7.66 Å was used. This value was chosen because previous work found it as a best fit to the $\Delta_r G$ data of **1DBA** to the molecular solvation model. Solving equation 3 for $\Delta\vec{\mu}$ gives a value of 22 D for the difference between the charge-separated state and the ground state dipole moments. Using 5.75 D for the ground state dipole moment[5] and assuming that the dipoles are collinear, the dipole moment of the charge separated state is ~28 D, which is close to the dipole moment of the charge separated state used in the molecular solvation model analysis. This value is also in good agreement with the HF/3-21G calculated value of 28.6 D for a simulacrum of the charge separated state of **1DBA** (the dipole moments of the charge-separated states of **1DBA** and **2DBA** should be similar).

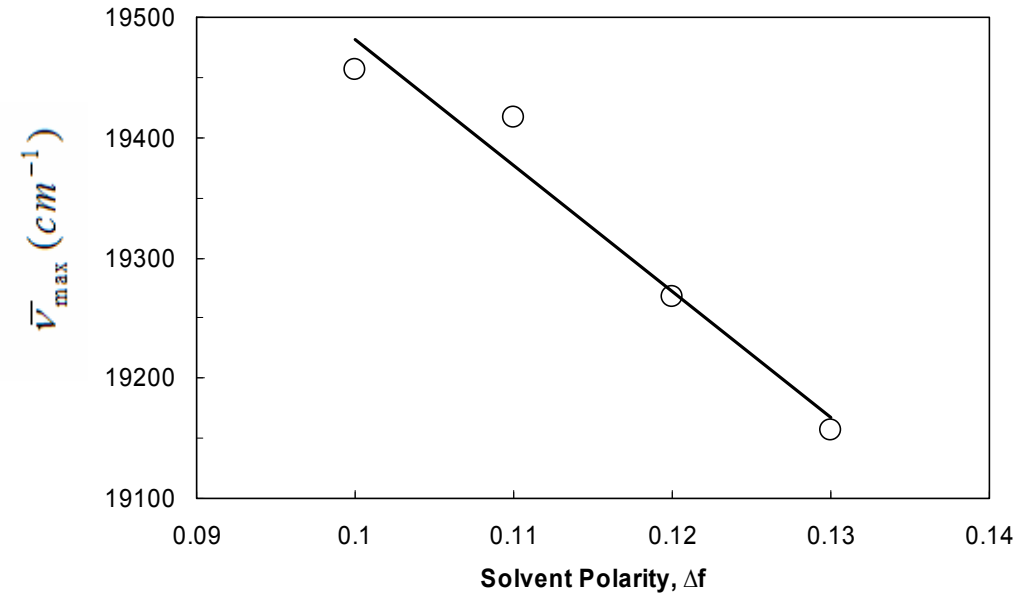

Figure 3.3 Lippert-Mataga plot for the charge transfer (CT) emission band of compound **2DBA** in different solvents.

Assuming that a unit charge is transferred, r_{dip} is equal to 5.8 Å for μ_{CS} of 28 D (i.e., the charge transfer distance, r_{dip} can be estimated from the relation $r_{dip} = \mu_{CS} / e$),. This value is smaller than the UHF/3-21G calculated center-to-center distance of 8.7 Å between the **DPMN** donor and the **DCV** acceptor groups in the charge-separated state geometry of a cognate of **2DBA** (*vide infra*). Although the reason for this difference remains unclear, it may reflect the fact that the negative and positive charges are delocalized over the respective **DCV** and **DPMN** groups (as predicted by UHF/3-21G calculations). Consequently calculation of r_{dip} assuming a point charge model may not be appropriate (The closest **DCV-DPMN** distance obtained from UHF/3-21G calculation in the charge separated state of the aforementioned cognate is 6.8 Å, between a **DCV** nitrogen and a **DPMN** CH ring carbon atom).

3.3.2 Analysis of Charge-Transfer Emission Spectra of 2DBA to obtain $\Delta_r G$ and λ_0

The charge recombination driving force for **2DBA** was estimated by simulation of the charge transfer emission lineshape predicted by Marcus[16]; i.e.

$$I_{emission}(\nu_{CS}) = \sum_j \frac{e^{-S} S^j}{j!} . \exp\left[-\frac{(jh\nu + \Delta G_{rec} + \lambda_0 + h\nu_{CS})^2}{4\lambda_0 kT} \right] \qquad \textbf{4}$$

Figure 3.4 compares the experimental difference spectra to simulated spectra predicted by equation 4 in mesitylene (panel A) and *p*-xylene (panel B) respectively. Such fits provide estimates of $\Delta_r G(CS \rightarrow S_0)$ and other electron-transfer parameters included in the semiclassical model: λ_0, λ_V, $h\nu$, and $\Delta G_r(CS \rightarrow S_0)$. The Gibbs energy

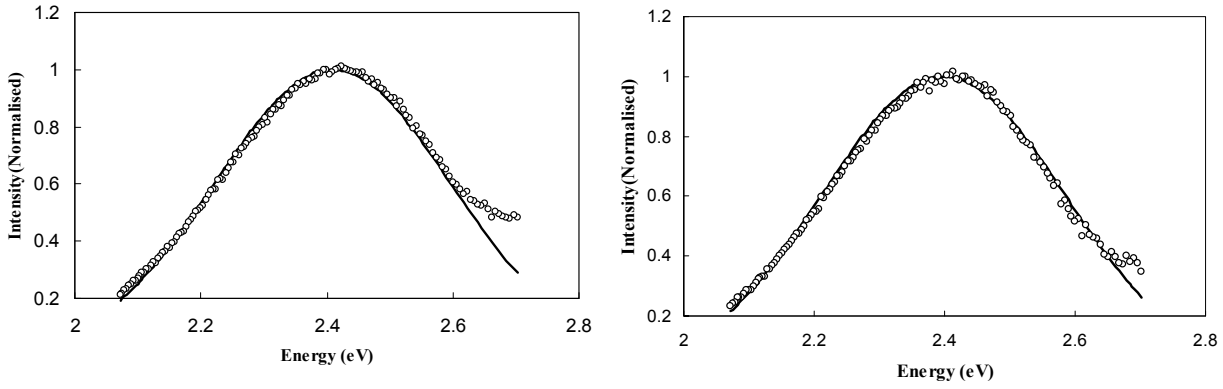

Figure 3.4 Experimental (o) and calculated (solid lines) charge-transfer emission spectra of **2DBA** in mesitylene (panel A) and in p-xylene (panel B). These spectra were calculated using λ_V =0.63eV, $\bar{\nu}$ = 1600 cm^{-1}, λ_0 =0.68 eV (for mesitylene and *p*-xylene) and $\Delta_r G(CS \rightarrow S_0)$ = -3.288 eV (mesitylene) and -3.277 eV (*p*-xylene).

$\Delta_r G(LE \rightarrow CS)$ can be obtained from $\Delta_r G(LE \rightarrow CS) = -\Delta G_r(CS \rightarrow S_0) - E_{00}$, where E_{00} is the excited state energy of the donor unit. Because different combinations of the four

parameters can accurately reproduce the experimental line shapes, the fitting parameters were constrained in the following way. The fits in fig. 3.4 were done with a constant value 0.63 eV for the λ_V parameter and a value of $\bar{\nu}$ ~1600 cm^{-1}; these values were used previously for similar molecules and were chosen for consistency with earlier work. Only λ_0 and $\Delta_r G(CS \rightarrow S_0)$ were adjusted in different solvents to optimize the fit.

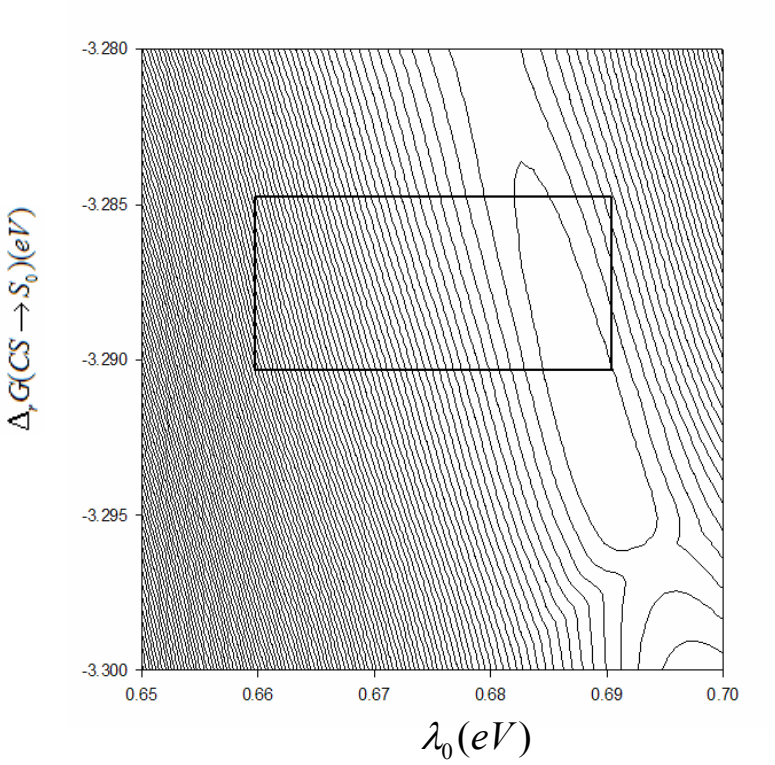

Figure 3.5 Contours of $\chi^2 / \chi_{Min}{}^2$ are shown for **2DBA** in mesitylene. Outside the rectangular region the fits to the charge transfer spectra visibly deviate from the experimental data for $\chi^2 / \chi_{Min}{}^2 \geq 5$

Figure 3.5 illustrates how the charge transfer emission fit quality, as measured by, $\chi^2 / \chi_{Min}{}^2$ changes with outer sphere reorganization energy (λ_0) and $\Delta_r G(CS \rightarrow S_0)$

values used in the fitting. The χ_{Min} represents the smallest value of χ obtained from the fitting. The boxed region in this case identifies the range for λ_0 and $\Delta_r G(CS \rightarrow S_0)$ over which the difference between the experimental and theoretical charge transfer emission spectra deviate visibly with a change of the $\chi^2 / \chi_{Min}{}^2 \geq 5$. Table 3.2 lists the different values of $\Delta_r G(CS \rightarrow S_0)$ and λ_0 obtained from the CT spectral fitting for different solvents. The line-shape derived estimates of λ_0 increases with increasing solvent dielectric constant.

Table 3.2 $\Delta_r G$ and λ_0 ; determined from the charge transfer emission spectra, using E_{00} = 3.40 eV [a]

Solvent	CT maxima (eV)	ε	$\Delta G(CS \rightarrow S_0)$ (eV)	λ_0 (eV)
Toluene	2.38	2.37	-3.26±0.04	0.69±0.02
Mesitylene	2.39	2.27	-3.29±0.01	0.68±0.01
p-Xylene	2.41	2.27	-3.28±0.02	0.68±0.01

[a,] The E_{00} was obtained from the mirror point between absorption and emission spectra in mesitylene for compound **2DBA**.

In previous work $\Delta_r G(LE \rightarrow CS)$ for **1DBA** was determined directly from the kinetic data by fitting the experimental data to the molecular solvation model for toluene, mesitylene and *p*-xylene and that model was calibrated to predict the free energy for the polar solvent

acetonitrile.[6] In that analysis the radius of the solute was optimized and found to be 7.66 Å; the ground state dipole moment was 5.75 D; and the excited state dipole moment was 28.64 D. The same analysis was carried out to determine the $\Delta_r G(LE \rightarrow CS)$ for **2DBA**. Because the fluorescence lifetime of **2DBA**

Table 3.3 $\Delta_r G(LE \rightarrow CS)$ **values for 1DBA and 2DBA in different solvents**

Solvent	Compound	$\Delta_r G$ (model) (eV)	$\Delta_r G$ (expt.) (eV)
Toluene	**1DBA**	-0.12	-0.12[a]
Mesitylene	**1DBA**	-0.09	-0.08[a]
p-Xylene	**1DBA**	-0.09	-0.09[a]
Acetonitrile	**1DBA**	-0.55	
Toluene	**2DBA**	-0.11	-0.14[b]
Mesitylene	**2DBA**	-0.08	-0.11[b]
p-Xylene	**2DBA**	-0.06	-0.12[b]
Acetonitrile	**2DBA**	-0.54	

[a] Obtained from Kinetic analysis [6]

[b] Obtained from CT emission spectra fitting

was nearly single exponential (~99% or greater) at all the temperatures and in all the solvents, the reaction Gibbs energy could not be experimentally determined for **2DBA** using the kinetic rate data. This indicates that the Gibbs energy for **2DBA** is more negative than -0.13 eV and it

can not be determined directly form the experiment. This observation implies that $\Delta_r G$ for **2DBA** is more negative than that for **1DBA.** The charge transfer fit parameters of **2DBA** in different solvents were used to determine the $\Delta_r G(LE \rightarrow CS)$ for **2DBA.** Table 3.3 compares the $\Delta_r G$ of **1 DBA** and **2DBA.** The Gibbs energy becomes more negative as the solvent becomes more polar, progressing from mesitylene and p-xylene, which have the least negative $\Delta_r G(LE \rightarrow CS)$, to toluene which is more negative, and finally to acetonitrile which is the most negative. Table 3.3 also reveals a reasonable agreement between the Gibbs energy for **2DBA** obtained from the charge transfer emission spectral fitting and that predicted from the molecular solvation model.

3.3.3 Kinetic analysis

With the reaction free energy and the internal reorganization energy parameters from the previous studies, it is possible to fit the temperature dependent rate constant data and extract the electronic coupling $|V_{CS}|$ and the solvent reorganization energy λ_0 for the charge separation process. $|V_{CS}|$ is treated as a temperature independent quantity, whereas the solvent reorganization energy has a temperature dependence because the solvation is temperature dependent. The temperature dependence of the solvent reorganization energy was predicted from the molecular solvation model and the best fit was used to extract the solvent reorganization energy at 295 K, as described previously. The fit of the temperature dependent rate constant data was used to determine the electronic coupling $|V_{CS}|$ and λ_0 (295 K), listed in Table 3.4. Figure 3.6 shows fits of the experimental rate constant to the model for compound **1DBA** and **2DBA** in mesitylene and acetonitrile. The rate data in toluene and p-

xylene behave similarly. The reverse order of the electron transfer rate for **1DBA** and **2DBA** in mesitylene and acetonitrile can be explained by their different reorganization energy value.[1]

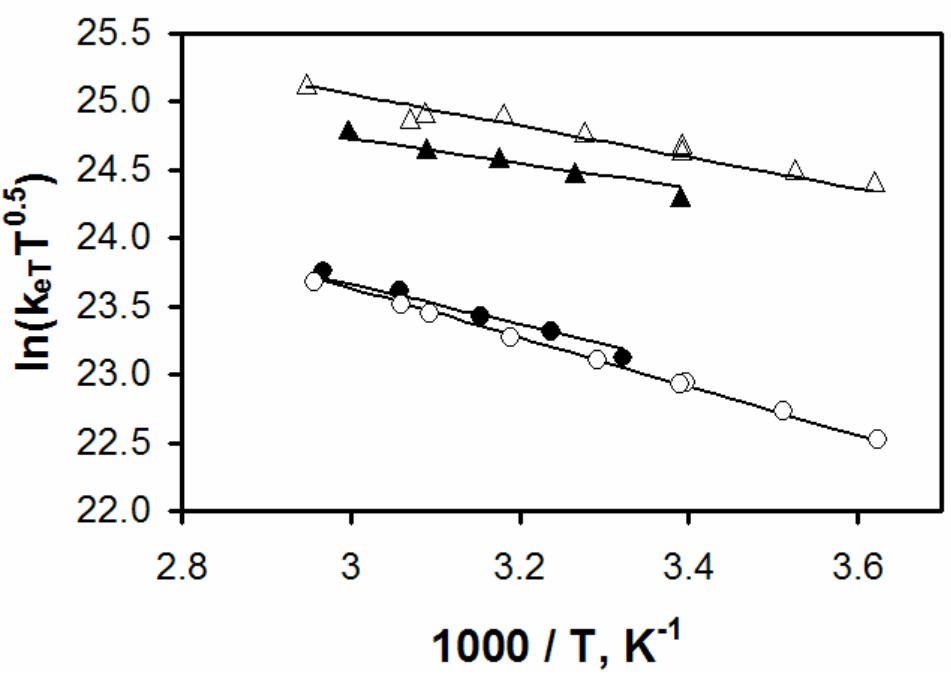

Figure 3.6 Experimental rate constant data are plotted versus 1/T, for **1DBA** in mesitylene (▲) and acetonitrile (●), and for **2DBA** in mesitylene (Δ) and in acetonitrile (○). The line represents the best fits to semiclassical equation.

Table 3.4 lists the solvent reorganization energies, λ_0, at 295 K and electronic couplings $|V_{CS}|$ that are obtained for the four solvents by fitting to the temperature dependent rate constant expression obtained from semiclassical model. In addition, the electronic coupling, $|V_{CR}|$, for the charge recombination in **2DBA** was computed using the charge transfer emission spectra (Table 3.4), as described in the next section

[1] The difference of reorganization energy between **1DBA** and **2DBA** is 0.09 eV in mesitylene but in acetonitrile the difference is 0.13 eV. This higher difference of λ_0 is responsible for reversal of the order.[17]

Table 3.4 Best fit of electronic coupling and reorganization energy (from the kinetic fit and from CT emission spectra) for 1DBA and 2DBA.

Compound	Solvent	$\lvert V_{CS}\rvert$ (cm^{-1}) [a]	$\lvert V_{CR}\rvert$ (cm^{-1}) [b]	λ_0 (eV) [c]	λ_0 (eV) [d]
	Toluene	147		0.70	
	Mesitylene	147		0.66	
1DBA	p-xylene	147		0.67	
	Acetonitrile	147		1.50	
	Toluene	274	467	0.79	0.69
	Mesitylene	274	453	0.75	0.68
2DBA	p-xylene	274	512	0.72	0.68
	Acetonitrile	274		1.63	

[a] Coupling obtained from the best fit rate data

[b] Coupling obtained form the CT emission spectral analysis using the distance 5.8 Å

[c] Reorganization energy obtained from best fit rate data

[d] Reorganization energy obtained from the CT emission spectra fit.

.

3.3.4 Calculation of the electronic coupling for charge recombination in 2DBA from CT emission spectra

Experimental evidence for a relatively close and solvent independent donor-acceptor distance in the charge separated state was obtained from the radiative rate constant (k_r) for the charge transfer fluorescence, which can be calculated from the fluorescence lifetime (τ) and quantum yield of the charge transfer fluorescence (Φ) via $k_r = \frac{\Phi}{\tau}$. It has been shown that the radiative rate constant (in s^{-1}) can be expressed by equation 5.[18]

$$k_r = (0.714 \times 10^{-5}) n^3 R^2 \left|V_{CR}\right|^2 \bar{\nu}_{CT} \qquad \mathbf{5}$$

In equation 5, R is the interchromophore distance in Å, n is the refractive index and $\left|V_{CR}\right|$ is the electronic coupling matrix element in cm^{-1}. Using the value of 5.8 Å for R, obtained from the Lippert-Mataga plot, the electronic coupling values tabulated in Table 6. The electronic coupling for **2DBA**, $\left|V_{CR}\right|$ is approximately 500 cm^{-1}. The above findings, from the temperature dependent rate data analysis, show that the electronic coupling for charge separation in **2DBA** is stronger than **1DBA**, by a factor of 1.9.

Table 3.4 shows that for **2DBA** the λ_0 (295 K) values obtained from the CT emission spectra fitting is less than the value obtained from the kinetic rate data. To analyse the error in the kinetic rate data fit, we have used different $\Delta_r G$ (295 K) values ranging from 0.06 eV to 0.10 eV in the fit to see how λ_0 (295 K) changes.

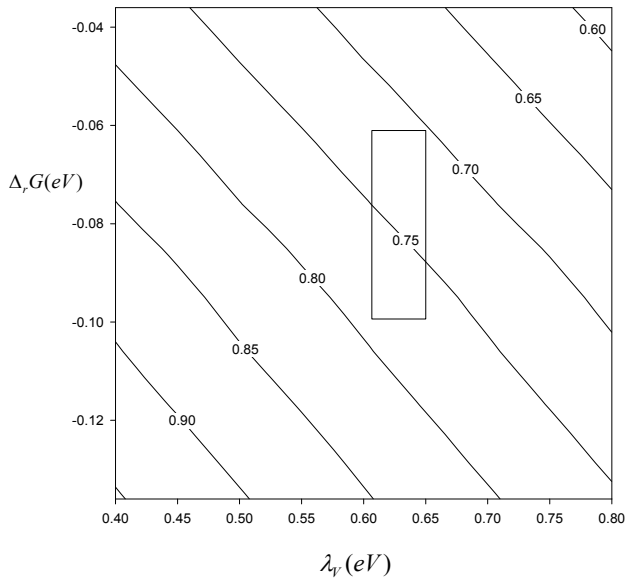

Figure 3.7 Contour plot of λ_0 (295 K) for 2DBA in mesitylene versus the assumed values of λ_V and $\Delta_r G$ (295 K). The constant contour lines are in units of eV. The box outlines the region defined by the estimate of λ_V (0.60-0.65 eV) and $\Delta_r G$ (295 K) ± 0.02 eV.

Figure 3.7 uses contour plots to illustrate the correlation between the λ_0 parameter and two of the other parameters $\Delta_r G$ (295 K) and λ_V. The box in figure 3.7 encloses a region corresponding to ±0.02 eV about the $\Delta_r G$ (295 K) calculated using the molecular solvation model and λ_V in the range of 0.60-0.65 eV. This limit provides a reasonable value of λ_0 ranging from 0.70- 0.79 eV obtained from kinetic rate data analysis.

3.3.5 Theoretical Calculations

A fully optimized gas phase geometry of the ground state of **2DBA** was obtained at the B3LYP/6-31G(d) level and is depicted in Figure 3.8a and 3.8b. The complete geometry optimization was carried out using Gaussian 03.[19]

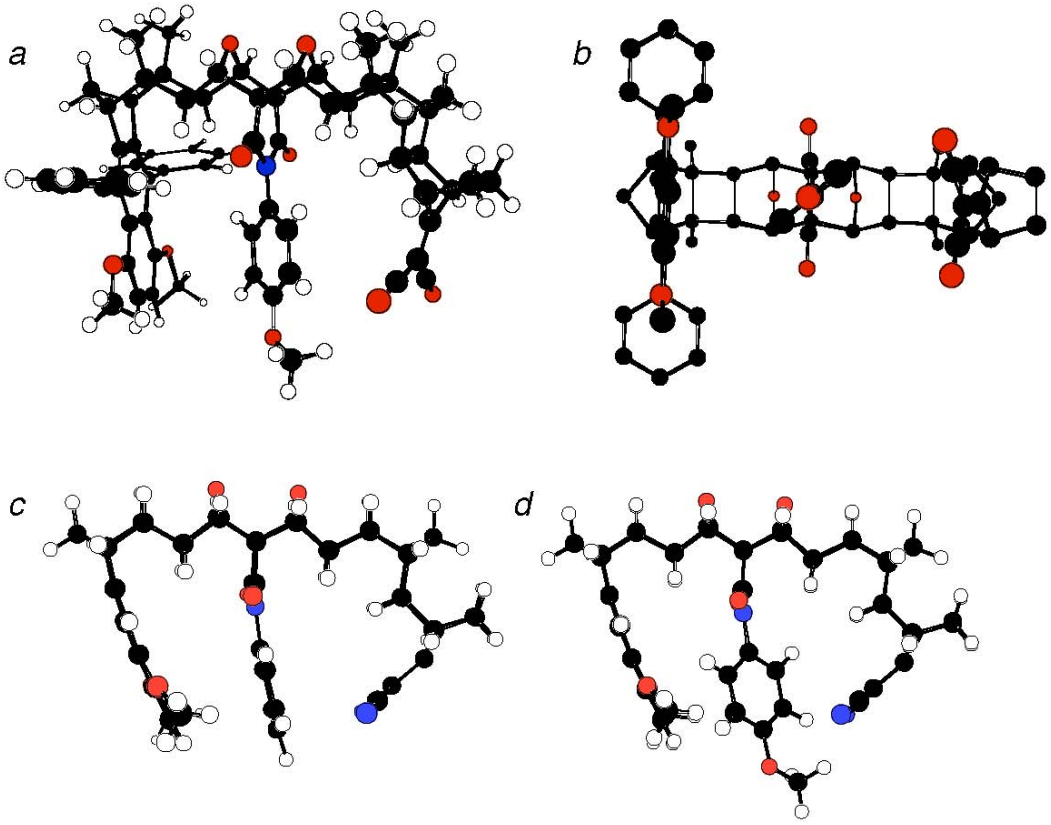

Figure 3.8 (a) B3LYP/6-31G(d) optimized ground state geometry of **2DBA**. (b) As for (a) but looking along the major axis of the pendant *p*-methoxyphenyl group; the hydrogen atoms having been omitted for clarity. (c) UHF/3-21G optimized geometry of the ^{1}A" charge-separated state of a simplified model for **1DBA**, referred to as **1DBA'** (i.e. **1DBA**, but with phenyl pendant group in place of *p*-ethylphenyl and with the dimethoxynaphthalene group in place of **DPMN**). The geometry was constrained to C_S symmetry. (d) Simulated geometry for the charge-separated state for **2DBA**, in which the bridge has the same geometry as that calculated for the charge-separated state of **1DBA'** but with the *p*-methoxyphenyl pendant twisted 48^{o} out of the plane of the imide ring.

The optimized ground state structure of **2DBA** is very similar to that computed for **1DBA** and various pendant-phenyl substituted cognates.[5,6,20] The pendant methoxyphenyl ring

is twisted 48° with respect to the plane of the imide ring, the closest distance between the **DPMN** and **DCV** chromophore units is 9.2 Å which is between a CH carbon atom of the former and an N atom of the latter, and the closest distances between the pendant group and the **DPMN** and **DCV** chromophore units are 3.8 - 3.9 Å (c.f. 47°, 9.4 Å and 3.8 - 3.9 Å, respectively for the compound having methylphenyl as pendant group).

Because of the large sizes of these U-shaped molecules, it was not feasible to compute the optimized geometry of the locally excited state of **2DBA**, which is relevant to the mechanism of photoinduced charge separation, using the CIS method. The strong similarities found between the ground state geometries of **1DBA** and **2DBA** most likely holds for the locally excited states of these systems. Consequently, the greater magnitude of the electronic coupling for photoinduced charge separation in **2DBA**, compared to **1DBA**, is unlikely to be caused by structural differences in the two systems. Two important classes of virtual ionic states namely $^{+}$DPMN-pendant^{-} and $^{+}$pendant-DCV^{-} contribute to the coupling for photoinduced electron transfer in these systems. However, for charge transfer from the locally excited state of the donor to the acceptor, the former ionic state is expected to be more important. Comparison with experimental data on monosubstituted benzenes suggests that the pendant groups' electron affinities (EA) (anisole EA= -1.09 eV and ethyl benzene EA= -1.17 eV[21]) are similar, but that **2DBA** should have a larger electronic coupling than **1DBA**. It may be that the second virtual ionic state $^{+}$pendant-DCV^{-} contributes, when the pendant group has a low ionization potential (IP) value. The IP for toluene and anisole are 8.83 and 8.39 eV respectively.[22] Whether one coupling mechanism dominates over the other, could, in principle, be resolved by studying a U-shaped system in which an electron withdrawing group is attached to the pendant aromatic ring at position 3 or 4. Unfortunately, all attempts to

synthesize such a system have so far met with failure.

Earlier UHF/3-21G gas phase calculations of charge-separated states revealed remarkable electrostatically driven changes in their geometries, compared to their ground state structures.[5,18,23] Regarding the U-shaped systems discussed in this paper, we were successful only in optimizing, at the UHF/3-21G level, the geometry of the charge-separated state of a cognate of **1DBA**, termed as **1DBA'**, in which the pendant group was phenyl and the dimethoxynaphthalene group, **DMN**, was the donor moiety (in place of **DPMN**). Furthermore, the geometry of the charge-separated state of **1DBA'** was constrained to possess C_S symmetry;[24] within this constraint, the electronic state of this charge-separated state is ^{1}A", thereby preventing collapse of the wavefunction to the ^{1}A**'** ground state during the geometry optimization.[23,24] The resulting optimized gas phase structure for the charge-separated state of **1DBA'** is shown in Fig. 3.8c, a particularly noteworthy feature being the strong pyramidalization of the **DCV** anion radical towards the **DPMN** cation radical whose rings are slightly bent, in the direction of the **DCV** moiety. Due to the imposed C_S symmetry constraint, the phenyl pendant group is roughly parallel to the imide ring. Such a conformation, in which the phenyl ring eclipses the imide carbonyl groups should be unstable, as it is in the ground state, and the relaxed phenyl-imide conformation in the charge separated state of **1DBA'** should resemble that computed for the ground state structure, i.e. with the phenyl ring twisted 48^0 with respect to the imide plane as depicted by the simulated structure in Fig. 3.8d.

The calculated UHF/3-21G dipole moment of **1DBA'** is 28.6 D[5] which is in good accord with the value of 28 D for **2DBA,** determined from the Lippert-Mataga plot. Also the distance between the centroids of the **DPMN** and **DCV** chromophore units in **1DBA'** was calculated to be 8.7 Å, although the closest contact between non-hydrogen atoms of the donor

and acceptor groups is only 6.8 Å. The closest non-hydrogen atom contacts between the pendant group in the charge-separated state of **1DBA'** and the **DMN** and **DCV** chromophores are 3.6 and 3.2 Å respectively and these are even smaller in the more reasonable structure depicted in Fig. 3.8d: 2.65 and 2.7 Å respectively. The significantly smaller chromophore-pendant contacts of 2.7 Å in the simulated charge-separated state (Fig.8d), compared to 3.8 Å in the ground state of **1DBA** (Fig. 3.8a) could well be responsible for the observed stronger electronic coupling of 453-512 cm^{-1} for charge recombination compare to charge separation, which is 274 cm^{-1} in **2DBA**.

3.4 Discussion

The electron transfer rate constant from the locally excited state of **DPMN** to **DCV** for **2DBA** is larger than that for **1DBA** in toluene, mesitylene and *p*-xylene solvents. This increase arises from the greater magnitude of the electronic coupling in **2DBA,** as found from analysis of the temperature dependent rate data. It is important to note that the electronic coupling obtained from the CT emission is the coupling between the charge separated state and the ground state (the charge recombination pathway) whereas the kinetic rate data provide the coupling between the locally excited state and the charge separated state. Whereas **1DBA** does not display charge transfer fluorescence, **2DBA** does, presumably because the magnitude of $|V_{CR}|$ for **2DBA** is substantially larger than for **1DBA**. Although the CT emission for **2DBA** is also not observed in acetonitrile, it is likely due to the non-radiative charge recombination

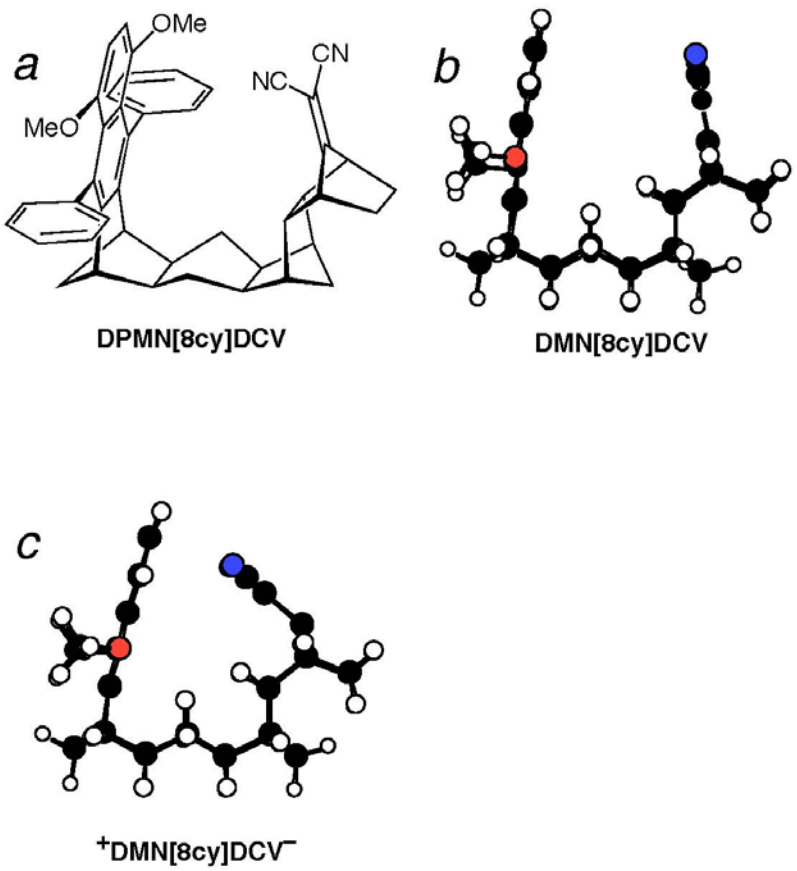

Figure 3.9. (a) Schematic of **DPMN[8cy]DCV**. (b) HF/3-21G optimised ground state structure of the cognate **DMN[8cy]DCV**, bearing the dimethoxynaphthalene donor in place of **DPMN**, and (c) UHF/3-21G optimised geometry of the ^{1}A" charge-separated state of **DMN[8cy]DCV**, constrained to C_S symmetry.

decay being rapid in this solvent. As the solvent polarity increases the driving force for charge recombination decreases and, within the context of the Marcus "inverted region" the rate of the non-radiative recombination process increases and becomes the dominant pathway in acetonitrile, quenching the charge transfer emission. The same effect was observed by Koeberg et al. in their study of the 8-bond U-shape system **DPMN[8cy]DCV** (Fig. 3.9a), which exhibited charge transfer fluorescence in weakly polar solvents but not in polar ones.[18]

It is illuminating to compare the strength of the electronic coupling for CT fluorescence of ~500 cm^{-1} for **2DBA** with the value of 374 cm^{-1} (in benzene) for **DPMN[8cy]DCV**.[18] Both systems possess similar U-shape configurations, but the latter lacks a pendant group. Even though the **DPMN** and **DCV** chromophores are connected by *twelve* bonds in **2DBA**, compared to only *eight* bonds in **DPMN[8cy]DCV** (see Fig. 3.9a), the electronic coupling strength for CT fluorescence in the former molecule is larger than that for the latter. This observation is best understood if the charge recombination (and charge separation) in **2DBA** takes place by the through-pendant mechanism, rather than by a through-bridge (i.e. through-bond) mechanism. The charge recombination mechanism in **DPMN[8cy]DCV** is discussed below.

An even more convincing demonstration of the extraordinarily large strength of the electronic coupling element for CT fluorescence in **2DBA** is to compare its magnitude (~500 cm^{-1}) with those for CT fluorescence in the series **DMN-*n*-DCV**, in which the donor and acceptor chromophores are connected to rigid norbornylogous bridges, *n* bonds in length, which possess the all-*trans* configuration.[8a] This all-*trans* configuration in **DMN-*n*-DCV** guarantees that electron transfer in these molecules takes place by the through-bond mechanism.[2C]

DMN-*n*-DCV

DMN-12-DCV

Extrapolating the experimental $|V_{CR}|$ values for the 4-, 6-, 8- and 10-bond systems leads to a predicted $|V_{CR}|$ value of ~6 cm^{-1} for the 12-bond system **DMN-12-DCV**. Because the 12-bond norbornylogous bridge in **2DBA** possesses *two* cisoid kinks, through-bridge-mediated electronic coupling in this molecule should be significantly *weaker* than that through the all-*trans* bridge in **DMN-12-DCV**.[2b,2c] In fact $|V_{CR}|$ for **2DBA** is ~90 times stronger than that estimated for **DMN-12-DCV**. Clearly, charge recombination from the charge- separated state of **2DBA** is not taking place by a through-bridge-mediated mechanism. These findings, together with the observation that the strength of the electronic coupling for photoinduced charge separation for **2DBA** is greater than that for **1DBA** leads to the unequivocal conclusion that charge separation and charge recombination processes must be taking place via the pendant aromatic ring in both **2DBA** and **1DBA**.

There is strong evidence that charge recombination in **DPMN[8cy]DCV** takes place directly, through-space, between the two chromophores, which is facilitated by the electrostatically enforced proximity of the two chromophores in the charge-separated state of this species (see Fig. 3.9c). Thus, the distance between the two centroids in the charge-separated state of **DPMN[8cy]DCV**, based on a model system (Fig. 3.9c), is only 4.4 Å,[18] which is sufficiently small to promote strong through-space interchromophore coupling in this species.[25] The distances between the pendant group and **DPMN** and **DCV** chromophores in the charge-separated state of **1DBA'** are between 3.4 Å and 2.7 Å, depending on the twist angle of the pendant phenyl ring (see previous section). These distances are significantly smaller than the aforementioned value computed for the charge-separated state of **DPMN[8cy]DCV**. Thus, the finding that the strength of the electronic coupling for CT

fluorescence is substantially larger for **2DBA**, compared to that for **DPMN[8cy]DCV**, is understandable.

A fit of the rate constant data as a function of temperature to Equation 2 was used to extract values for the solvent reorganization energy (see Table 3.4) for **1DBA** and **2DBA**. The solvent reorganization energy values of **2DBA** are higher than **1DBA** in all the solvents. The difference between their solvent reorganization energy values is highest for the most polar solvent acetonitrile and least for *p*-xylene. Since the pendant groups in **1DBA** and **2DBA** have comparable sizes, the difference is likely caused by differences in the polarities of the pendant groups in these molecules, the electronegative oxygen atom making the methoxyphenyl pendant group in **2DBA** more polar than ethylphenyl group in **1DBA**. The CT emission fit was also used to determine the solvent reorganization energy for charge recombination in **2DBA** (Table 3.4). The values obtained from CT emission spectra fitting is somewhat smaller than the values obtained from the kinetic rate data and correlates with more negative values of $\Delta_r G$ obtained from CT emission fit (Table 3.3).

The $\Delta_r G$ values for **1DBA** were obtained from the kinetic fit of the experimental data to the molecular solvation model whereas fitting to the CT emission was used to calculate $\Delta_r G$ values of **2DBA** experimentally in different solvents. The magnitude of $\Delta_r G$ is least negative in *p*-xylene and is most negative in polar solvent acetonitrile. The $\Delta_r G$ for **2DBA** can not be determined from kinetic fit as $\Delta_r G$ is too negative (from CT emission fitting); however the estimated free energy obtained from the molecular solvation model for **2DBA** is somewhat lower than the free energy of **1DBA**. This finding indicates that there is some error associated with the fitting. To estimate the error we have used the contour plot of

reorganization energy values as a function of different free energy values in the fit in mesitylene (Fig. 3.7). The plot provides reasonable values for the reorganization energy ranging from 0.70-0.79 eV and $\Delta_r G$ values close to the values obtained from the CT emission fit.

3. 5 Conclusion

The electron transfer in U-shaped molecules **1DBA** and **2DBA** containing two different pendant groups in the cleft between the donor and acceptor group was studied. **2DBA** shows CT emission in nonpolar and weakly polar solvents. The magnitude of the electronic coupling for photoinduced charge separation in **1DBA** and **2DBA** were found to be 147 and 274 cm^{-1}, respectively. The origin of this difference lies in the electronic nature of the pendant aromatic group, since charge separation occurs by tunneling through the pendant group, rather than through the bridge. The charge transfer fluorescence for **2DBA** in non-polar solvents was used to determine the electronic coupling for charge recombination, $|V_{CR}|$, the magnitude of which is ~ 500 cm^{-1}, much larger than that for charge separation. This difference can be explained by changes in the geometry of the molecule in the relevant states; because of electrostatic effects, the **DPMN** and **DCV** chromophores are about 1Å closer to the pendant group in the CS state than in the locally excited state. Consequently the through-pendant-group electronic coupling is stronger in the CS state – which controls the CT fluorescence process – than in the locally excited state – which controls the CS process. The magnitude of $|V_{CR}|$ for **2DBA** is almost two orders of magnitude greater than that in **DMN-12-DCV**, having the same length bridge as for the former molecule, but lacking a pendant group. This result unequivocally demonstrates the operation of the through-pendant-group mechanism of electron transfer in the pendant-containing U-shaped systems of the type **1DBA** and **2DBA**.

Our observation of the modulation of the strength of electronic coupling in the U-shaped system **2DBA**, brought about by electrostatically driven changes in molecular geometry, suggests an intriguing approach to the generation of long-lived charge-separated species: build a U-shaped system possessing a doubly positively chaged acceptor, D-B-A^{2+} (e.g. A^{2+} = viologen). Photoinduced electron transfer should generate D^{+}-B-A^{+}. Repulsive electrostatic interactions should drive the singly positively chaged chromophores further apart, thereby weakening the electronic coupling for charge recombination. Such an effect has been observed and explained in terms of this mechanism.[26]

3. 6 Acknowledgement

We acknowledge financial support from the Australian Research Council and the US National Science Foundation (CHE-041545).

3.7 Appendix

Table 3.5 Fluorescence decay of DBA molecules in toluene

System	Toluene							
	T(K)	Donor τ (ps)	A1%	τ_1 (ps)	τ_2 (ps)	k_{for} (s^{-1})	k_{back} (s^{-1})	$\Delta_r G$ (eV)
1DBA	295.0	4203	99.0	399	25515	2.24×10^{9}	2.59×10^{7}	-1.13×10^{-1}
	305.6	3980	98.5	355	39882	2.52×10^{9}	4.63×10^{7}	-1.05×10^{-1}
	314.7	3814	98.0	324	41885	2.77×10^{9}	6.58×10^{7}	-1.01×10^{-1}
	323.9	3663	97.0	279	42236	3.21×10^{9}	1.15×10^{7}	-9.30×10^{-2}
	336.6	3479	95.8	264	38555	3.35×10^{9}	1.70×10^{7}	-8.64×10^{-2}
2DBA	285.3	4634	90.0	317	1353	2.77×10^{9}	3.42×10^{7}	-1.12×10^{-1}
	295.2	4150	91.0	258	1315	2.90×10^{9}	4.32×10^{7}	-1.13×10^{-2}
	295.6	4155	93.0	290	1054	3.57×10^{9}	3.64×10^{7}	-1.07×10^{-2}
	304.0	3981	91.0	246	1170	3.16×10^{9}	6.40×10^{7}	-1.17×10^{-2}
	314.6	3809	90.0	237	870	3.73×10^{9}	5.26×10^{7}	-1.24×10^{-1}
	317.9	3734	92.0	255	1264	3.90×10^{9}	3.88×10^{7}	-1.15×10^{-1}
	323.6	3644	92.0	230	956	3.60×10^{9}	6.34×10^{7}	-1.14×10^{-1}
	339.3	3413	91.0	202	730	4.55×10^{9}	6.29×10^{7}	-1.25×10^{-1}

Table 3.6 Fluorescence decay of DBA molecules in p-Xylene

System	*p*-Xylene							
	T(K)	Donor τ (ps)	A1%	τ_1 (ps)	τ_2 (ps)	k_{for} (s^{-1})	k_{back} (s^{-1})	$\Delta_r G$ (eV)
1DBA	295.0	4051	97.9	418	48039	2.10×10^{9}	5.53×10^{7}	-9.24×10^{-2}
	305.1	3834	97.0	364	46308	2.40×10^{9}	8.94×10^{7}	-8.66×10^{-2}
	314.6	3641	96.1	339	44762	2.56×10^{9}	1.26×10^{8}	-8.18×10^{-2}
	323.1	3488	94.9	306	41869	2.82×10^{9}	1.80×10^{8}	-7.66×10^{-2}
	333.6	3317	93.4	265	36500	3.23×10^{9}	2.69×10^{8}	-7.14×10^{-2}
2DBA	276.2	3729	88.0	384	15115	1.59×10^{9}	8.62×10^{7}	-7.2×10^{-2}
	283.7	3573	90.0	352	16258	1.63×10^{9}	10.9×10^{7}	-9.1×10^{-2}
	294.2	3379	91.9	313	11447	2.86×10^{9}	3.75×10^{7}	-10.9×10^{-2}
	294.2	3297	90.8	291	5987	3.01×10^{9}	6.39×10^{8}	-9.82×10^{-2}
	305.8	3315	91.2	263	6478	3.46×10^{9}	3.77×10^{8}	-11.9×10^{-2}
	314.3	3073	91.3	248	5748	3.63×10^{9}	6.42×10^{7}	-11.8×10^{-2}
	324.4	2905	91.3	222	8714	4.08×10^{9}	6.01×10^{7}	-12.2×10^{-1}
	335.9	2925	92.6	242	8651	3.73×10^{9}	4.92×10^{7}	-12.5×10^{-2}
		2816	91.3	204	10180	4.47×10^{9}	5.89×10^{7}	

Table 3.7 Fluorescence decay of DBA molecules in acetonitrile

System		Acetonitrile		
	T(K)	Donor τ (ps)	τ_1 (ps)	k_{ET} (s^{-1})
1DBA	301	11375	1382	6.36×10^8
	309	11102	1172	7.63×10^8
	317	10472	1069	8.40×10^8
	327	9897	918	9.88×10^8
	337	9389	806	1.13×10^9
2DBA	276	9455	2120	3.67×10^8
	285	9470	1830	4.42×10^8
	295	9035	1550	5.35×10^8
	295	9904	1590	5.30×10^8
	303	9165	1380	6.17×10^8
	314	8802	1200	7.22×10^8
	324	8292	1030	8.51×10^8
	327	8415	979	9.02×10^8
	338	8134	857	10.4×10^8

3. 8 References

1. (a) Barbara, P. F.; Meyer, T. J.; Ratner, M. A. *J. Phys. Chem*. **1996**, *100*, 13148. (b) Electron Transfer-From Isolated Molecules to Biomolecules, *Adv. Chem. Phys*. Jortner, J.; Bixon, M., Eds.; Wiley: New York, 1999.

2. (a) Hush, N. S.; Paddon-Row, M. N.; Cotsaris, E.; Oevering, H.; Verhoeven, J. W.; Heppener, M. *Chem. Phys. Lett*. **1985**, *117*, 8. (b) Oliver, A. M.; Craig, D. C.; Paddon-Row, M. N.; Kroon, J.; Verhoeven, J. W. *Chem. Phys. Lett*. **1988**, *150*, 366. (c) Paddon-Row, M. N. *Acc. Chem. Res*. **1994**, *27*, 18.

3. (a) Zeng, Y.; Zimmt, M. B. *J. Phys. Chem*. **1992**, *96*, 8395. (b) Oliver, A. M.; Paddon-Row, M. N.; Kroon, J.; Verhoeven, J. W. *Chem. Phys. Lett*. **1992**, *191*, 371.

4. (a) Closs, G. L.; Miller, J. R. *Science* **1988**, *240*, 440. (b) Guldi, D. M.; Luo, C.; Prato, M.; Troisi, A.; Zerbetto, F.; Scheloske, M.; Dietel, E.; Bauer, W.; Hirsch, A.; *J. Am. Chem. Soc*. **2001**, *123*, 9166.

5. Napper, A. M.; Head, N. J.; Oliver, A. M.; Shephard, M. J.; Paddon-Row, M. N.; Read, I.; Waldeck, D. H. *J. Am. Chem. Soc*. **2002**, *124*, 10171.

6. Liu, M.; Chakrabarti, S.; Waldeck, D. H.; Oliver, A. M.; Paddon-Row, M. N. *Chem. Phys*. **2006**, *324*, 72.

7. Napper, A. M.; Read, I.; Waldeck, D. H.; Head, N.J.; Oliver, A. M.; Paddon-Row, M. N. *J. Am. Chem. Soc*. **2000**, *122*, 5220.

8. (a) Oevering, H.; Verhoeven, J. W.; Paddon-Row, M. N.; Warman, J. M. *Tetrahedron* **1989**, *45*, 4751. (b) Oevering, M. N.; Paddon-Row, M. N.; Heppener, H.; Oliver, A. M.; Cotsaris, E.; Verhoeven, J. H.; Hush, N. S. *J. Am. Chem. Soc*. **1987**, *109*, 3258.

9. Kumar, K.; Kurnikov, I. V.; Beratan, D. N.; Waldeck, D. H.; Zimmt, M. B. *J. Phys. Chem. A,* **1998**, *102*, 5529.

10. Read, I.; Napper, A. M.; Zimmt, M. B.; Waldeck, D. H. *J. Phys. Chem. A* **2000**, *104*, 9385.

11. Matyushov, D. V.; Voth, G. A. *J. Chem. Phys*. **1999**, *111*, 3630.

12. (a) Paddon-Row, M. N.; Oliver, A. M.; Warman, J. M.; Smit, K. J.; de Hass, M. P.; Oevering, H.; Verhoeven, J. W. *J. Phys. Chem.* **1988**, *92*, 6958. (b) Warman, J. M.; Smit, K. J.; de Hass, M. P.; Jonker, S. A.; Paddon-Row, M. N.; Oliver, A. M.; Kroon, J.; Oevering, H.; Verhoeven, J. W. *J. Phys. Chem*. **1991**, *95*, 1979.

13. Wasielewski, M. R.; Minsek, D. W.; Niemczyk, M. P.; Svec, W. A.; Yang, N. C. *J. Am. Chem. Soc*. **1990**, *112*, 2823.

14. Morais, J.; Huang, R. R.; Grabowski, J. J.; Zimmt, M. B. *J. Phys. Chem*. **1993**, *97*, 13138.

15. (a) Mataga, N.; Kaifu, Y.; Koizumi, M. *Bull. Chem. Soc. Jpn*. **1955**, *28*, 690. (b) Mataga, N.; Kaifu, Y.; Koizumi, M. *Bull. Chem. Soc. Jpn.* **1955**, *29*, 465.

16. (a) Marcus, R. A. *J. Phys. Chem*. **1989**, *93*, 3078. (b) Cortes, J.; Heitele, H.; Jortner, J. *J. Phys. Chem*. **1994**, *98*, 2527.

17. When the fitting was done in acetonitrile keeping the difference of reorganization energy between **1DBA** and **2DBA** 0.09 eV (same as mesitylene), the molecular solvation theory predicts higher values of k_{ET} for **2DBA** than **1DBA** but leads to a bad fit between the experimental and theoretical prediction of **2DBA**.

18. Koeberg, M.; Groot-de, M.; Verhoeven, J. W.; Lokan, N. R.; Shephard, M. J.; Paddon-Row, M. N. *J. Phys. Chem. A* **2001**, *105*, 3417.

19. Frisch, M. J.;Trucks, G. W.;Schlegel, H. B.;Scuseria, G. E.;Robb, M. A.; Cheeseman, J. R.;Montgomery, J. A.;Vreven, J. A. Jr.;Kudin, K. N.; Burant, J. C.; Millam, J. M.;Iyengar, S. S.;Tomasi, J.;Barone, V.;Mennucci, B.;Cossi, M.;Scalmani, G.;Rega, N.;Petersson, G. A.;Nakatsuji, H.;Hada, M.;Ehara, M.;Toyota, K.;Fukuda, R.;Hasegawa, J.;Ishida, M.;Nakajima, T.;Honda, Y.;Kitao, O.;Nakai, H.;Klene, M.;Li, X.;Knox, J. E.;Hratchian, H. P.;Cross, J. B.;Adamo, C.;Jaramillo, J.;Gomperts, R.;Stratmann, R. E.;Yazyev, O.;Austin, A. J.;Cammi, R.;Pomelli, C.;Ochterski, J. W.;Ayala, P. Y.;Morokuma, K.;Voth, G. A.;Salvador, P.;Dannenberg, J. J.;Zakrzewski, V. G.;Dapprich, S.;Daniels, A. D.;Strain, M. C.; Farkas, O.;Malick, D. K.;Rabuck, A. D.;Raghavachari, K.;Foresman, J. B.;Ortiz, J. V.;Cui, Q.;Baboul, A. G.;Clifford, S.;Cioslowski, J.;Stefanov, B. B.;Liu, G.; Liashenko, A.;Piskorz, P.;Komaromi, I.;Martin, R. L.;Fox, D. J.;Keith, T.; Al-Laham, M. A.;Peng, C. Y.;Nanayakkara, A.;Challacombe,Gill, P. M. W.;Johnson, B.;Chen, W.;Wong, M. W.;Gonzalez, C.;Pople, J. A.Gaussian, Inc., Pittsburgh PA, 2003.

20. Liu, M.; Waldeck, D. H.; Oliver, A.; Head, N. J.; Paddon-Row, M. N. *J. Am. Chem. Soc.* **2004**, *126*, 10778.

21. Jordan, K. D.; Burrow, P. D. *Acc. Chem. Res.* **1978**, *11*, 341.

22. Toluene: Kimura, K. Handbook of He(I) photoelectron spectra of fundamental organic molecules, **1981**, Japan Sci. Soc. Press, Tokyo. Anisole: Kobayashi, T.; Nagakura, S. *Bull. Chem. Soc. Japan* **1974**, *47*, 2563.

23. (a) Shephard, M. J.; Paddon-Row, M. N. *J. Phys. Chem. A* **1999**, *103*, 3347. (b) Shephard, M. J.; Paddon-Row, M. N. *J. Phys. Chem. A* **2000**, *104*, 11628.

24. Fully optimized charge-separated state geometries, with no symmetry constraints, could be calculated using some sort of CI procedure, the simplest being CIS. However, preliminary attempts to optimize the charge separated state of **1DBA'**, even using the relatively small 3-21G basis set, met with such huge computational overheads that they were aborted.

25. Paddon-Row, M. N.; Jordan, K. D.; Through-Bond and Through-Space Interactions in Unsaturated Hydrocarbons: Their Implications for Chemical Reactivity and Long-Range Electron Transfer. In *Modern Models of Bonding and Delocalization*; Liebman, J. F., Greenberg, A., eds.; VCH Publishers: New York, 1988; Vol. 6; pp 115.

26. (a) Jolliffe, K. A.; Bell, T. D. M.; Ghiggino, K. P.; Langford, S. J.; Paddon-Row, M. N. *Angew. Chem., Int. Ed.* **1998**, *37*, 916. (b) Bell, T. D. M.; Jolliffe, K. A.; Ghiggino, K. P.; Oliver, A. M.; Shephard, M. J.; Langford, S. J.; Paddon-Row, M. N. *J. Am. Chem. Soc.* **2000**, *122*, 10661.

4.0 CHAPTER FOUR

Solvent Dynamical Effects on Electron Transfer in U-Shaped Donor-Bridge-Acceptor Molecules

This work has been submitted as Chakrabarti, S.; Liu, M.; Waldeck, D. H.; Oliver, A. M.; Paddon-Row, M. N. to J. Phys. Chem. B

This study explores how the electron transfer in a class of donor-bridge-acceptor (DBA) supermolecules is affected by the dynamical response of the solvent. These DBA molecules have a pendant group in the line of sight which provides intermediate coupling strengths of a few hundred wavenumbers and can be tuned by substituents added to the pendant. This design allows the measurement of electron transfer rates from a regime in which the mechanism is nonadiabatic to a regime in which the solvent friction modifies the rate substantially. The rate constants and mechanistic parameters are compared with the expectations of models for solvent dynamical effects on the reaction rate.

4.1 Introduction

The influence of solvent dynamics on chemical reactions is important for understanding chemical processes in polar and viscous solvents.[1-3] In particular, this work addresses electron transfer reactions of Donor-Bridge-Acceptor (**DBA**) molecules in the

solvent controlled regimes. Previous work[4,5] showed that the photoinduced electron transfer reaction for molecule **3** (see Figure 4.1) changes from a nonadiabatic electron tunneling mechanism at high temperature in the solvent N-metylacetamide (NMA) to a solvent controlled mechanism at low temperature, involving the nuclear motion as the rate limiting step of the reaction. This mechanism change was observed in solvents having high viscosity and long Debye relaxation times, but not in low viscosity solvents having short Debye relaxation times. It was postulated that the mechanism change arose from a solvent friction effect, in which the polarization relaxation time of the solvent controls the rate by controlling the characteristic time spent in the transition state (curve crossing) region.

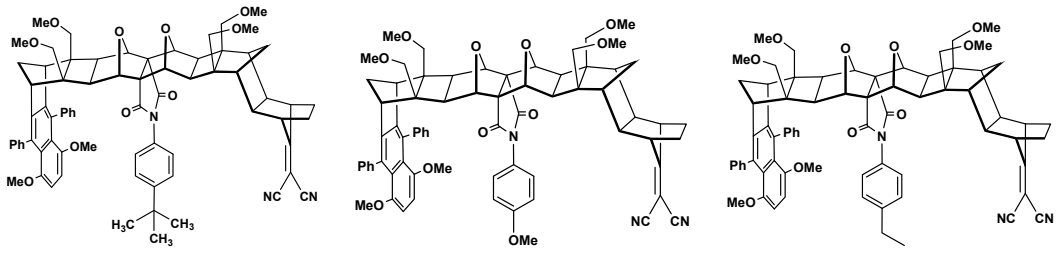

Figure 4.1 The molecular structure of three U-shaped Donor- Bridge-Acceptor (DBA) molecules having different pendant units are shown here

The U-shaped molecules **1**, **2** and **3** are designed so that electron transfer occurs by way of electron tunneling through the pendant group. The DBA molecules in Figure 4.1 have the same 1,4 diphenyl-5,8-dimethoxynaphthalene (**DPMN**) donor unit and 1,1-dicyanovinyl (**DCV**) acceptor unit connected through a highly curved bridge unit that holds the donor and the acceptor moieties at a well defined distance and fixed orientation. A pendant group is covalently attached to the bridge unit and occupies the cavity between the donor and acceptor. It has been shown that in such systems the electron tunnels from the donor to acceptor via the

pendant groups.[6,7] The semiclassical equation with a single effective quantum mode can be successfully applied to describe the electron transfer rate constants at high temperatures in nonpolar and weakly polar solvents. The resulting rate constant expression takes the form[8]

$$k_{NA} = \frac{2\pi}{\hbar} |V|^2 \frac{1}{\sqrt{4\lambda_o \pi k_B T}} \sum_{n=0}^{\infty} \exp(-S)\left(\frac{S^n}{n!}\right) \exp\left[-\frac{\left(\Delta_r G + \lambda_o + nh\nu\right)^2}{4\lambda_0 k_B T}\right] \qquad \mathbf{1}$$

where λ_o is the medium reorganization energy; $\Delta_r G$ is the Gibbs energy; $S = \frac{\lambda_v}{h\nu}$ and λ_v is the internal reorganization energy. The $h\nu$ term is the energy spacing of the single effective quantum mode that is coupled to the electron transfer reaction. These last two terms account for the high frequency component of the reorganization energy, and for these systems it is characteristic of the donor and acceptor groups. (See Reference 8 for a more detailed description.)

Previously, $\Delta_r G(LE \rightarrow CS)$ for **1**, **2** and **3** was determined experimentally from the kinetic data in the solvents toluene, mesitylene, and *p*-xylene.[9,10] In these systems an equilibrium exists between the charge separated state and the locally excited state so that $\Delta_r G$ could be determined experimentally. These data were used to calibrate the solute molecule parameters of a molecular solvation model. [11-13]

This study extends the earlier work by exploring how the solvent dynamics affects the charge transfer of **1**, **2** and **3** in N-methyl propionamide (NMP). These solute molecules are chosen to explore how the change from a nonadiabatic electron transfer mechanism to a solvent controlled electron transfer mechanism depends on the strength of the solute molecule's electronic coupling. NMP has a large static dielectric constant and slow polarization response time, which results from its hydrogen bonded structure, and this allows

the dynamical solvent effect to be observed. The Zusman model was used to fit the experimental results over a wide temperature range (from 337 K to 230 K) and obtain an outer sphere solvent reorganization energy (λ_0) and $\Delta_r G$ for compounds **1**, **2** and **3** in NMP (Table 2). The experimental rates in the low temperature regimes are analyzed and discussed in terms of three different models that account for solvent dynamics.

4.2 Background

Electron transfer reactions are commonly viewed as occurring in one of three possible regimes that are distinguished by the strength of their electronic coupling $|V|$ and the characteristic response time of the solvent medium. When the electronic coupling is weak $|V| << k_BT$ and the solvation response is rapid, the reaction is nonadiabatic (dashed curve in Figure 4.2) and the rate constant is proportional to $|V|^2$. In this regime, the system may move through the curve crossing region $q^{\ddagger}$ many times before the electronic state change occurs; hence the electronic tunneling event (curve hopping) is the rate limiting step. A second regime is adiabatic electron transfer, where $|V| >> k_BT$ (solid curves in Figure 4.2). In this limit, the electronic state evolves from reactant to product as the nuclear motion proceeds through the transition state. The third regime is solvent controlled electron transfer, in which the electronic coupling may be weak at the transition state, but the characteristic time spent in the curve crossing region is long enough that nearly every passage through the crossing region results in a change of electronic state. Hence the reaction appears adiabatic, in the sense that the rate is limited by the nuclear dynamics rather than by the electron tunneling probability. This latter limit is discussed more in the next sections, in terms of different theoretical models.

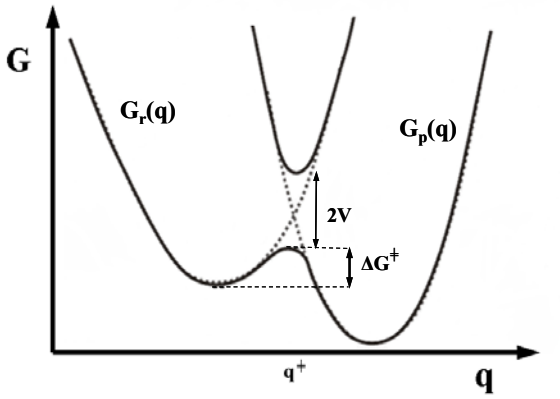

Figure 4.2 This diagram illustrates the adiabatic (the solid curves) - strong coupling - and nonadiabatic (the diabatic dashed curves) – weak coupling limits. (Taken from reference 8)

A. *Zusman Model*

According to Zusman[14-16] the electron transfer rate constant (k_{ET}) can be expressed as a serial combination of the normal nonadiabatic electron transfer rate constant (k_{NA}) and a solvent-controlled electron transfer rate constant (k_{SC}), namely

$$\frac{1}{k_{ET}} = \frac{1}{k_{SC}} + \frac{1}{k_{NA}} \qquad \textbf{2}$$

When $k_{SC} >> k_{NA}$, the overall electron transfer rate k_{ET} can be described well by the semiclassical expression for k_{NA} (Equation 1). On the other hand if the solvent's polarization relaxation is the rate limiting step then $k_{ET} \sim k_{SC}$, because $k_{SC} << k_{NA}$, and the contribution of k_{NA} to the overall rate constant is small.

In the classical limit (quantized vibrational modes ignored) Zusman finds that k_{SC} can be expressed by

$$k_{SC,z} = \frac{1}{\tau_S}\sqrt{\frac{\lambda_0}{\pi^3 k_B T}}\sin\left[\pi\sqrt{\frac{\Delta G^{\neq}}{\lambda_0}}\right]\exp(-\Delta G^{\neq}/k_B T) \qquad \textbf{3}$$

In which $\Delta G^{\neq} = (\Delta_r G + \lambda_0)^2 / 4\lambda$, which predicts that the electron transfer rate constant is inversely proportional to the solvation time τ_S. Since the solvation time increases rapidly with decreasing temperature in viscous solvents, the solvation dynamics can become rate limiting at low temperature. Correspondingly, the solvation time gets faster at higher temperature and the electron transfer rate becomes less dependent on solvent friction as the temperature increases. If we define a reduced electron transfer time τ^*_{ET} by

$$\tau^*_{ET} = \sqrt{\frac{1}{\lambda_0 k_B T}} \frac{\exp(-\Delta G^{\neq} / k_B T)}{k_{ET}} \qquad \textbf{4}$$

and substitute into Equations 2 and 3, we find that

$$\tau^*_{ET,Z} = \frac{\sqrt{\pi^3}}{\lambda_0 \sin\left(\pi\sqrt{\frac{\Delta G^{\neq}}{\lambda_0}}\right)} \tau_S + \sqrt{\frac{1}{\lambda_0 k_B T}} \frac{\exp(-\Delta G^{\neq} / k_B T)}{k_{NA}} \qquad \textbf{5}$$

In the approximation that the first term in the summation over vibronic states in equation 1 dominates the sum, the rate constant expression k_{NA} reduces to the classical expression with an effective electronic coupling $|V_{eff}| = |V| \exp(-S/2)$ and equation 5 takes the form.

$$\tau^*_{ET,Z} = \frac{\sqrt{\pi^3}}{\lambda_0 \sin\left(\pi\sqrt{\frac{\Delta G^{\neq}}{\lambda_0}}\right)} \tau_S + \frac{\hbar}{\sqrt{\pi}} \frac{1}{|V_{eff}|^2} \qquad \textbf{6}$$

Although λ_0 and $\Delta_r G$ are each temperature dependent, their net contribution to the temperature dependence in Equation 6 is weak over the temperature range studied so that τ^*_{ET} is effectively a linear function of τ_S.

B. *Mukamel Model*

Sparpaglione and Mukamel have developed a model[17,18] for electron transfer rates in polar solvents that includes dynamical solvent effects and interpolates between the nonadiabatic and adiabatic limits. This model uses a time correlation function to describe the solvent response, which allows the treatment of non-Debye solvent models. Their expression for the electron transfer rate constant is given by

$$k_{ET,SM} = \frac{2\pi}{\hbar}\left|V^2\right| \frac{1}{\sqrt{4\pi\lambda_0 kT} + \frac{2\pi\left|V^2\right|\tau_a}{\hbar}} \exp\left(-\frac{(\Delta_r G + \lambda_0)}{4kT\lambda_0}\right) \qquad \mathbf{7}$$

in which the symbols have their usual meaning and τ_a is a characteristic solvent response time. This formulation corresponds to a limit in which the characteristic time $\tau \sim \sqrt{\frac{h^2}{8kT\lambda_0}}$ is shorter than solvent timescales relevant to the electron transfer and the back electron transfer is neglected.[19,20] For τ_a short enough the nonadiabatic limit (classical version of Eqn 1) is recovered, and in the solvent controlled limit (τ_a long enough) one finds that

$$k_{SC,SM} = \frac{1}{\tau_a}\exp\left(-\frac{(\Delta_r G + \lambda_0)}{4kT\lambda_0}\right) \qquad \mathbf{8}$$

This latter result differs from Zusman's result; compare to Eqn 3. Using the definition of τ^*_{ET} (Eqn 4) and substituting in equation 9, we find that

$$\tau^*_{ET,SM} = \frac{\hbar}{\sqrt{\pi}\left|V^2\right|} + \frac{\tau_a}{\sqrt{\lambda_0 kT}} \qquad \mathbf{9}$$

Under the approximation that the solvation time is a property of the solvent and not dependent on the details of the solute (e.g., size of dipole moment, radius of the solute), we

can use the solvation time from dynamic Stokes Shift measurements[5] to write $\tau_a = \tau_S$. This result differs from that found from the Zusman model. Although a plot of τ^*_{ET} versus τ_S has the same intercept in these models, the slope of the line is predicted to be different.

C. *Two- Dimensional Electron Transfer Model*

Sumi, Nadler and Marcus[21,22] introduced a two-dimensional electron transfer model to describe the influence of solvent dynamics. This model views the reaction as proceeding along a two dimensional-reaction coordinate, containing a nuclear coordinate (*q*) and a solvent polarization coordinate (*X*). They found the reaction rate by solving a diffusion-reaction equation for diffusive motion along *X* and treating the motion along *q* through a rate constant *k*(X), which is X dependent but depends on the "fast" motions in the normal way (equation 1). The population probability is described by

$$\frac{\partial P(X,t)}{\partial t} = D\frac{\partial}{\partial X}\left[\frac{\partial}{\partial X} + \frac{1}{k_B T}\frac{dV}{dX}\right]P(X,t) - k(X)P(X,t) \qquad \textbf{10}$$

where D is the diffusion coefficient, $V(X)$ is the effective potential for the solvent polarization coordinate, and $P(X,t)$ is a probability distribution function for the reactant population. This model predicts that solvents with long polarization relaxation times have a "*power-law*" dependence of the average survival time on the solvent relaxation time. They solve the diffusion reaction equation for four limiting cases. The first case is called the "slow reaction limit" and corresponds to the motion along *X* which is fast compared to the motion along *q*, so the reaction does not depend on solvent frictional coupling. The second case is known as "wide reaction window" and represents a situation in which the internal reorganization energy is much larger than the solvent reorganization so that the reaction may

proceed over a range of X values but the reaction rates at different X values are the same. In the third ("narrow reaction window") and fourth ("non-diffusing limit") cases the motion along the polarization coordinate is slow compared to k(X) and the solvent friction has a significant effect on the electron transfer rate. In the "narrow reaction window" limit, Sumi and Marcus assume the electron transfer occurs at a particular value of $X=X_0$ and the reaction rate is controlled by the time evolution of the reactant population along X, which can be nonexponential. In the "non-diffusing" limit, the reaction occurs at a range of X values and the nonexponentiality of the rate arises from a distribution of k(X).

Although Sumi, Marcus, and Nadler discussed four limiting cases, only two of these are relevant to the present study. One is the "slow reaction limit" which applies for the high temperature data reported here, and the other is the "narrow reaction window" and it applies to the low temperature data. For the "narrow reaction window" case, they showed that the average survival time increases gradually with increasing solvent relaxation time with a slope between zero and unity. Also they find that the logarithm of the average survival time τ_c increases linearly with an increase in the activation barrier with a slope between zero and one. Hence, the dependence of the average survival time on activation energy barrier $\Delta G^{\neq} / k_B T$ over some intermediate values of activation barrier can be approximated as $\tau_c \infty \exp(\frac{\alpha \Delta G^{\neq}}{k_B T})$, where α is a parameter between zero and one. Comparison of the experimental data for **1**, **2**, and **3** with this model are discussed in the results section.

4.3 Experimental

The synthesis of the U-shaped supermolecules **1**, **2** and **3** is similar to that reported elsewhere.[23] The solvent NMP was purchased from TCI America. NMP was fractionally

distilled three times under vacuum. The freshly purified fraction was used in all the experiments. Each solution was freeze-pump-thawed a minimum of seven cycles or more to eliminate dissolved oxygen.

Time resolved fluorescence kinetics of **1**, **2** and **3** were measured using the time-correlated single photon counting technique. Each sample was excited at 330 nm by the frequency-doubled cavity-dumped output of a Coherent CR599-01 dye laser, using DCM (4-dicyanomethylene-2-methyl-6-p-dimethylamino-styryl-4H-Pyran) dye, which was pumped by a mode locked Vanguard 2000-HM532 Nd:YAG laser purchased from Spectra-Physics. The dye laser pulse train had a repetition rate of 300 kHz. Pulse energies were kept below 1 nJ, and the count rates were kept below 3 kHz to prevent pile up effects. All fluorescence measurements were made at the magic angle, and data were collected until a standard maximum count of 10,000 was observed at the peak channel.

The steady-state and time-resolved fluorescence kinetics for **1, 2** and **3** and their donor only analogues were carried out in NMP as a function of temperature (O.D ~ 0.10). The temperature ranged from 226 K to a high of 353 K. The experimental high range of temperature was controlled by an ENDOCAL RTE-4 chiller and the temperature was measured using a "type-K" thermocouple (Fisher-Scientific), accurate to within 0.1 ºC. Measurements in the lower temperature range employed a VPF Cryostat (Janis Research Company, Inc.) and a model 321 Autotuning Temperature Controller (LakeShore Cryotronics, Inc.) with a silicon diode sensor.

Temperature measurements were improved from the earlier described design by incorporating another "type-T" thermocouple directly on the surface of the sample cell to monitor the temperature, in addition to the silicon sensor used for temperature control, which

is not directly in contact with the sample cuvette. The temperatures measured at the sample cell's surface are close to those measured when a thermocouple is directly inserted into the liquid sample, within 1K, but they are systematically higher than the temperature measured from the diode sensor. The worst case was observed at the lowest temperature (220K), which had a 10K difference.

Table 4.1 Properties of Solvent NMP at 303K

Solvent	n[a]	ε_S[a]	τ_D (ps)[b]	τ_S (ps)[c]	η (cP)[a]	μ (D)[d]
NMP	1.43	164.4	100	42	4.60	4.29

[a] The refractive index n, relative static dielectric constant ε, and shear viscosity η are taken from the Beilstein database; [b] Taken from reference 5; [c] The solvation time is extracted from the best fit of the dynamic Stokes shift measurements, [d] The dipole moment μ was calculated using Gaussian/MP2/6- 31G.

The instrument response function was measured using a sample of colloidal $BaSO_4$. The fluorescence decay curve was fit by a convolution and compare method using IBH-DAS6 analysis software. Independent experiments on individual donor only molecules at the measured temperatures, always a single exponential fluorescence decay, was used to determine the intrinsic fluorescence decay rate of the locally excited state. The DBA molecules, **1**, **2** and **3** have a small amount of donor only impurity. The measurement of the donor only molecule's fluorescence decay characteristic for each solvent and temperature allowed this contribution to the decay to be subtracted from the data and obtain the decay law of the DBA molecules**.**

Fitting the rate constant data by the semiclassical equation (equation 1) and the low temperature analysis were performed using Microsoft Excel 2003. In fits by a molecular solvation model the electronic coupling was treated as an adjustable parameter for each solute

molecule and the reorganization energy was treated as an adjustable parameter. The internal reorganization parameters were obtained from the charge transfer spectra of a similar compound and were kept fixed since the solute has the same donor and acceptor group. The molecular solvation model was calibrated for compounds **1**, **2** and **3** in weakly polar and nonpolar solvents, and it was used to predict the Gibbs free energy and reorganization energy in the polar solvent NMP.

4.4 Results and Analysis

Steady-State Spectra:

Steady-state UV-Vis absorption and emission spectra of compounds **1**, **2** and **3** in N-methylpropionamide (NMP) are shown in figure 4.3. The spectral features of the DBA molecules **1**, **2** and **3** are dominated by the donor 1,4-dimethoxy-5,8-diphenylnaphthalene (**DPMN**) unit, which has two transition bands in the UV region assigned to $^1A \rightarrow {}^1L_b$, and the $^1A \rightarrow {}^1L_a$ transition.[10] Consequently excitation at 330 nm produces a locally excited state on the **DPMN** portion of the molecule. Compounds **1**, **2** and **3** differ by the substituent at the *para* position of the pendant phenyl group, located in the cleft. It is evident that the emission bands of **1** and **3** are nearly identical, and that **2** differs somewhat in the red edge/tail. An earlier study in nonpolar and weakly polar solvents showed that a charge transfer band could be identified for **2** in weakly polar and nonpolar solvents. While its emission is expected to be quenched in the highly polar NMP, it may cause some residual broadening on the spectrum's red tail. These results suggest that there is little difference in the steady state emission spectra in these molecules.

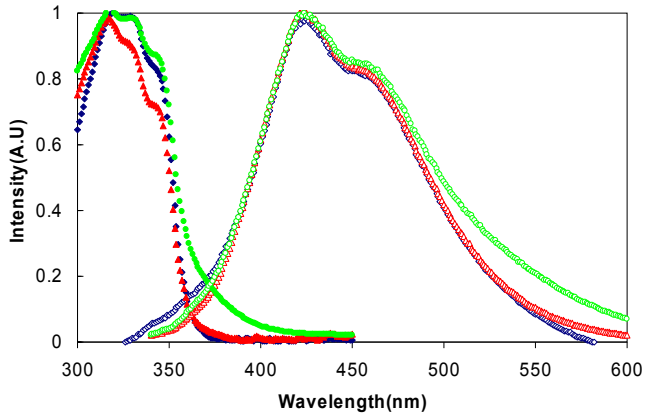

Figure 4.3 Figure showing steady-state absorption and emission spectra of compound **1** (red) compound **2** (green), and compound **3** (blue) in NMP.

Fluorescence Decay Time Analysis

Similar to the results reported earlier for compound **3** in NMP, the fluorescence decays of **1** and **2** in NMP can be fit by a single exponential decay law at high temperature, but become less exponential at lower temperature and are strongly nonexponential at low temperature. In contrast, the decay kinetics of these compounds can be fit by a single exponential decay in acetonitrile at all temperatures studied here, and the nonadiabatic expression (equation 1) provides a good description of the rate constant over the whole temperature range for these compounds. Details can be found in the supplementary materials.

Because the decay law is not single exponential, the electron transfer rate constant is not well-defined in NMP. To quantify the rate in terms of an effective rate constant, a correlation time τ_c is computed from the fluorescence decay law. Because the decay law of the DBA molecule could be described by a sum of exponentials (most commonly two exponentials), τ_c was calculated from , $\tau_C = \sum_i f_i \tau_i$ where, τ_i is the time constant for component *i* and f_i is the amplitude of component *i*. As described previously[4,5], the electron

transfer rate is obtained from $k_{ET} = k_{obs} - k_f$, where k_f is the fluorescence decay rate of the donor only molecule and k_{ET} is the experimentally determined electron transfer rate constant. By subtracting the intrinsic lifetime of the locally excited state (modeled as the donor-only lifetime), an effective electron transfer rate constant was found, *i.e.*, $k_{ET} = 1/\tau_c - k_f$.

Figure 4.4 shows the rate constant data plotted as a function of the inverse temperature. The rate constants for all three compounds are similar at low temperatures; however they systematically deviate from one another at higher temperatures. The *t*-butyl substituted compound (**1**) deviates most significantly and at

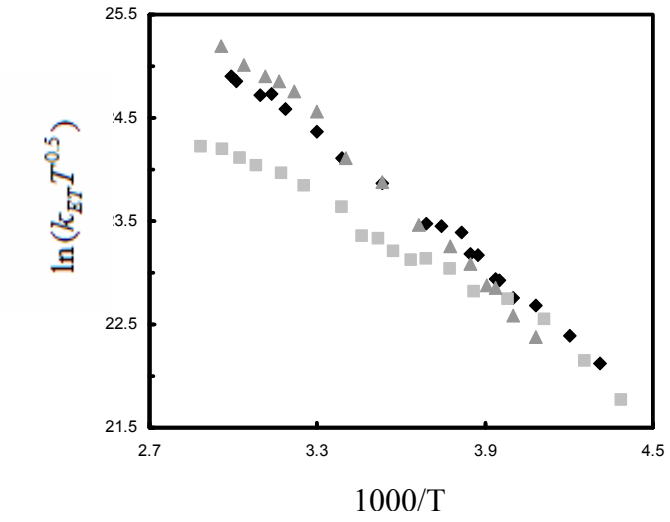

Figure 4.4 This figure shows experimental electron transfer rate constant of compound **1** (square), **2** (triangle), **3** (diamond) in NMP.

a temperature of about 260 K to 270 K. The data for **2** and **3** are more similar but show a systematic deviation at temperatures above 310 K. In previous work comparing **3** with a compound containing a propyl pendant group[5], this overlap of electron transfer rates was explained in terms of a dynamic solvent effect whose importance can be gauged by a

characteristic time for the solvent's polarization response. For NMP, a temperature in the 260 to 270 K range corresponds to a solvation time of about 240 ps and at the relatively higher temperature of 310 K it is about 55 ps. These solvation times are taken from dynamic Stokes shift measurements[5]. This trend in characteristic times for the different solutes correlates with the change in electronic coupling |V| that has been reported for these three molecules; i.e., |V(**2**)|>|V(**3**)|>|V(**1**)| and can be predicted by the Zusman and Mukamel model; discussed later.

Modeling the Rate Constant

Previously, we used a molecular solvation model to fit the high temperature data in nonpolar and weakly polar solvents and obtained values for the electronic coupling between the donor and acceptor moieties of **1**, **2** and **3**. We also showed that use of the same model for the NMP solvent was unable to fit the data over the whole temperature range. Although Equation 1 fits the high temperature experimental data, it fails to give a good fit in the low temperature range. This behavior was explained by the importance of the dynamic solvent effect at low temperature. The present analysis uses equation 2 so that the contributions of the dynamic solvent effect are included and a quantitative description of the electron transfer rate constant over the whole temperature range is possible.

Figure 4.5 shows fits of the experimental rate constant data k_{ET} as a function of temperature to Equation 2, using the Zusman model for k_{SC}. In these fits the reorganization energy and Gibbs energy were treated as adjustable parameters (values are reported in Table 2). Other parameters λ_v, $\hbar\omega$, and τ_s (see reference 5) were

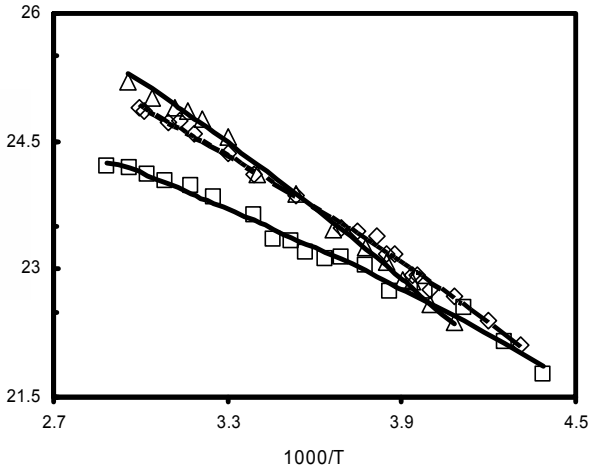

Figure 4.5 This figure plots the electron transfer rate constant data of compound **1** (square), compound **2** (triangle), compound **3** (diamond) in NMP. The straight lines represent best fit equation 2.

obtained from previous studies and kept fixed during this analysis. Table 4.2 lists the electronic coupling, Gibb's energy, and reorganization energy values obtained from these fits. The electronic coupling values for **2** and **3** were held constant at the values reported previously; however, it was necessary to change the electronic coupling value for **1,** from that reported earlier, in order to obtain reasonable values of the reorganization energy and Gibbs energy change. Table 4.2 reports the best fitting parameters for the data of **1**, **2** and **3**. To be self consistent with earlier work, we have taken this new electronic coupling value for **1** and used it to fit our previous data in weakly polar and nonpolar solvents and were able to obtain reasonable fits; this analysis is provided in the Supplementary Material.

From the data at high temperature, it can be observed that the electron transfer rate of **2** is higher than **3** in NMP and **1** has the lowest electron transfer rate. This trend is consistent with the respective electronic coupling values reported in Table 4.2. The electronic coupling magnitude of **2** with a methoxy substituted pendant unit is highest among the three molecules.

This may be associated with the electron affinity.[13] The somewhat lower value for the t-butyl substituted pendant, as compared to the ethyl substituted pendant, could reflect a decrease in overlap that results from steric constraints.

Table 4.2 Fitting parameters for compound 1, 2 and 3 in NMP at 295K[a]

Compound	[b] $\lvert V \rvert$ (cm^{-1})	λ_0 [b] (eV)	$\Delta_r G$ [b] (eV)
1	90	1.24	-0.35
2	273	1.59	-0.57
3	147	1.50	-0.52

[a] Values of λ_V =0.63 eV and $\hbar\omega$ =1600 cm^{-1} are determined from charge-transfer spectra of related species. [b] Obtained from the fit keeping the electronic coupling $\lvert V \rvert$ same as obtained from previous study for **2** and **3** but modifying the value for **1**.

The reorganization energy and Gibbs free energy parameters reported in Table 4.2 vary somewhat among the three compounds, but this variation is within the error of fitting. If one assumes that the first term in the summation of Equation 1 dominates over the other terms in its contribution to the sum (hence the nonadiabatic rate constant), then the activation barrier for the reaction is $\Delta G^{\neq} = (\Delta_r G + \lambda_0)^2 / 4\lambda_0$. Using the parameters in Table 4.2, we find that the activation barrier ranges from 0.160 eV to 0.164 eV for these three compounds. The similarity in the activation barrier (and energetic parameters) is consistent with the similar size, shape, and chemical structure of the molecules. This similarity is found even though the rate constant data appear to deviate substantially from one another as the temperature changes.

The self-consistency of this analysis can be evaluated by considering the dependence of the rate constant on the solvation time, via Equation 6 (or 8). The different kinetic models predict that the electron transfer rate constant is inversely proportional to the solvation time when the reaction proceeds in the solvent friction regime, but that it becomes independent of solvent friction when the solvation time is rapid.

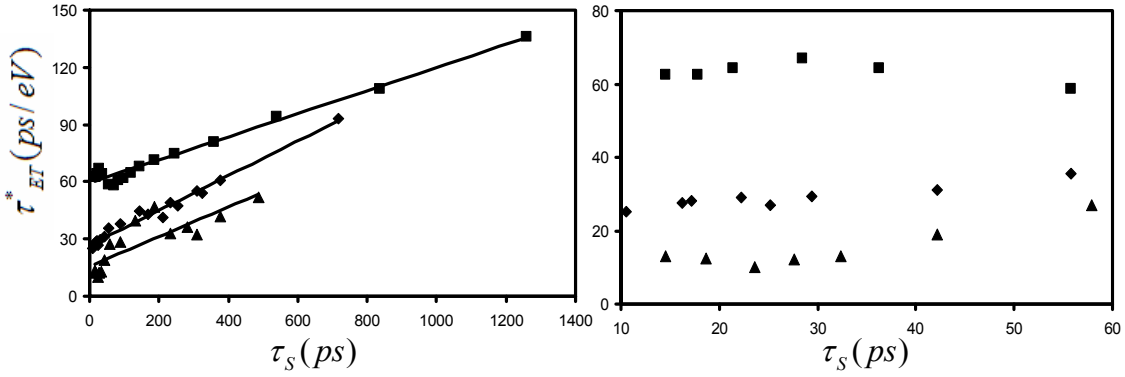

Figure 4.6 Plot of τ^*_{ET} versus τ_S for **1** (square), compound **2** (triangle) and compound **3** (diamond) in NMP. Panel A shows the plot over the whole range of data, and panel B expands the plot in the high temperature region $0 \le \tau_S \le 60$ ps (60 ps corresponds to the room temperature) for compound **1**, **2** and **3**.

Figure 4.6 plots the value of τ^*_{ET} for **1**, **2** and **3** in NMP versus the solvation time of NMP over the temperature range 250 to 350K. For all these systems a good linear correlation between τ^*_{ET} and the solvation time at low temperature is found in the range of large values of τ_S (> 60ps). The intercept from the fit to equation 6 gives an effective electronic coupling $|V_{eff}|$ = 22 cm^{-1}, 49 cm^{-1} and 28 cm^{-1} for compound **1**, **2** and **3** respectively. Using the fact that $|V| = |V_{eff}|.\exp\left(\frac{S}{2}\right)$ and S=3.2 (obtained from earlier studies using charge transfer spectra),

gives electronic coupling values of 109 cm^{-1} for **1**, 242 cm^{-1} for **2**, and 139 cm^{-1} for **3**. These values are derived by extrapolation from the data in the low temperature/solvent controlled limit (see Equations 6 and 8); yet they are in excellent agreement with those obtained by analysis over the whole temperature range using Eqn 2 (compare to values in Table 4.2) and to values obtained from studies in weakly polar and nonpolar solvents using Matyushov's molecular solvation model (see references 9 and 10).

The dependence of τ^*_{ET} on the solvation time τ_S was fit to Equation 6 and the slopes obtained are 0.061 eV^{-1}, 0.078 eV^{-1}, and 0.091 eV^{-1} respectively for **1**, **2**, and **3**. In contrast, a calculation of the slopes from the parameters in Table 2 gives 5.20 eV^{-1}, 4.57 eV^{-1} and 5.29 eV^{-1} for **1**, **2** and **3**. These calculated values are around 50 times bigger than those seen experimentally. Similarly the dependence of τ^*_{ET} on the solvation time τ_S was fit to equation 9 and the slopes obtained are 0.071 eV^{-1} for **1**, 0.079 eV^{-1} for **2**, and 0.089 eV^{-1} for **3** which are similar to the slopes obtained from Zusman model. The slopes obtained theoretically from equation 9 for **1**, **2**, and **3** are 5.63 eV^{-1}, 4.97 eV^{-1} and 5.12 eV^{-1} respectively which are also similar to those obtained from equation 6.

Although the Zusman and Mukamel models fail to predict the slope quantitatively, they each provide an accurate description of the data otherwise.

Adiabaticity Parameter

Zusman derived a criterion to assess whether the dynamic solvent effect is important in an electron transfer reaction. If the inequality

$$\frac{\pi^2 |V|^2 \tau_S}{\hbar \lambda_0} \exp(-S) >> \left(\sin \frac{\pi}{2} \left(\frac{\Delta_r G}{\lambda_0} + 1 \right) \right) \quad \textbf{11}$$

holds, then the solvent friction should be important. If the reaction occurs in the range of a small driving force, $|\Delta_r G| << \lambda_0$, and an effective electronic coupling can be defined as $|V_{eff}| = |V| \exp(-S/2)$, then equation 10 becomes $\frac{\pi^2 \tau_S |V_{eff}|^2}{\hbar \lambda_0} >> 1$. The dynamic solvent effect can be interpreted as a solvent driven change of adiabaticity in the reaction, characterized by an adiabaticity parameter g, where

$$g = \frac{|V_{eff}|^2 \pi^2 \tau_S}{\hbar \lambda_0} \quad \textbf{12}$$

When g >> 1, the reaction is solvent controlled, and when g << 1 no dynamic solvent effect is observed. Equation 11 shows that the crossover (g=1) between the nonadiabatic regime (g < 1) and the solvent controlled regime (g > 1) depends on τ_S, $|V_{eff}|$, and the solvent reorganization energy.

In the Mukamel model one can also define an adiabaticity parameter g_{SM}, which is given by

$$g_{SM} = \frac{|V|^2 \tau_S \sqrt{\pi}}{\hbar \sqrt{\lambda_0 k_B T}} \quad \textbf{13}$$

and depends on |V|, τ_S, and λ_0; however it scales as $1/\sqrt{\lambda_0}$ rather than $1/\lambda_0$. When g_{SM}<<1, Eqn 12 reduces to the semiclassical Eqn 1; and when g_{SM}>>1 the rate constant becomes $k_{ET} = \frac{1}{\tau_S} e^{-\Delta G^{\neq}/kT}$ so that the rate is controlled by the solvent relaxation time and the activation energy barrier.

Using the parameters in Table 4.2 and Eqn 12, the Zusman model predicts that dynamic solvent effect should manifest itself when τ_S >> 24 ps for compound **1**, τ_S >> 2 ps for compound **2,** and τ_S >> 6 ps for compound **3** in NMP. The experimental results (Figure 4) indicate that **2** and **3** are in the solvent controlled limit (coalescence of rates) when τ_S is near 56 ps which fulfills the Zusman condition. For **1** the solvent controlled limit is reached at around 240 ps, again fulfilling the Zusman condition. These comparisons show that the experimentally observed trend in the rate data can be understood via the Zusman model.

The adiabaticity parameter obtained from Mukamel model can be used to draw similar comparisons. In this case the model predicts that when τ_S >> 37 ps for compound **1**, τ_S >> 5 ps for compound **2,** and τ_S >> 12 ps for compound **3** in NMP. These values are little different from those obtained using the Zusman model.

Though the Zusman model and Mukamel analysis provide a very good agreement between the effective electronic coupling values obtained from the low temperature analysis with those obtained from equation 1 at high temperatures, they overestimate the scaling with the solvent response time (slopes in Figure 4.6A). This failure could result from our modeling of the characteristic polarization relaxation times τ_S and τ_a in those models. In both cases the polarization relaxation times were modeled as the correlation time found from dynamic Stokes Shifts measurements of a dye molecule in the solvent NMP. The solvation response in NMP is non-exponential, and it may be that the faster components of the solvation response control the electron transfer dynamics. If so, then the solvation time used here is too large by some factor and this could account for a decreased slope.

Two-Dimensional View of Reaction

In the Sumi-Marcus description the reaction rate is quantified by considering the average survival probability Q(t) of the locally excited state. Q(t) is the fraction of reactant molecules that have not transferred their electron by time *t*, and it can be obtained directly from the fluorescence decay law. They considered both the correlation time $\tau_c = \int_0^\infty Q(t)dt$ and the average decay time $\bar{\tau} = \frac{1}{\tau_c}\int_0^\infty tQ(t)\,dt$ to describe their results. These survival times

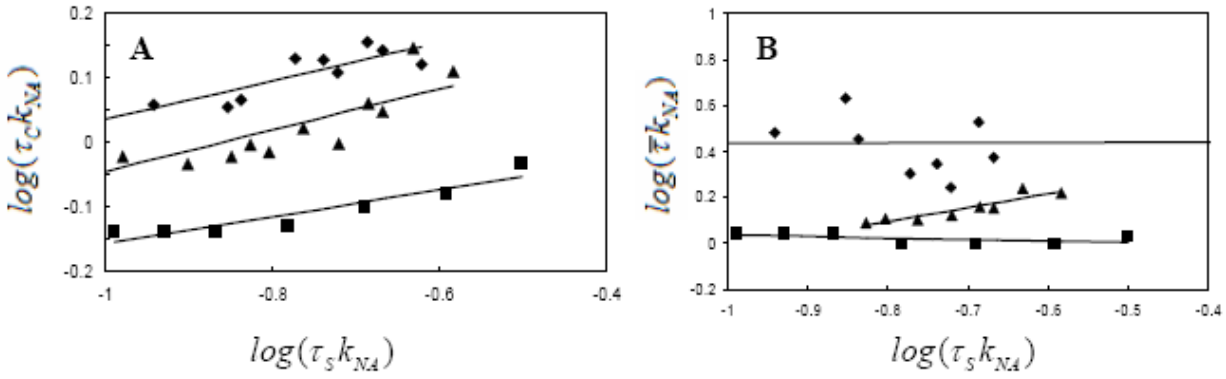

Figure 4.7 Plot of log ($\tau_c k_{NA}$) versus log $\tau_s k_{NA}$ for compound **1** (square), **2** (traingle) and compound **3** (diamond) in NMP (panel A). Plot of log ($\tau_S k_{NA}$) versus log $\tau_s k_{NA}$ for compound **1** (square), **2** (triangle) and compound **3** (diamond) in NMP (panel B). These plots show only the low temperature range. k_{NA} is extracted from the fit of the high temperature data to the nonadiabatic model.

provide valuable information about the timescale and temporal characteristic of the reaction rate. For example, if $\tau_c = \bar{\tau}$ then Q(*t*) is a single exponential decay, whereas $\tau_c \neq \bar{\tau}$ indicates a nonexponential decay law. Performing this analysis for the kinetics of **1, 2** and **3** in NMP,

substantiates the inferences drawn above and the manifestation of solvent friction effects. Figure 4.7 plots $\log(\tau_c k_{NA})$ (Panel A) and $\bar{\tau} k_{NA}$ (panel B) as a function of $\log(\tau_s k_{NA})$ in NMP for **1**, **2** and **3** over the low temperature range studied here. k_{NA} is extracted from the fit of the high temperature kinetic rate data to the nonadiabatic

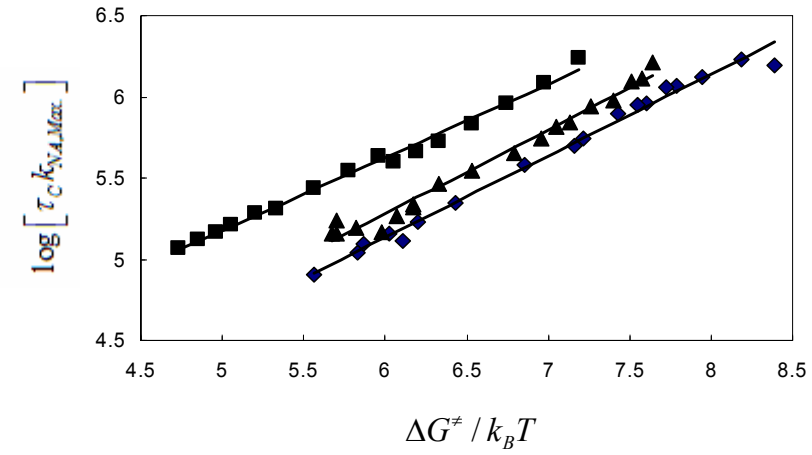

Figure 4.8 Plot of $\log(\tau_c k_{NA,Max.})$ versus $\Delta G^{\neq} / k_B T$ for compound **1** (square), **2** (triangle) and compound **3** (diamond) in NMP (panel B). k_{NA} is extracted from the fit of the high temperature data to the nonadiabatic model.

semiclassical electron transfer model. The shift of the solute data from one another may be understood from their different λ_v/λ_0 values as shown by Sumi and Marcus. In our study, because $\lambda_v/\lambda_0 \sim 0.5 < 1$ and $\exp(-\Delta G^{\neq} / k_B T) < 1$, the reaction proceeds in the narrow reaction window limit. According to Sumi, Marcus and Nadler, the log-log plots will be linear with a slope of unity in the classical limit ($\lambda_v/ \lambda_0 = 0$,), but the slope will lie between zero and 1 for different values of λ_v/λ_0. From the figure 4.7A it is clear that the product of τ_c and k_{ET} increase gradually as a function of $\tau_s k_{ET}$. The slope for compound **1**, **2** and **3** is 0.21, 0.32 and 0.30 respectively in Fig. 4.7A which is less than unity as predicted by Nadler and Marcus. In

Figure 4.7B the data points for **1** and **2** show a somewhat linear behavior which may suggest a weak solvent dynamic effect but for **3** the data are too scattered to draw a conclusion and it must be qualitative only.

To better understand the data in terms of the two-dimensional model Figure 4.8 plots of $\log(\tau_c k_{NA,Max.})$ as a function of $\Delta G^{\neq} / k_B T$ for compound **1**, **2** and **3** over the whole temperature range (Figure 4.8). $k_{NA,Max.}$ stands for the electron transfer rate constant evaluated from the semiclassical non-adiabatic electron transfer rate under zero activation barrier. According to the Sumi-Marcus model the plot in Figure 4.8 should be linear, as observed. The data for compounds **1**, **2** and **3** in Figure 4.8 have slopes ranging from about 0.45 to 0.52 which are less than unity, as predicted by Sumi and Marcus. These experimental findings indicate that the solvent response influences the electron transfer rate constant and that the effect becomes more pronounced with increasing solvent relaxation time at low temperature.

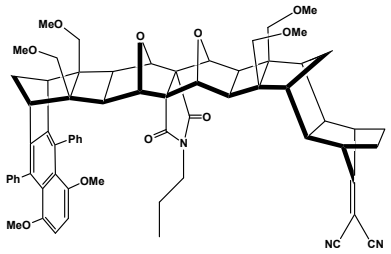

4, $|V| \sim 62$ cm^{-1}

Comparing **1**, **2**, and **3** with another previously studied molecule **4** (reported to have |V| = 62 cm^{-1}) shows a dependence of the observed dynamic solvent effect on the electronic coupling. In each case, the 'switchover' in mechanism is defined empirically as the temperature at which the rate constant of a solute molecule coincides with that of **2**. The switchover to a dynamic solvent effect for **4** in NMP was reported to occur when the $\tau_S \sim 309$ ps. For **1** the solvent controlled limit is reached at around 240 ps, and the switchover of mechanism from nonadiabatic to solvent controlled regime when the solvation time is near 56

ps for **2** and **3** (same ET rate). This comparison shows that with decreasing electronic coupling values (Table 4.2) a longer characteristic polarization relaxation time is required to observe a dynamic solvent effect.

4.5 Discussion and conclusion

This work explores the transition from nonadiabatic electron transfer to solvent controlled electron transfer for the U-shaped Donor-Bridge-Acceptor molecules **1**, **2** and **3** in NMP. The rate data were compared with models that interpolate between the nonadiabtic and solvent controlled limits; each of the models provides a semiquantitatively accurate description of the behavior in terms of a dynamic solvent effect, The solvent controlled limit is manifest even though the electronic couplings lie in the intermediate ($\left| V \right| \sim k_B T$) to weak ($\left| V \right| < k_B T$) coupling regime.

The electron transfer rate constants were fit by the Zusman model over the whole temperature range. Fitting the experimental rate data to the model was used to obtain the Gibbs free energy and the reorganization energy for compounds **1**, **2** and **3** in NMP (Table 2). As reported in the earlier work, the electron transfer rate constants fall below the nonadiabatic electron transfer rates predicted by the semiclassical equation.

The locally excited state's population decay changes from a single exponential decay at high temperature to a nonexponential decay which can be analyzed in terms of two exponentials at low temperature in these molecules. This observation indicates that the time evolution of the reactant population along X must be considered at low temperature and increasing solvation time This conclusion is supported by the difference between the

correlation time and average time (Figure 7) measures of the rate, as anticipated by the Sumi-Marcus model.

The low temperature rate constants for **1**, **2**, and **3** in NMP were compared to three different models for the solvent dynamical effect. Both Zusman's model[14-16] and Mukamel's model[17-18] predict that the rate constant should correlate with the characteristic time for the solvent polarization relaxation. The data were shown to correlate with the characteristic solvation rate, $1/\tau_s$ which was modeled for NMP by dynamic Stokes shifts measurements on a dye molecule. At high temperature the rate constant is found to be independent of $\tau_{s.}$ and at low temperature the rate constant scales linearly with $1/\tau_s$; see Figure 4.6. Quantitative comparisons with these models give an electronic coupling that is in good agreement with the value found using semiclassical electron transfer equation (equation 1) to fit the rate data at high temperatures. In addition, the models' criteria for 'adiabaticity' (g parameter) are satisfied, however the models' estimates of the characteristic time for the transition from nonadiabatic to solvent control (via the criterion of g=1) are somewhat weaker than what is found using the solvation time from the dynamic Stokes shift measurements. Although the plot of τ^*_{ET} versus the solvation time τ_s reveals a linear correlation at low temperatures, the slopes of the plot disagrees significantly from the theoretical prediction.

Different possibilities can be identified for the discrepancy between the predictions of Zusman's model and the observed dependence of τ^*_{ET} on τ_s. One possibility is that the solvation time obtained from the dynamic Stokes shift measurement.[5] The solvation response of NMP was found to be nonexponential, so that a correlation time for the response was calculated and used in the comparisons of Figure 4.6. It may be that this characteristic time is not appropriate for the electron transfer rate. For example, it may be that only a portion (e.g.,

the high frequency/short time components) of the response function is relevant for the electron transfer reaction. A second limitation of the Zusman and Mukamel treatments arises from their high friction (Smoluchowski) limit for the solvent frictional coupling. Recently, Gladkikh[23] et al extended Zusman's ideas to the intermediate friction regime and different barrier shapes. They found that the Zusman model overestimated the transfer rate by up to 10^3 and that the dynamics is a sensitive function of $|V|$ (or distance). Although quantitative details of these models may be questioned, they appear to capture the physical essence of the process and link with the correct nonadiabatic limit.

The electron transfer in **1**, **2** and **3** appears to lie in the narrow reaction window limit of the Sumi-Nadler-Marcus treatment. The ratio of $\lambda_v/\lambda_0 \sim 0.5$ and the nonexponentiality of the locally excited state's population decay support the interpretation that the reaction precedes in the narrow reaction window regime. In this limit, the electron transfer reaction occurs predominantly at a particular solvent polarization value of X_0 and the nonexponentiality arises from the time evolution of the reactant population along X. Other considerations of the Sumi-Marcus treatment, e.g. the electron transfer rate is proportional to the solvation rate, are similar to the Zusman prediction. The important difference between the two models in this limit is that Sumi-Marcus predicts a nonexponential decay law, as observed, whereas the Zusman and Mukamel treatments do not explicitly address this issue. The Sumi-Marcus treatment successfully explains the electron transfer behavior of **1**, **2** and **3** at low temperature in NMP, however it is difficult to draw direct quantitative comparisons with the model.

The characteristic solvation time required to observe the solvent dynamic effect increases with decreasing electronic coupling values. This can be explained from Zusman and

Mukamel model. According to equation 12 and 13 the τ_S should decrease with increasing electronic coupling $|V|$ in order to satisfy the criterion g=1.

By exploring the electron transfer dynamics of three different U-shaped molecules as a function of temperature in the slowly relaxing solvent NMP, the change in electron transfer mechanism from a nonadiabatic reaction to a friction controlled reaction is observed. Comparison to the different theoretical models indicates that the solvent dynamics plays a crucial important role in the electron transfer path. The observation that the decay law becomes nonexponential as the solvent relaxation time slows down supports the conclusion that solvent dynamics affect the electron transfer at lower temperature. This study also provides new insights into the factors governing the dynamics of electron transfer through non-bonded contacts in the solvent control limit.

4.6 Acknowledgement

This work was supported by the US National Science Foundation (CHE-0415457 and CHE-0718755) and by the Australian Research Council. The authors also thank Dr. R. A. Butera for technical assistance.

4.7 Appendix

Table 4.3 Fluorescence decay of 1 DBA molecules in toluene

T(K)	τ_1 (ps)	A_1 (%)	τ_2 (ps)	A_2 (%)	Donor τ (ps)	k_{ET} (s^{-1})
228	5198	45	2236	47	13755	$1.98 X10^8$
235	4588	27	1974	66	12349	$2.87 X10^8$
243	4687	13	1649	80	11007	$3.88 X10^8$
251	4613	9	1301	85	9889	$5.22 X10^8$
259	4824	6	1062	87	8947	$6.52 X10^8$
265	4582	5	950	88	8240	$7.51 X10^8$
271	4054	5	836	88	7793	$8.61 X10^8$
275	5358	7	784	88	7429	$7.53 X10^8$
284	4879	7	646	88	6628	$9.14 X10^8$
295	3972	7	512	89	5782	$1.15 X10^9$
308	3171	7	408	88	5056	$1.48 X10^9$
315	3101	7	383	88	4703	$1.54 X10^9$
324	2719	6	337	89	4266	$1.79 X10^9$
331	2419	6	315	90	4027	$1.95 X10^9$
338	2289	7	281	89	3766	$2.09 X10^9$
347	1969	6	276	90	3513	$2.32 X10^9$

Table 4.4 Fluorescence decay of 2 DBA molecules in NMP

2 in NMP excited at 330nm

T(K)	τ_1 (ps)	A_1 (%)	τ_2 (ps)	A_2 (%)	Donor τ (ps)	k_{ET} (s^{-1})
245	4381	27	1547	63	11710	3.33×10^8
250	3739	31	1449	57	10767	3.52×10^8
254	3114	22	1107	68	10094	5.27×10^8
260	2837	14	916	75	9197	7.13×10^8
265	2044	21	832	66	8541	7.70×10^8
270	2341	11	717	78	7955	9.69×10^8
276	2664	7	622	83	7349	1.14×10^9
283	2327	6	523	84	6711	1.39×10^9
294	2154	6	410	85	5873	1.73×10^9
311	641	5	324	83	4849	2.73×10^9
316	614	7	271	83	4606	3.16×10^9
321	466	7	166	80	4391	3.99×10^9
337	365	7	155	80	4211	4.10×10^9

Table 4.5 Fluorescence decay of 2 DBA molecules in NMP

3 in NMP excited at 330nm

T(K)	τ_1 (ps)	A_1 (%)	τ_2 (ps)	A_2 (%)	Donor τ (ps)	k_{ET} (s^{-1})
232	4124	42	1958	52	12922	2.65×10^8
238	5658	13	1811	84	11817	3.44×10^8
245	6021	8	1444	89	10709	4.54×10^8
250	4124	10	1435	84	9974	4.84×10^8
253	6506	6	1148	91	9638	5.72×10^8
254	3979	8	1248	86	9650	5.75×10^8
258	4422	6	1002	89	8973	7.19×10^8
260	6211	5	912	92	8840	7.23×10^8
262	2722	6	872	88	8585	8.85×10^8
267	3854	4	813	89	8187	9.36×10^8
271	5149	4	725	92	7554	9.56×10^8
283	4021	4	518	93	6651	1.37×10^9
295	3456	3	420	93	5818	1.73×10^9
304	2989	3	338	94	5245	2.15×10^9
314	2659	3	290	94	4647	2.52×10^9
324	2253	3	242	94	4203	3.01×10^9
333	2119	3	224	94	3798	3.26×10^9

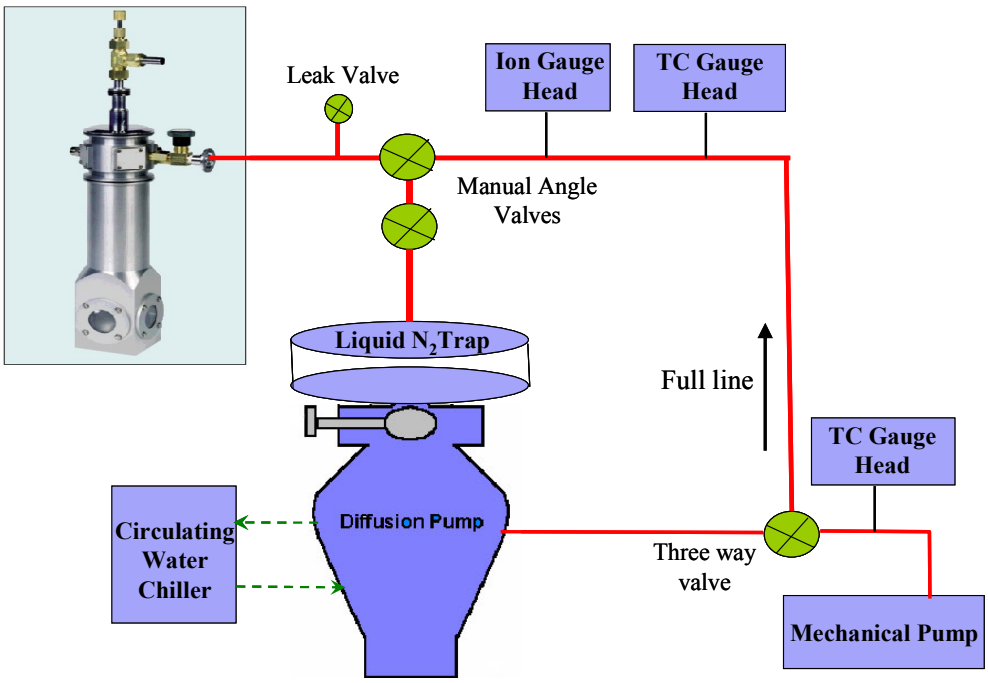

Figure 4.9 Cryostat Low Temperature Instrument

4.8 References

(1) Su, S.-G.; Simon, J. D. *J. Chem. Phys.* **1988**, *89*, 908.

(2) Okada, A. *J. Phys. Chem. A* **2000**, *104*, 7744.

(3) McGuire, M.; McLendon, G. *J. Phys. Chem.* **1986**, *90*, 2549.

(4) Liu, M.; Waldeck, D. H.; Oliver, A. M.; Head, N. J.; Paddon-Row, M. N. *J. Am. Chem. Soc.* **2004**, *126*, 10778.

(5) Liu, M.; Ito, N.; Maroncelli, M.; Waldeck, D. H.; Oliver, A. M.; Paddon-Row, M. N. *J. Am. Chem. Soc.* **2005**, *127*, 17867-17876.

(6) Napper, A. M.; Read, I.; Waldeck, D. H.; Head, N. J.; Oliver, A. M.; Paddon-Row, M. N. *J. Am. Chem. Soc.* **2000**, *122*, 5220.

(7) Napper, A. M.; Head, N. J.; Oliver, A. M.; Shephard, M. J.; Paddon-Row, M. N.; Read, I.; Waldeck, D. H. *J. Am. Chem. Soc.* **2002**, *124*, 10171.

(8) Zimmt, M. B.; Waldeck, D. H. *J. Phys. Chem. A* **2003**, *107*, 3580.

(9) Liu, M.; Chakrabarti, S.; Waldeck, D. H.; Oliver, A. M.; Paddon-Row, M. N. *Chemical Physics* **2006**, *324*, 72.

(10) Chakrabarti, S.; Liu, M.; Waldeck, D. H.; Oliver, A. M.; Paddon-Row, M. N. *J. Am. Chem. Soc.* **2007**, *129*, 3247.

(11) Read, I.; Napper, A.; Zimmt, M. B.; Waldeck, D. H. *J. Phys. Chem. A* **2000**, *104*, 9385.

(12) Matyushov, D. V.; Voth, G. A. *J. Chem. Phys.* **1999**, *111*, 3630.

(13) Gupta, S.; Matyushov, D. V. *J. Phys. Chem. A* **2004**, *108*, 2087.

(14) Zusman, L. D. *Electrochimica Acta* **1991**, *36*, 395.

(15) Zusman, L. D. *Chemical Physics* **1980**, *49*, 295.

(16) Zusman, L. *J. Chem. Phys.***1995**, *102*, 2580.

(17) Sparpaglione, M.; Mukamel, S. *J. Chem. Phys.* **1988**, *88*, 3263.

(18) Sparpaglione, M.; Mukamel, S. *J. Chem. Phys.* **1988**, *88*, 4300.

(19) Ponnu, A.; Sung, J.; Spears, K. G. *J. Phys. Chem. A* **2006**, *110*, 12372.

(20) Moran, A. M.; Aravindan, P.; Spears, K. G. *J. Phys. Chem. A* **2005**, *109*, 1795.

(21) Sumi, H.; Marcus, R. A. *J. Chem. Phys.* **1986**, *84*, 4894.

(22) Nadler, W.; Marcus, R. A. *J. Chem. Phys.* **1987**, *86*, 3906.

(23) Gladkikh, V.; Burshtein, A. I.; Rips, I. *J. Phys. Chem. A* **2005**, *109*, 4983.

5.0 CHAPTER FIVE

Experimental Demonstration of Water Mediated Electron-Transfer through Bis-Amino Acid Donor-Bridge-Acceptor Oligomers

This work has been submitted as Chakrabarti, S.; Parker, F. L. M.; Morgan, C.; Schafmeister, C. E.; Waldeck, D. H. to J. Am. Chem. Soc.

This work compares the photo-induced unimolecular electron transfer rate constants for two different molecules (**D-SSS-A** and **D-RRS-A**) in water and DMSO solvents. The **D-SSS-A** solute has a cleft between the electron donor and electron acceptor unit, which is able to contain a water molecule but is too small for DMSO. The rate constant for **D-SSS-A** in water is significantly higher than that for **D-RRS-A**, which lacks a cleft, and significantly higher for either solute in DMSO. The enhancement of the rate constant is explained by an electron tunneling pathway that involves water molecule(s).

Water molecules influence electron transport in biomolecules and play a key role in biologically vital processes in living cells.[1-3] The importance of water in determining the activation energy for electron transfer (ET) reactions is well appreciated. Recent theoretical work shows that placement of a few water molecules between electron donor and acceptor moieties can change the electronic tunneling probability between them.[4-6] Although some experimental studies investigate electron tunneling in frozen water,[7,8] an experimental study

of electron tunneling through water molecules under ambient conditions is lacking. This work investigates the role of water molecules by studying the photoinduced electron transfer rate in two Donor-Bridge-Acceptor (DBA) bis-amino acid oligomers that contain a keto pyrene group as an acceptor unit and dimethylaniline (DMA) as a donor unit in water and DMSO. The DBA molecules differ by their bridge stereochemistry (Figure 5.1). One amide rotamer of the **D-SSS-A** bridge forms a cleft between the donor and acceptor whereas the **D-RRS-A** bridge geometry does not form any well defined cleft. Here SSS and RRS indicate the stereochemistry at the 2 and 4 positions of the pyrrolidine ring and at the α-carbon of the dimethylalanine residue, respectively. This difference in geometry also provides two different "*line-of-sight*" donor to acceptor distances 4.6 Å and 9.7 Å, respectively, but the same number and types of covalent bonds through the bridge.[9]

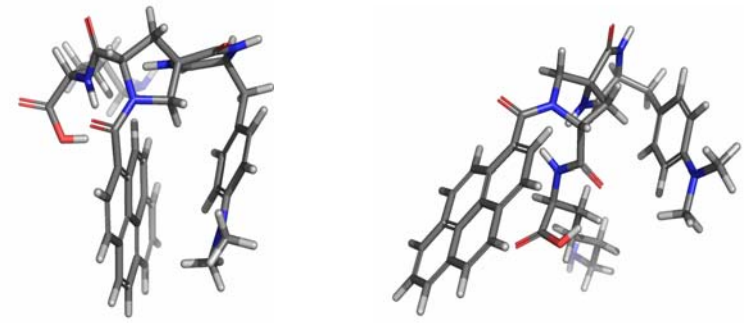

D-SSS-A **D-RRS-A**

Figure 5.1 Bis-Amino acid Donor-Bridge-Acceptor molecules with different bridge stereochemistry.

Earlier work in organic solvents shows that photoinduced electron transfer in DBA supermolecules with a cleft between the donor and acceptor moieties can proceed by electron tunneling through solvent molecules residing in the cleft.[10-13] The ET rates of the two compounds in Figure 1 were studied in two different solvents, water and dimethyl sulfoxide (DMSO), as a function of temperature to probe the effect of water molecules on the ET kinetics and compare to DMSO as a 'control' solvent. Synthesis of the bis-amino acid oligomers with different length has been reported elsewhere[14] (see the supporting information). The molecules in Figure 5.1 have the same donor and acceptor unit, and ET occurs when the keto-pyrene moiety is electronically excited by 330 nm light. This donor and acceptor pair has been used for intramolecular ET studies in different organic solvents in the past.[15,16] The pH of the water solution was kept ~7 to avoid any protonation of the amine group of the dimethylaniline donor unit.[17]

Two decay times were observed for these molecules. We assume that the longer decay time may be coming from either the acceptor-only impurity present in the solution or from the less populated conformers where the donor and acceptor are far apart from each other. This study uses the short decay time to evaluate the electron transfer rate constant which is the characteristic of the more populated conformer with a cleft (Fig. 1). Details can be found in the Appendix section.

The electron transfer rate constants as a function of temperature are shown in Figure 5.2 for the two **DBA** compounds in water and DMSO. The rate constant in **D-SSS-A** is about three times larger in water than in DMSO and is three times larger than the rate constant measured in **D-RRS-A**. In each solvent system, the ET rate displays a temperature

dependence, and the activation energies are very similar (ranging from 1.5 kJ/mol to 2.1 kJ/mol.

The electron transfer rate constants as a function of temperature are shown in figure 5.3 for the two **DBA** compounds in water and DMSO. The rate constant in **D-SSS-A** is about three times larger in water than in DMSO and is three times larger than the rate constant measured in **D-RRS-A**. In each solvent system, the ET rate displays a temperature dependence, and the activation energies are very similar (ranging from 1.5 kJ/mol to 2.1 kJ/mol).

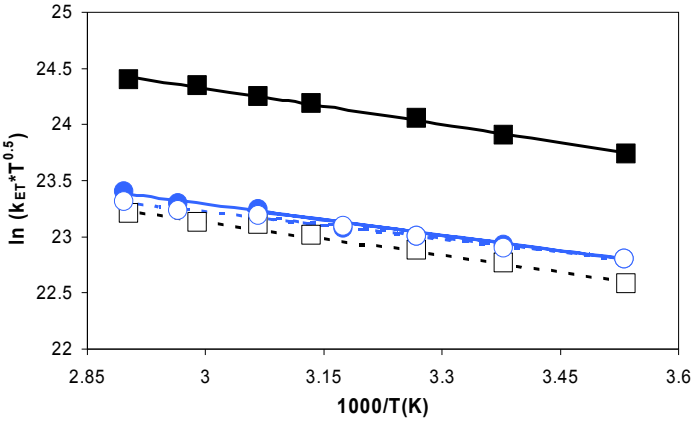

Figure 5.2 These plots show the temperature dependence of the ET rate constant k_{ET} in two solvents: **D-SSS-A** in water (black closed square) and DMSO (blue closed circle); **D-RRS-A** in water (black open square) and DMSO (blue open circle). The solid lines represent k_{ET} predicted from Marcus semiclassical ET equation.

The semiclassical electron transfer theory expresses the electron transfer rate constant as the product of the square of the electronic coupling, $|V|^2$, and the Franck-Condon weighted density of states (FCWDS). Using the semiclassical Marcus equation[18,19] to calculate the rate

constant requires knowledge of the electronic coupling (|V|), the Gibbs free energy (ΔG), the solvent reorganization energy (λ), and the internal reorganization energy parameters.[20,21] The internal reorganization energy parameters (λ_V and ν) are primarily determined by the molecular characteristics of the donor and acceptor, and the values for pyrene and dimethylaniline were taken from a previous study[15] to be λ_V = 0.19 eV and ν = 1400 cm^{-1}. The lines show fits of the experimental rate data to this model. This analysis considers the Gibbs energy and the electronic coupling |V| as adjustable parameters. The solvent reorganization energy λ_S was calculated using a continuum model.[22,23] The values for the reorganization energies were kept constant throughout the analysis; i.e., no temperature dependence was included.

The electronic coupling and the Gibbs energy obtained from the fit is reported in Table 5.1. The Gibbs energy is found to be more negative for compound **D-SSS-A** than **D-RRS-A** in water and DMSO. The difference in Gibbs energy for **D-SSS-A** and **D-RRS-A** likely reflects the difference in Coulomb stabilization in the charge separated state, however an accurate assessment will require modeling that includes the electrostatic properties and polarizability of the solvent molecules, as well as the solute.[24,25] The electronic coupling obtained from the ET rate in DMSO solvent are very close for the two solutes; however, the electronic coupling value obtained for **D-SSS-A** in water is significantly higher than that found for **D-RRS-A** in water. In each of the cases the coupling values are modest and consistent with a nonadiabatic coupling mechanism.

Table 5.1 Electron transfer parameters ($|V|$, ΔG, λ_{Total}) and rotamer populations for **D-SSS-A** and **D-RRS-A**

DBA	Solvent	$\|V\|$ (cm-1)	ΔG (eV)	λ_0 (eV)
D-SSS-A	H2O	22	-1.12	1.42
D-RRS-A	H2O	11	-0.86	1.14
D-SSS-A	DMSO	8	-0.83	1.12
D-RRS-A	DMSO	7	-0.64	0.91

[a] Population ratio of two amide rotamers at 330 – 333K

One-dimensional proton nuclear magnetic resonance experiments indicate that D-SSS-A in both D_2O and DMSO and D-RRS-A in D_2O at 330 - 333 K each occupy two rotameric conformations with essentially identical population ratios (see Table 1). In both solvents, the more populated conformation of D-SSS-A is the cleft conformation shown in figure 1, in which the pyrene is rotated close to the dimethylaniline hydrogens indicated by the upfield chemical shifts of the DMA peaks. This indicates that the conformational preferences of the DBA molecules at these temperatures is solvent independent and thus the difference in ET rate must be caused by other factors.

Two different mechanisms can be proposed to explain the higher |V| found for the **D-SSS-A** in water system. The similarity of the electronic coupling for **D-RSS-A** in DMSO and water suggests that the coupling is determined by a bridge-mediated superexchange interaction, hence it is solvent independent. In contrast, the cleft molecule **D-SSS-A** shows a solvent dependence (a larger |V| for water than for DMSO). Taking the donor to acceptor

distance of 4.5 Å and accounting for their π-cloud extents, the space available in the cleft is about 1.2 Å.[27] This value is comparable to the van der Waals radius of a water molecule (*ca.* 1.4 Å) but significantly smaller than that of a DMSO molecule (*ca.* 2.5 Å).[28] Hence we postulate that for DMSO the electron tunneling must occur through the 'empty' cleft or by way of the bridge, whereas in water a solvent molecule can reside in the cleft and mediate the electron tunneling or bind alongside the cleft to act as a bridge between the donor and acceptor. The enhancement in |V| for **D-SSS-A** in water, over that for **D-RRS-A**, may reflect a change in the tunneling pathway from a bridge mediated process to electron tunneling by way of the solvent molecule in the cleft between the donor and acceptor unit. An alternative mechanism to explain the observations involves proton motion that is coupled to the ET;[29-31] i.e., a proton coupled electron transfer (PCET). In this mechanism the electron transfer occurs through a hydrogen bond network between the donor and acceptor. To evaluate this possibility, the ET rate was measured for these two DBA compounds in deuterium oxide (D_2O). A significant normal kinetic isotope effect was observed ($k_{ET,\ H2O}/k_{ET,\ D2O} = 1.49$ for **D-SSS-A** and $k_{ET,\ H2O}/k_{ET,\ D2O} = 1.17$ for **D-RRS-A** at 295K). Both molecules display an isotope effect, however it is more pronounced in **D-SSS-A.** The detailed origin of the enhancement of the rate for **D-SSS-A** in water requires further investigation.

Whichever of the above mentioned mechanisms is operative, it seems clear that electron transfer for **D-SSS-A** involves one or more water molecules as part of the reaction path. The observation of an isotope effect that is stronger for the **D-SSS-A** system than for the **D-RRS-A** system suggests that hydrogen bonded network(s) involving protons play an important role in the reaction. It is expected that the hydrogen bond networks could be quite different for the two solutes. Because the ET rate is significantly higher for **D-SSS-A** in water than for **D-**

RRS-A in water, and either solute in DMSO, suggests that water molecules play a special role for the **D-SSS-A**. A comparison of the solvent molecule size to the size of the cleft suggests that the electron transfer may occur by tunneling directly from the donor to the acceptor by way of a water molecule in the cleft, rather than by way of the DBA molecule's bridge. In terms of the semiclassical model, the higher ET rate constant for **D-SSS-A** in water as compared to DMSO can be attributed to a higher electronic coupling. An analysis using this model and a dielectric continuum description for the solvent reorganization energy indicates that the electronic coupling values for **D-RRS-A** and for either solute in DMSO are very similar (see Table 1), whereas that for **D-SSS-A** in water is three times larger. These experimental results in water substantiate earlier theoretical predictions that water molecules located in the vicinity of donor and acceptor units can mediate the electronic coupling; i.e., the electron transfer proceeds by tunneling through water molecule(s).

5. 2 Acknowledgement

We acknowledge financial support from the US National Science Foundation (CHE-0415457 and CHE-0718755).This research was supported by the NIH/NIGMS (GM067866) to C.E.S.

5. 3 Appendix

General Methods.

Pro4ss and Pro4rr (see supplemental figure 1) were synthesized according to literature procedure Anhydrous N-methylpyrrolidinone, Anhydrous Dimethylformamide, Anhydrous Dichloromethane, redistilled Diisopropylethylamine,Tetrakis(triphenylphosphine)palladium0, Borane:dimethylamine complex, Pyrenecarboxylic acid, Allyl chloroformate, and 37% Formaldehyde solution were purchased from Aldrich. Tetrahydrofuran, Triethylamine and Trifluoroacetic acid were purchased from Alfa Aesar. Palladium on Carbon and HATU were purchased from Genscript, Fmoc-4-nitrophenylanaline was purchased from TCI organics. Fmoc-Lys(Boc)-OH was purchased from Novabiochem.

Flash Chromatography was perfored on an ISCO CombiFlash Companion with cartridges filled with Bodman 32-63 D (60Å) grade silica gel.

Analytical HPLC-MS analysis was performed on a Hewlett-Packard Series 1200 with a Waters Xterra MS C18 column (3.5um packing, 4.6 mm x 100mm) with a solvent system of water/acetonitrile with 0.1% formic acid at a flow rate of 0.8mL/min.

Preparatory Scale HPLC purification was performed on a Varian Prostar Prep HPLC with a Waters Xterra column (5um packing, 19mm x 100mm) with a solvent system of water/acetonitrile with 0.1% formic acid at a flow rate of 12mL/min.

NMR experiments were performed on a Bruker 500mHz NMR with a chemical shifts (δ) reported relative to DMSO-d6 or $CDCl_3$ residual solvent peaks.

HRESIQTOFMS analysis was performed by Ohio State University.

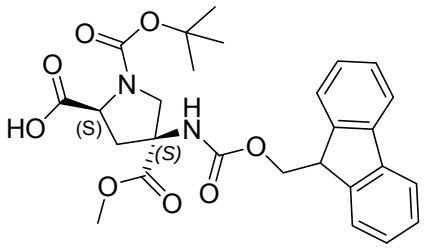

Pro4ss

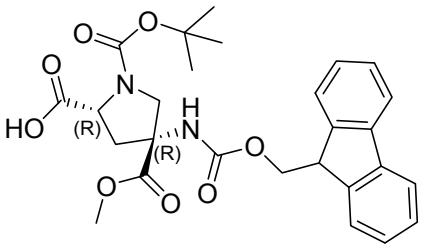

Pro4rr

Structures of Pro4ss and Pro4rr

Synthetic Methods.

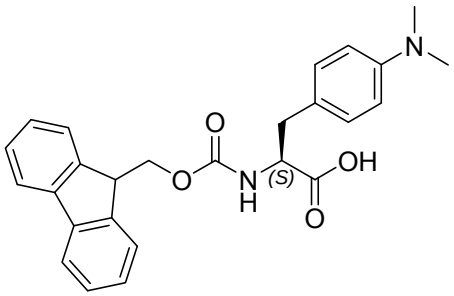

(S)-2-(((9H-Fluoren-9-yl)methoxy)carbonylamino)-3-(4-(dimethylamino)phenyl)propanoic acid (sc1)

(S)-2-(((9H-Fluoren-9-yl)methoxy)carbonylamino)-3-(dimethylamino)phenyl)propanoic acid (sc1):

To a solution of Fmoc-4-nitrophenylanaline (1g, 2.3mmoles) in tetrahydrofuran/methanol (46mL, 1:1) was added 37% Formaldehyde (aq) (480uL, 4.6mmoles) followed by 69 mg of Palladium on Carbon. The reaction mixture was then degassed under vacuum, charged with H_2 (g), stirred overnight, concentrated under reduced pressure and purified by chromatography on silica (gradient elution over 16 column volumes from dichloromethane to 5% methanol in dichloromethane. Desired fractions were combined

and concentrated under reduced pressure to yield (sc1) as a dark yellow solid (860 mg, 2.0mmoles, 87%). Purity was assessed by analytical HPLC-MS (See Supplementary Figure 1) ^{1}H NMR (500 MHz, rt, $CDCl_3$): δ 9.19 (br s, 1H), 7.77 (d, J = 7.55 Hz, 2H), 7.60 (t, J = 6.95 Hz, 2H), 7.41 (t, J = 7.40 Hz, 7.45 Hz, 2H), 7.32 (t, J = 7.40 Hz, 7.45 Hz, 2H), 7.10 (d, J = 8.20 Hz, 2H), 6.86 (d, J = 8.20 Hz, 2H), 5.53 (d, J = 7.65 Hz, 1H), 4.66 (q, J = 7.30 Hz, 3.00 Hz, 7.30 Hz, 1H), 4.35 (q, J = 7.30 Hz, 3.00 Hz, 7.30 Hz, 1H), 4.22 (t, J = 7.00 Hz, 7.00 Hz, 1H), 3.18 (m, 2H), 2.89 (s, 6H); HRESIQTOFMS calcd for $C_{26}H_{27}N_2O_4$ ($M + H^+$) 431.1971, measured 431.1967 (0.9ppm).

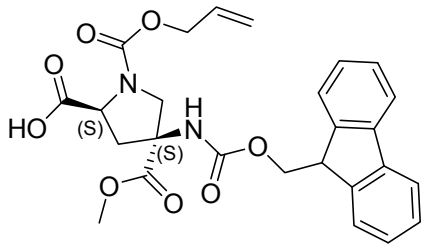

(2S,4S)-4-(((9H-fluoren-9-yl)methoxy)carbonylamino)-1-(allyloxycarbonyl)-4-(methoxycarbonyl) pyrrolidine-2-carboxylic acid (sc2)

(2S,4S)-4-(((9H-fluoren-9-yl)methoxy)carbonylamino)-1-(allyloxycarbonyl)-4-(methoxy carbonyl) pyrrolidine-2-carboxylic acid (sc2):

To a solution of Pro4ss (1g, 1.96mmoles) in dichloromethane (14mL) was added trifluoroacetic acid (6mL). The reaction mixture was stirred for 4 hours then concentrated under reduced pressure. The residue was dissolved in tetrahydrofuran (10mL). Triethylamine (820uL, 5.88mmoles) was added followed by Allyl chloroformate (230uL, 2.15mmoles). The

reaction mixture was stirred overnight, cooled to 0°C, and acidified with 6M hydrochloric acid. The product was extracted with ethyl acetate. The organic portions were combined, washed with brine, dried over sodium sulfate, filtered, concentrated under reduced pressure and purified by chromatography on silica (gradient elution over 16 column volumes from dichloromethane to 5% methanol in dichloromethane. Desired fractions were combined and concentrated under reduced pressure to yield (sc2) as a light yellow solid (914mg, 1.85mmoles, 94%). ^{1}H NMR (500 MHz, rt, DMSO-d6): δ 8.49 (bs, 1H), 8.11 (d, J = 7.45 Hz, 2H), 7.92 (d, J = 7.05 Hz, 2H), 7.64 (t, J = 7.30 Hz, 7.4 Hz, 2H), 7.56 (t, J = 7.30 Hz, 7.20 Hz, 2H), 6.17 (m, 1H), 5.52 (t, J = 16.7 Hz, 16.7 Hz, 1H), 5.43 (dd, J = 10.5 Hz, 17.9 Hz, 10.5 Hz, 1H), 4.77 (m, 2H), 4.54 (m, 4H), 4.29 (dd, J = 11.2 Hz, 24.2 Hz, 11.2 Hz, 1H), 3.82 (s, 3H), 3.80 (m, 1H), 3.11 (m, 1H).

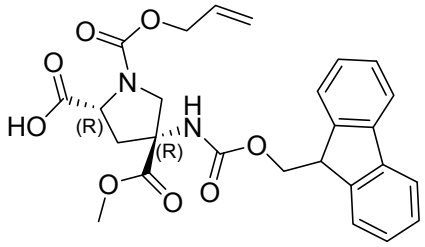

(2R,4R)-4-(((9H-fluoren-9-yl)methoxy)carbonylamino)-1-(allyloxycarbonyl)-4-(methoxycarbonyl) pyrrolidine-2-carboxylic acid (sc3)

(2R,4R)-4-(((9H-fluoren-9-yl)methoxy)carbonylamino)-1-(allyloxycarbonyl)-4-(methoxy carbonyl) pyrrolidine-2-carboxylic acid (sc3):

To a solution of Pro4rr (1g, 1.96mmoles) in dichloromethane (14mL) was added trifluoroacetic acid (6mL). The reaction mixture was stirred for 4 hours then concentrated under reduced pressure. The residue was dissolved in tetrahydrofuran (10mL). Triethylamine

reaction mixture was stirred overnight, cooled to 0°C, and acidified with 6M hydrochloric acid. The product was extracted with ethyl acetate. The organic portions were combined, washed with brine, dried over sodium sulfate, filtered, concentrated under reduced pressure and purified by chromatography on silica (gradient elution over 16 column volumes from dichloromethane to 5% methanol in dichloromethane. Desired fractions were combined and concentrated under reduced pressure to yield (sc3) as a light yellow solid (882mg, 1.78mmoles, 91%). ^{1}H NMR (500 MHz, rt, DMSO-d6): δ 8.49 (bs, 1H), 8.11 (d, J = 7.45 Hz, 2H), 7.92 (d, J = 7.05 Hz, 2H), 7.64 (t, J = 7.30 Hz, 7.4 Hz, 2H), 7.56 (t, J = 7.30 Hz, 7.20 Hz, 2H), 6.17 (m, 1H), 5.52 (t, J = 16.7 Hz, 16.7 Hz, 1H), 5.43 (dd, J = 10.5 Hz, 17.9 Hz, 10.5 Hz, 1H), 4.77 (m, 2H), 4.54 (m, 4H), 4.29 (dd, J = 11.2 Hz, 24.2 Hz, 11.2 Hz, 1H), 3.82 (s, 3H), 3.80 (m, 1H), 3.11 (m, 1H).

General procedure(A): attachment to Wang resin:

To a solution of the amino acid (10 equivalents based on resin loading) in dichloromethane (3mL/mmole of amino acid) was added diisopropylcarbodiimide (5 equivalents based on resin loading). The reaction mixture was allowed to stir for 30 minutes, concentrated under reduced pressure, reconstituted in dimethylformamide (5mL/mmole of amino acid) and added to a pre-swelled (in dimethylformamide) portion of resin in a solid phase reactor. To this solution was added dimethylaminopyridine (0.1 equivalents based on amino acid). The reaction mixture was stirred for 1 hour. The resin was filtered and washed with dimethylformamide, isopropanol, and dimethylformamide.

General procedure (B): HATU (2-(7-Aza-1H-benzotriazole-1-yl)-1,1,3,3-tetramethyluronium hexafluorophosphate) coupling:

To a solution of amino acid (3 equivalents based on resin loading) and HATU (3 equivalents based on resin loading in N-methylpyrrolidine (5mL/mmole of amino acid) was added diisopropylethylamine (6 equivalents based on resin loading). The reaction mixture was added to a pre-swelled (in dimethylformamide) portion of resin in a solid phase reactor and stirred for 45 minutes. The resin was filtered and washed with dimethylformamide, isopropanol, and dimethylformamide.

General procedure (C): Fmoc deprotection:

A solution of 20% of piperidine in dimethylformamide (15mL/mmole based on resin loading) was added to a pre-swelled (in dimethylformamide) portion of resin in a solid phase reactor and stirred for 15 minutes. The resin was filtered and washed with dimethylformamide, isopropanol, and dimethylformamide.

General procedure (D): Alloc deprotection:

A solution of borane:dimethylamine complex (6 equivalents based on resin loading) in dichloromethane (10mL/mmole based on resin loading) was added to a pre-swelled (in dimethylformamide) portion of resin in a solid phase reactor and stirred for 5 minutes. To this solution was added a solution of tetrakis(triphenylphosphine)palladium0 (0.1 equivalents based on resin loading) in dichloromethane (10mL/mmole based on resin loading). The reaction mixture was stirred for 1 hour. The resin was filtered and washed with dimethylformamide, isopropanol, and dimethylformamide.

General procedure (E): liberation from Wang resin:

A solution of 5% triisopropylsilane and 5% water in trifluoroacetic acid (25 mL/mmole based on resin loading was added to a portion of resin (successively washed with dichloromethane and methanol, and thoroughly dried under vacuum) and stirred for 4 hours. The resin was filtered and washed with trifluoroacetic acid. The filtrate was concentrated, reconstituted in 75% acetonitrile in water (0.05% formic acid) and freeze-dried.

Solid Phase Oligomer Assembly

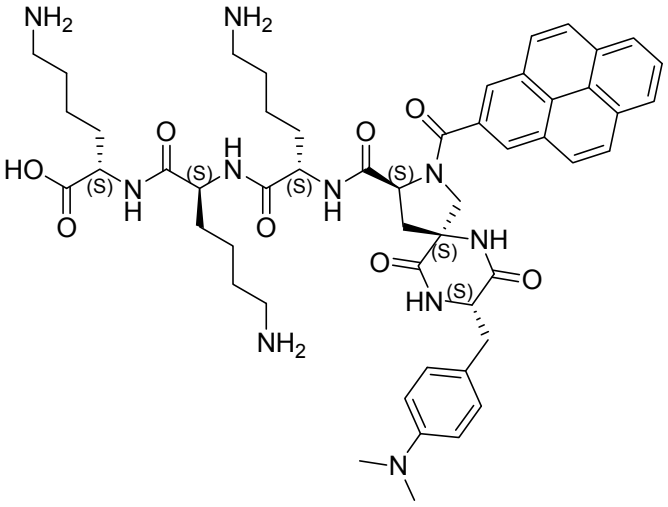

D-SSS-A (sc4)

D-SSS-A (sc4):

Wang resin (200mg, 150umoles loading) was placed in a 15mL solid phase reactor. Fmoc-Lys(Boc)-OH (703mg, 1.5mmoles) was attached according to general procedure (A) using dichloromethane (4.5mL), diisopropylcarbodiimide (116uL, 750umoles), dimethylformamide (4.5mL), and dimethylaminopyridine (18.3mg, 150umoles). The terminal Fmoc group was removed according to general procedure (C) using 20% piperidine in dimethylformamide (2.25mL).

Fmoc-Lys(Boc)-OH (211mg, 450umoles) was coupled according to general procedure (B) using HATU (171mg, 450umoles), N-methylpyrrolidinone (2.25mL), and diisopropylethylamine (156uL, 900umoles). The terminal Fmoc group was removed according to general procedure (C) using 20% piperidine in dimethylformamide (2.25mL).

Fmoc-Lys(Boc)-OH (211mg, 450umoles) was coupled according to general procedure (B) using HATU (171mg, 450umoles), N-methylpyrrolidinone (2.25mL), and diisopropylethylamine (156uL, 900umoles).

(sc2) (223mg, 450umoles) was coupled according to general procedure (B) using HATU (171mg, 450umoles), N-methylpyrrolidinone (2.25mL), and diisopropylethylamine (156uL, 900umoles). The terminal Fmoc group was removed according to general procedure (C) using 20% piperidine in dimethylformamide (2.25mL).

Fmoc-DMA-OH (sc1) (194mg, 450umoles) was coupled according to general procedure (B) using HATU (171mg, 450umoles), N-methylpyrrolidinone (2.25mL), and diisopropylethylamine (156uL, 900umoles). The terminal Fmoc group was removed according to general procedure (C) using 20% piperidine in dimethylformamide (2.25mL) and the reaction time was extended to 1 hour.

The Alloc group was removed according to general procedure (D) using borane:dimethylamine complex (53mg, 900umoles) in dichloromethane (2.5mL) and tetrakis(triphenylphosiphine)palladium0 (17mg, 15umoles) in dichloromethane (2mL). Pyrenecarboxylic acid (111mg, 450umoles) was coupled according to general procedure (B) using HATU (171mg, 450umoles), N-methylpyrrolidinone (2.25mL), and diisopropylethylamine (156uL, 900umoles).

(sc4) was liberated from the resin according to general procedure (E) using 3.75 mL of the cleavage cocktail. The residue was reconstituted in 75% acetonitrile in water (0.05% formic acid) and purified by reverse-phase chromatography (gradient elution over 30 minutes from water (0.1% formic acid) to 50% acetonitrile (0.05% formic acid) in water (0.1% formic acid). Desired fractions were combined and freeze-dried to yield (4) as a white powder. Purity was assessed with analytical HPLC-MS; mobile phase, (gradient elution over 30 minutes from water (0.1% formic acid) to 50% acetonitrile (0.05% formic acid) in water (0.1% formic acid), UV detection at 274nm, tR = 13.458 ESI-MS *m/z* (relative intensity):

229.10 (80.9%), 480.25 (100.0%), 959.30 (81.6%), 960.35 (51.0%), HRESIQTOFMS calculated for $C_{52}H_{67}N_{10}O_8$ ($M + H^+$) 959.5143 measured 959.5115 (2.9ppm).

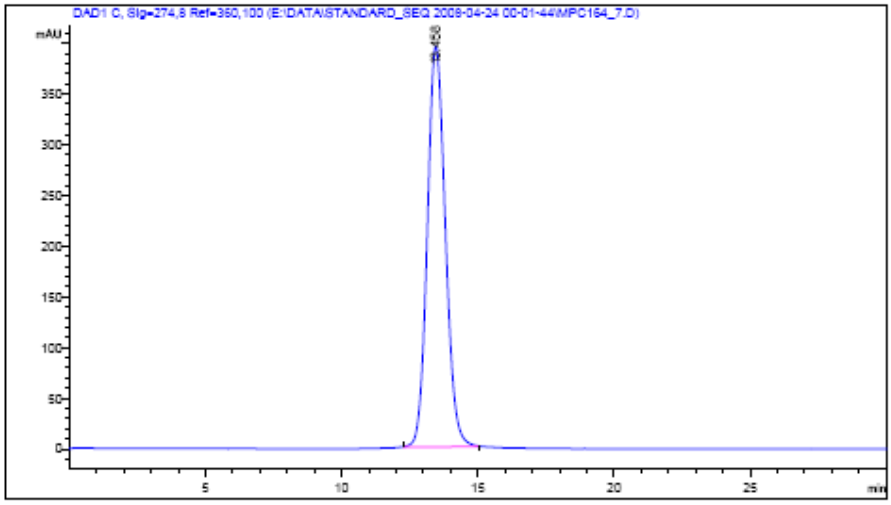

Figure 5.3 Reverse-Phase purified chromatogram of (sc4). UV detection at 274nm, tR = 13.458 ESI-MS *m/z* 959.30 (calculated for 958.51)

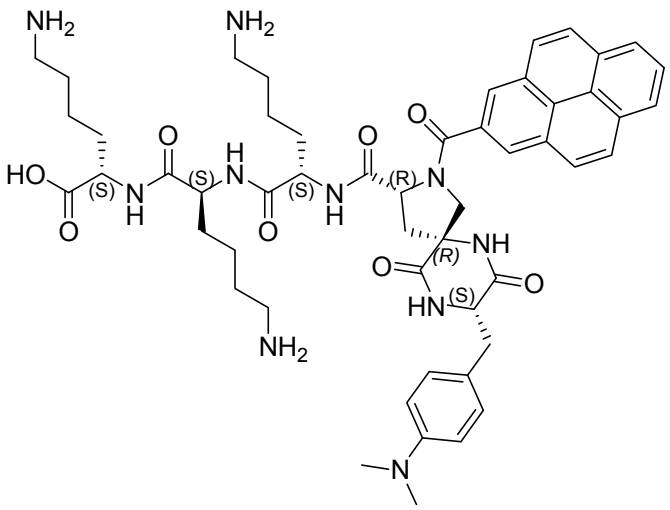

D-RRS-A (sc5)

D-RRS-A (5):

Wang resin (200mg, 150umoles loading) was placed in a 15mL solid phase reactor. Fmoc-Lys(Boc)-OH (703mg, 1.5mmoles) was attached according to general procedure (A) using dichloromethane (4.5mL), diisopropylcarbodiimide (116uL, 750umoles), dimethylformamide (4.5mL), and dimethylaminopyridine (18.3mg, 150umoles). The terminal Fmoc group was removed according to general procedure (C) using 20% piperidine in dimethylformamide (2.25mL).

Fmoc-Lys(Boc)-OH (211mg, 450umoles) was coupled according to general procedure (B) using HATU (171mg, 450umoles), N-methylpyrrolidinone (2.25mL), and diisopropylethylamine (156uL, 900umoles). The terminal Fmoc group was removed according to general procedure (C) using 20% piperidine in dimethylformamide (2.25mL).

Fmoc-Lys(Boc)-OH (211mg, 450umoles) was coupled according to general procedure (B) using HATU (171mg, 450umoles), N-methylpyrrolidinone (2.25mL), and diisopropylethylamine (156uL, 900umoles).

(sc3) (223mg, 450umoles) was coupled according to general procedure (B) using HATU (171mg, 450umoles), N-methylpyrrolidinone (2.25mL), and diisopropylethylamine (156uL, 900umoles). The terminal Fmoc group was removed according to general procedure (C) using 20% piperidine in dimethylformamide (2.25mL).

Fmoc-DMA-OH (sc1) (194mg, 450umoles) was coupled according to general procedure (B) using HATU (171mg, 450umoles), N-methylpyrrolidinone (2.25mL), and diisopropylethylamine (156uL, 900umoles). The terminal Fmoc group was removed according to general procedure (C) using 20% piperidine in dimethylformamide (2.25mL) and the reaction time was extended to 1 hour.

The Alloc group was removed according to general procedure (D) using borane:dimethylamine complex (53mg, 900umoles) in dichloromethane (2.5mL) and tetrakis(triphenylphosiphine)palladium0 (17mg, 15umoles) in dichloromethane (2mL). Pyrenecarboxylic acid (111mg, 450umoles) was coupled according to general procedure (B) using HATU (171mg, 450umoles), N-methylpyrrolidinone (2.25mL), and diisopropylethylamine (156uL, 900umoles).

(sc5) was liberated from the resin according to general procedure (E) using 3.75 mL of the cleavage cocktail. The residue was reconstituted in 75% acetonitrile in water (0.05% formic acid) and purified by reverse-phase chromatography (gradient elution over 30 minutes from water (0.1% formic acid) to 50% acetonitrile (0.05% formic acid) in water (0.1% formic acid)). Desired fractions were combined and freeze-dried to yield (5) as a white powder. Purity was assessed with analytical HPLC-MS; mobile phase, (gradient elution over 30 minutes from water (0.1% formic acid) to 50% acetonitrile (0.05% formic acid) in water (0.1% formic acid), UV detection at 274nm, tR = 13.410 ESI-MS *m/z* (relative intensity):

229.10 (80.9%), 480.25 (100.0%), 959.30 (81.6%), 960.30 (51.0%), HRESIQTOFMS calculated for $C_{52}H_{67}N_{10}O_8$ ($M + H^+$) 959.5143, measured 959.5102 (4.3ppm).

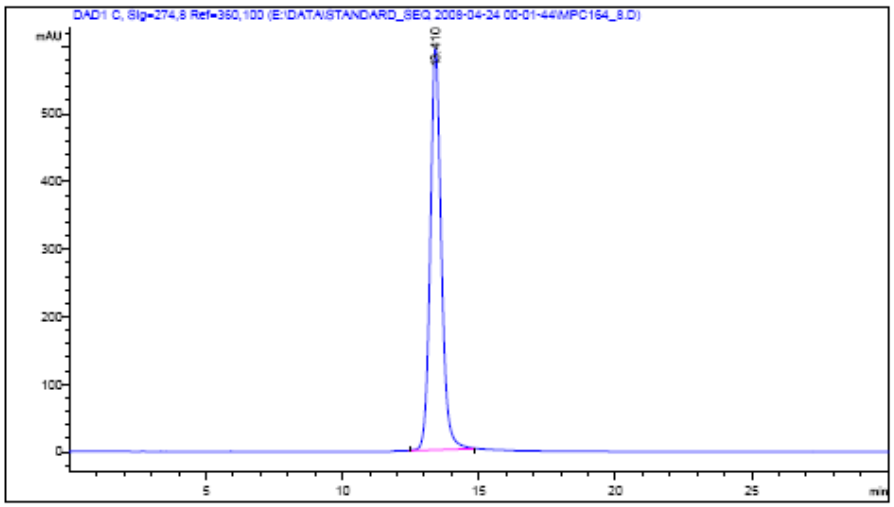

Figure 5.4 Reverse-Phase purified chromatogram of (sc4). UV detection at 274nm, tR = 13.410 ESI-MS *m/z* 959.30 (calculated for 958.51)

Oligomer Characterization

Oligomer NMR samples were prepared at 20 mM concentration in DMSO or D_2O. The NMR samples were treated with 10 uL of a 1M TFA-d to bring the final solution pH was 4.87-4.9 and were transferred to Shigemi Tubes. The NMR experiments were performed on a Bruker 500mHz instrument at elevated temperatures (330-333K). The pH and temperature settings were determined experimentally to provide optimized resolution of spectra. However all spectrum display a mixture of rotamers attributed to the slow rotation of the pyrene carboxamide.

NMR Experiment	Supplemental Figure	Integration of Conformer A	Integration of Conformer B	Relative population A:B
(sc4) D_2O	3	1.6691	1.0000	63:37
(sc4) DMSO	4	1.8444	1.0000	65:35
(sc5) D_2O	5	1.7281	1.0000	63:37

Table 5.2 NMR analysis of conformer ratio. Integration of the Aromatic protons on the Dimethylanaline displayed as a ratio of the two slowly exchanging tertiary amide rotamers Rotamers A and B for (sc4) refer to the rotameric species of the pyrenecarboxamide modeled in Supplemental Figure 4. Rotamer A is the more shielded (up-field) constituent and Rotamer B is the less shielded (down-field) constituent. Both rotamers A and B of sc5 have their dimethylaniline hydrogens shifted downfield because the relative stereochemistry of this molecule holds the dimethylaniline group out of the pyrene shielding cone permanently.

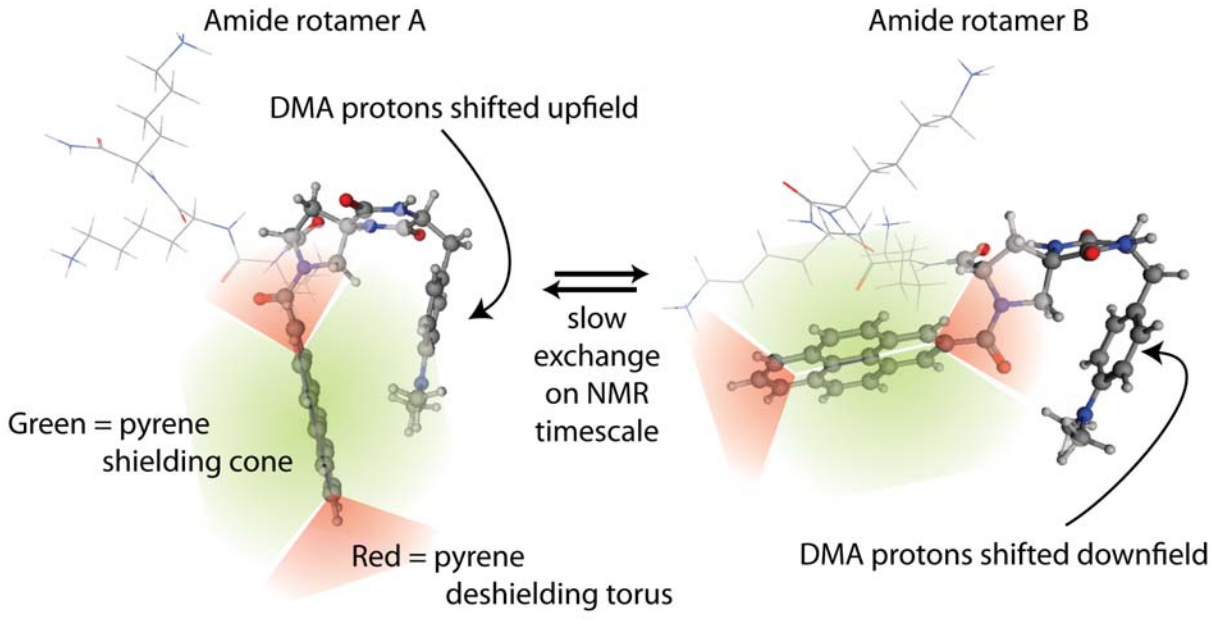

Figure 5.5 Molecular models of pyrenecarboxamide rotamers in (sc4)

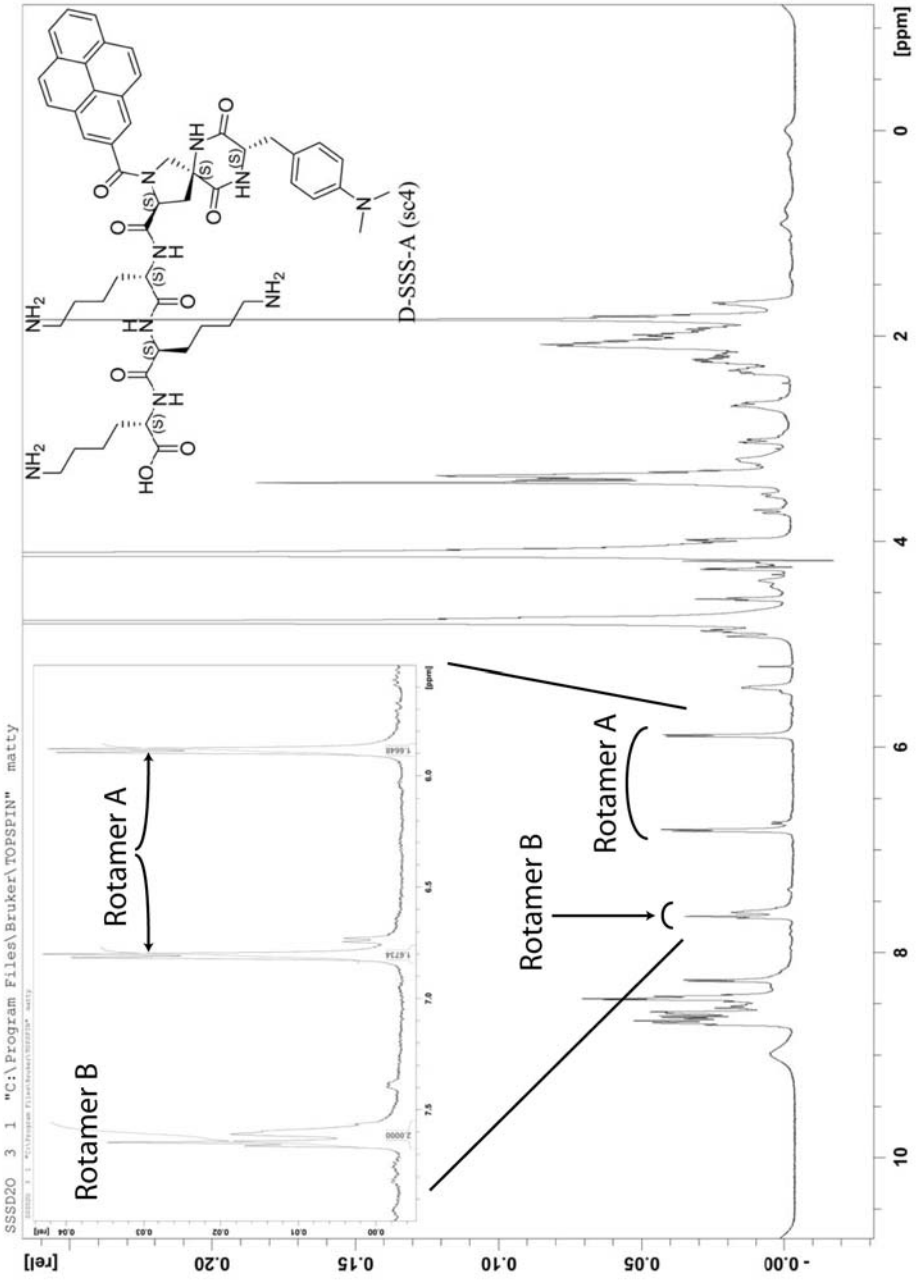

Figure 5.6 ^{1}H NMR (500 MHz, D_2O, 333K) of D-SSS-A (sc4)

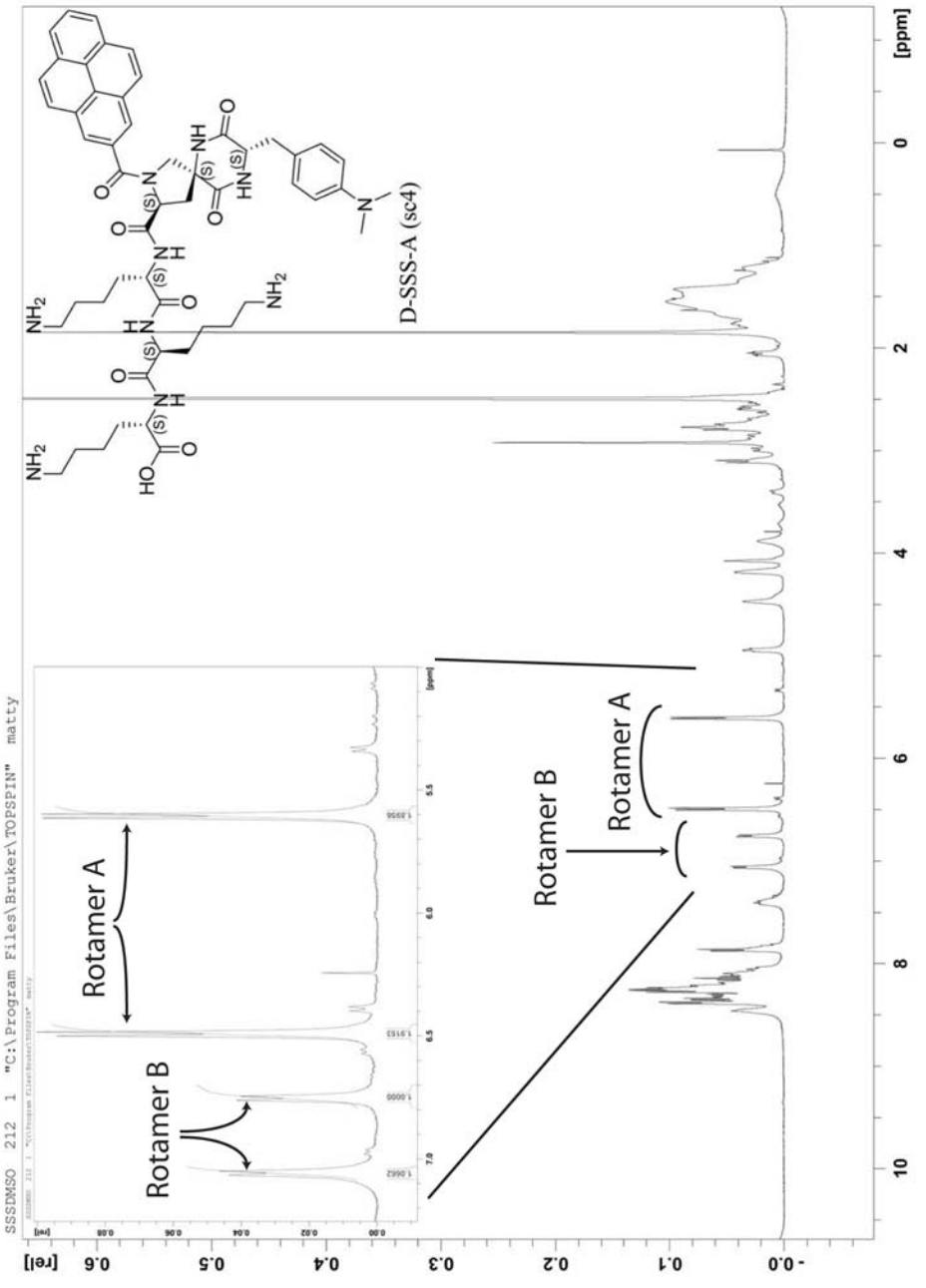

Figure 5.7 ^{1}H NMR (500 MHz, DMSO, 330K) of D-SSS-A (sc4)

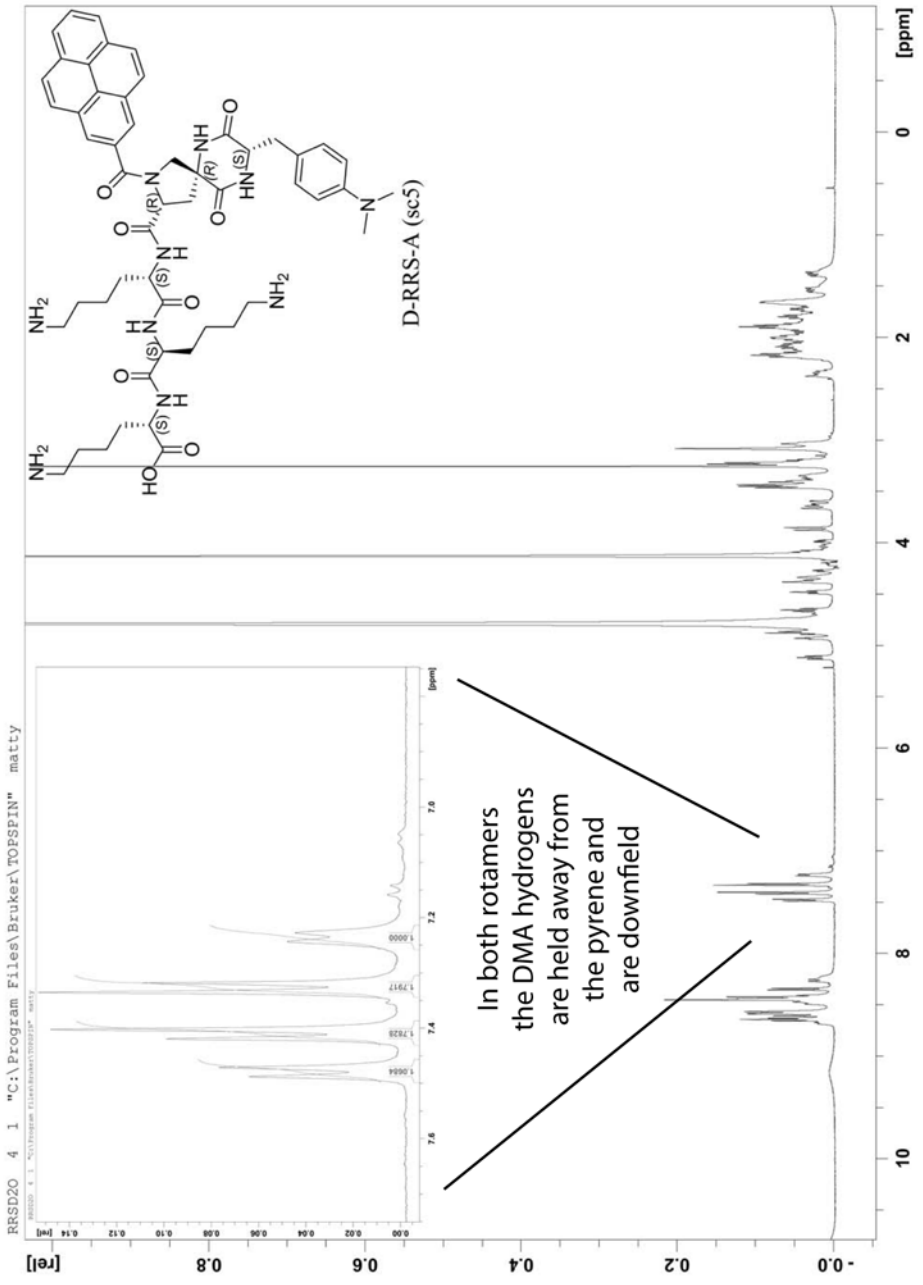

Figure 5.8 ^{1}H NMR (500 MHz, D_2O, 333K) of D-RRS-A (sc5)

Fitting of the experimental data to the semiclassical electron transfer equation

The semiclassical model for electron transfer in the nonadiabatic limit begins with a Fermi's Golden Rule expression for the transition rate; namely

$$k_{ET} = (2\pi / \hbar)\left|V\right|^2 FCWDS$$

where $\hbar$ is Planck's constant divided by 2π, $\left|V\right|$ is the electronic coupling matrix element, and FCWDS is the Franck-Condon weighted density of states. Previous work has successfully applied the Golden Rule rate constant expression with a single effective quantum mode, and described k_{ET} by the semiclassical rate equation.

$$k_{ET} = \frac{4\pi^2}{h} |V|^2 \frac{1}{\sqrt{4\lambda_S \pi k_B T}} \sum_{n=0}^{\infty} \exp(-S)\left(\frac{S^n}{n!}\right)\exp\left[-\frac{(\Delta G + \lambda_S + nh\nu)^2}{4\lambda_S k_B T}\right] \qquad \mathbf{1}$$

where λ_S is the solvent reorganization energy; ΔG is the reaction free energy; $S = \frac{\lambda_v}{h\nu}$ and λ_v is the internal reorganization energy. The *hν* term refers to the average energy spacing of a single effective quantized mode frequency in the electron transfer reaction and is a characteristic of the solute. The sum is performed over the vibrational states of the effective quantum mode. The quantities *hν* and λ_v are determined primarily by the donor and acceptor groups and is not sensitive to their separation. This analysis uses a value of 1400 cm^{-1} for the single effective quantized mode *ν* and 0.19 eV for the solute reorganization energy λ_v. This effective frequency is comparable to typical carbon-carbon stretching frequencies in aromatic ring systems and taken from our previous work carried out on C-shaped DBA molecules having the similar donor and acceptor groups (reference 15 mentioned in the reference section of the text).

Calculation of reorganization energy considering the elliptical cavity

The reorganization energy λ_S for the compounds **D-SSS-A**, **D-RRS-A** in water and DMSO were calculated from the continuum model of solvation using the following equation where the solvent cavity is considered to be ellipsoidal.

$$\lambda_S = \frac{\Delta\mu^2}{2AB^2}\left(\frac{1}{D_{OP}} - \frac{1}{D_S}\right)\sum_{n=1}^{n=\infty} X_n \qquad \mathbf{2}$$

and $$X_n = (1/2)(2n+1)\left[1-(-1)^n\right]k(k^2-1)Q_n(k)/P_n(k) \qquad \mathbf{3}$$

where $\Delta\mu$ is the dipole moment difference, $P_n(k)$ and $Q_n(k)$ are the Legendre polynomial of the first kind and second kind respectively. 2A and 2B are the lengths of the major axis and the minor axis of the ellipsoid. k is given by $k = \sqrt{\frac{A^2}{A^2 - B^2}}$.

The molecular diameters for D-RRS-A were taken to be 13.5 Å, 5 Å, and 8 Å, and for D-SSS-A, they were taken to be 8 Å, 5 Å, and 10 Å. This model is for a symmetric ellipsoid, so calculations were done using 13.5 Å and 6.5 Å (average of other two axis) for D-RRS-A and 8 Å and 7.5 Å (average of other two axis) for D-SSS-R . The computed values of $\sum_{n=1}^{n=\infty} X_n$ for D-SSS-A and D-RRS-A are 0.951645 and 0.702741 respectively.

If we assume that a full charge moves across the center-to-center distance in D-SSS-A, it will produce a dipole moment of 22 D. If we carry out similar calculation on D-RRS-A the dipole moment value we obtain is 46 D, which is quite large. If the dipole moment change from D-SSS-A to D-RRS-A is assumed to scale as the effective radius increase from D-SSS-A and D-RRS-A. Then a dipole moment of 24 D is obtained for D-RRS-A.

$(1/D_{op}-1/D_s)$ for water, and DMSO which are 0.55 and 0.437 respectively, we can use Equation 2 to obtain the reorganization energy of D-SSS-A in water of 1.42 eV, and the reorganization energy of D-RRS-A in water of 1.14 eV (for $\Delta\mu \sim 24$ D) [we find 3.67 eV for $\Delta\mu = 46$ D]. Similarly, the reorganization energy of D-SSS-A in DMSO is 1.12 eV, and the reorganization energy of D-RRS-A in DMSO is 0.91 eV (for $\Delta\mu \sim 24$ D) [we find 2.91 eV for $\Delta\mu = 46$ D].

In the current work λ_S was calculated using the equation 2 and kept fixed for water and DMSO. The electronic coupling $|V|$ and the free energy change $\Delta_r G$ were used as adjustable parameters in equation 1. Using all the parameters λ_S, λ_V, ν, ΔG (adjustable), $|V|$ (adjustable) in equation 1, we can calculate the semiclassical electron transfer rate. The calculated k_{ET} values were fitted to the experimental electron transfer rate constant values using the "*Solver*" function in Excel 2007. The values of the Gibbs energy and electronic coupling were reported in the text are found from this fit.

Experimental Rate Constant Data

The fluorescence decay laws of the molecules D-SSS-A and D-RRS-A were found to be double exponential in both water and DMSO. The long lifetime component is of smaller amplitude, ranging from 10% to 25% of the decay law, and it has a relaxation time that is close to that found for the acceptor only control molecule studied in solution (SSS-A). While this lifetime component may reflect some acceptor only impurity in the sample, it more likely corresponds to D-SSS-A and D-RRS-A rotamers that have the pyrene moiety rotated away from the donor. The lifetimes suggest that the electron transfer rate constant for these rotamers is small compared to the acceptor's intrinsic fluorescence decay (see table 4). The

short decay time components, which dominate the decay law, are assigned to the rotamers in which the pyrene and dimethylaniline moieties define a cleft. Given that the rate constant in D-RRS-A do not change between DMSO and water, suggests that the electronic coupling is bridge mediated in this case, but differs between the rotamers. Conformational effects on the efficiency of bridge mediated charge transfer have been previously studied for other systems.

2. Decay law fitting paramters

Table 5.3 D-SSS-A and D-RRS-A in water and DMSO excited at 330nm

T(K)	τ_1 (ps)	A_1 (%)	τ_2 (ps)	A_2 (%)	Acceptor Only τ_3 (ps)	k_{ET} (s^{-1})
D-SSS-A					**SSS-A**	
296	676	81	12419	19	12620	1.42×10^9
306	590	79	11103	21	12419	1.57×10^9
319	534	79	12766	21	11842	1.77×10^9
326	509	80	11236	20	11673	1.88×10^9
335	470	89	8034	11	11336	2.02×10^9
345	460	88	7497	12	11308	2.18×10^9
D-RRS-A					**SSS-A**	
296	2180	74	12644	26	12620	9.14×10^8
306	1890	82	12410	18	12419	1.15×10^9
308	1600	80	12318	20	12400	1.48×10^9
319	1580	84	12207	16	11842	1.54×10^9
326	1460	80	11842	20	11673	1.79×10^9
335	1450	86	11840	14	11336	1.95×10^9
345	1360	81	11657	19	11308	2.09×10^9

D-SSS-A and D-RRS-A in DMSO excited at 330nm

T(K)	τ_1 (ps)	A_1 (%)	τ_2 (ps)	A_2 (%)	Acceptor Only τ_3 (ps)	k_{ET} (s^{-1})
D-SSS-A					**SSS-A**	
296	1690	79	16371	21	15538	5.34×10^8
306	1590	78	13261	22	14045	5.82×10^8
315	1490	80	12096	20	12860	6.25×10^8
326	1290	82	10523	18	12096	6.79×10^8
345	1280	81	9867	19	9867	7.73×10^8
D-RRS-A					**SSS-A**	
296	1740	82	12644	18	15538	5.26×10^8
306	1580	81	12410	19	14045	5.65×10^8
315	1470	79	12318	21	12860	6.00×10^8
326	1350	80	12207	20	12096	6.42×10^8
345	1220	80	11842	20	9867	7.16×10^8

5.4 References

1. Beratan, D. N.; Onuchic, J. N. *Protein Electron Transfer*; Bendall, D. S., Ed.; BIOS Scientific Publishers Ltd.: Oxford, 1996; p 23.
2. Berg, J. M..; Stryer, L.; Tymoczko J. L. *Biochemistry*, 5th Ed.; Freeman: New York, 2002.
3. Page, C. C.; Moser, C. C.; Chen, X.; Dutton, P. L. *Nature* **1999**, *402*, 47.
4. Lin, J.; Balabin, I. A.; Beratan, D. N. *Science* **2005**, 310, 1311.
5. Migliore, A.; Corni, S.; Felice, R. D.; Molinari, E. *J. Phys. Chem. B* **2006**, *110*, 23796.
6. Miyashita, O.; Okamura, M. Y.; Onuchic, J. N. *Proc. Natl. Acad. Sci. U.S.A.* **2005**, *102*, 3558.
7. Wenger, O.S.; Leigh, R. M.; Villahermosa, H. B.; Gray, H. B.; Winkler, J. R. *Science*, **2005**, *307*, 99.
8. Ponce, H. B.; Gray, H. B.; Winkler, J. R. *J. Am. Chem. Soc*. **2000**, *122*, 8187.
9. The distances are center to center distances between the pyrene and dimethylaniline group found by molecular mechanics minimization of the molecular geometries *in vacuo*.
10. Zimmt, M. B.; Waldeck, D. H. *J. Phys. Chem. A*. **2003**, *107*, 3580.
11. Read, I.; Napper, A.; Kaplan, R.; Zimmt, M. B.; Waldeck, D. H. *J. Am. Chem. Soc.* **1999**, *121*, 10976.
12. Kumar, K.; Kurnikov, I.; Beratan, D. N.; Waldeck, D. H.; Zimmt, M. B. *J. Phys. Chem. A*. **1998**, **102**, 5529.
13. Troisi, A.; Ratner, M. A.; Zimmt, M. B. *J. Am. Chem. Soc*. **2004**, *126*, 2215.
14. Levins, C. G.; Schafmeister, C. E. *J. Am. Chem. Soc*. **2003**, *125*, 4702.

15. Nadeau, J. M.; Liu, M.; Waldeck, D. H.; Zimmt, M. B. *J. Am. Chem. Soc*. **2003**, *125*, 15973.

16. Galoppini, E.; Fox, M. A. *J. Am. Chem. Soc.* **1996**, *118*, 2299.

17. The pK_a of the dimethylaniline is 5.1. Around pH 7 100% of the molecule will be free amine whereas at pH 4.5 only 20% of the molecules will contain free amine group in the dimethylamine donor unit.

18. Marcus, R. A.; Sutin, N. *Biochim. Biophys. Acta* **1985**, *811*, 265.

19. Bixon, M.; Jortner, J. *Adv. Chem. Phys.* **1999**, *106*, 35.

20. Liu, M.; Chakrabarti, S.; Waldeck, D. H.; Oliver, A. M.; Paddon-Row, M. N. *Chem. Phys***.** **2006**, *324*, 72.

21. Chakrabarti, S.; Liu, M.; Waldeck, D. H.; Oliver, A. M.; Paddon-Row, M. N. *J. Am. Chem. Soc*. **2007**, *129*, 3247.

22. Sharp, K.; Honig, B. *Annu. Rev. Biophys*. *Chem.* **1990**, *19*, 301.

23. Newton, M. D.; Basilevsky, M. V.; Rostov, I. V. *Chem. Phys*. **1998**, *232*, 201.

24. Matyushov, D. V.; Voth, G. A. *J. Chem. Phys*. **1999**, *111*, 3630.

25. Read, I.; Napper, A. M.; Zimmt, M. B.; Waldeck, D. H. *J. Phys*. *Chem. A* **2000**, *104*, 9385.

26. The reorganization energy were calculated using the continuum model considering the solute as an ellipsoidal cavity according to the papers Chem. Phys. Lett, **1977**, *49*, 299-304 & JPC, **1986**, 90, 3657-3668).

27. The thickness of an aromatic ring is approximately 3.4 Å. Thus the π orbitals of each aromatic chromophore in the **D-SSS-A** molecule extend into the cleft by about 1.7 Å, leaving a 1.2 Å gap between the donor and the acceptor.

28. The molecular radii were estimated from volume increments given by A. Bondi, *J. Phys. Chem.* **1964**, 68 441.

29. Turro, C.; Chang, C. K.; Leroi, G. E.; Cukier, R. I.; Nocera, D. G. *J. Am. Chem. Soc*. **1992,** *114*, 4013.

30. Cukier, R. I.; Nocera, D. G. *Annu. Rev. Phys. Chem.* **1998**, *49*, 337.

31. Hodgkiss, J. M.; Damrauer, N. H.; Presse, S.; Rosenthal, J.; Nocera, D. G. *J. Phys. Chem. B* **2006**, *110*, 18853.

6.0 CHAPTER SIX

Electron transfer between donor-acceptor units separated by a distance is the primary event in many important biological and technological processes. Long distance (nanometers) electron transfer is important in supramolecular chemistry and molecular biology. This work described how the electron-transfer rate can proceed by the efficient electron tunneling from a donor moiety to an acceptor moiety through a pendant group (or solvent molecule) located in the '*line- of- sight*' between the donor and acceptor groups in different U-shaped Donor-Bridge-Acceptor (DBA) molecules. The efficiency of electron transfer in these molecules depends on the extent of interaction of the pendant group (or the solvent molecule) with the donor and acceptor moieties.

Chapters 2 and 3 describe how the presence of different pendant groups can modulate the electron coupling between the donor and the acceptor. In chapter 2, a series of molecules were investigated having an aromatic pendant unit in between the donor and acceptor. Different parameters like the Gibbs energy, reorganization energy, and electronic coupling values were determined from the experimental rate data. The reaction free energy for different U-shaped DBA molecules in weakly polar solvents was used to calibrate a molecular solvation model which yields the reaction free energy and the reorganization energy. This model was then used to predict these parameters in polar solvents. The electronic coupling values obtained from this study clearly indicated that the electron transfer rates depend on the

electronic nature of the substituted group present on the pendant phenyl ring. When aliphatic groups were present on the pendant phenyl ring, the electronic coupling values obtained are very similar. Alkyl substitution on the phenyl ring has little effect on its electron properties, hence a superexchange picture predict no large change in the electron coupling. Similarly, the Gibbs energy obtained from these studies supports the fact that the energetics of the electron transfer reaction in these molecules is not very different. Some change in the reorganization energies and difference in the reorganization energies between the polar solvents and the non-polar solvents indicate that the change in effective molecular volume or the different dipole moments of the pendant groups may be important to consider.

Chapter 3 discussed a comparison study in which the pendant phenyl ring is methoxy substituted. This change in functionality on the phenyl ring of the pendant supermolecules can change the electronic coupling. This system has an electronic coupling for its forward electron transfer of 275 cm^{-1}, nearly twice that of the aliphatic group substituted pendant unit. Its electronic coupling for the back electron transfer (charge separated state to ground state) is even higher, nearly 500 cm^{-1}, and we were able to observe charge transfer emission spectra. Our analysis of these data gave solvent reorganization energies that are only 10% higher than that found for the aliphatic substituted pendant units. Hence, the substitution of the phenyl can be used to tune the value of electronic coupling, |V| without significantly having to modify the structure of the molecule and change other parameters.

Chapter 4 described the evaluation of the electron transfer rate constants at low temperature in slow solvents (solvents having slow relaxation time). The results indicate that in NMP at low temperature the solvent plays an important role in the electron transfer reaction in these U-shaped DBA molecules. Solvent molecules can influence a chemical reaction by

solvation and they can also interact dynamically by exchanging energy and momentum through friction with the reacting species. It is well known that solvation is important in electron transfer reactions, at the same time the dynamic solvent effects can also play a key role in electron transfer reactions. This work explored how the solvent dynamics affected charge transfer in U-shaped **DBA** molecules by comparing the photoinduced electron transfer of the three DBA molecules with different electronic coupling values as a function of temperature in N-methyl propionamide (NMP). The Zusman model was used to fit the experimental results over the whole temperature range (from high to low) and obtain an outer sphere solvent reorganization energy and Gibbs energy. The low temperature experimental results are also analyzed and discussed in terms of different kinetic models.

Chapter 5 described the extension of electron transfer studies in DBA molecules to water solvent and the presence of water molecules in the cleft between donor and acceptor. It is well known that water molecules can tune the electron transfer pathways in a highly efficient way by modulating the activation energy of the electron transfer. We have studied electron transfer for two DBA molecules with two different cleft sizes and showed that electron tunneling event through water molecules is likely. It was observed that when only few water molecules were able to fit into the cleft the electronic transfer rate became higher as compared to the cleft where more and more water molecules can enter. We were able to show that water molecules can influence significantly the electron transfer pathways in these systems through the hydration layer formed between the donor and acceptor, which is not possible for aprotic solvents like DMSO. We were also able to determine the different mechanistic parameters, and it was observed that presence of water molecules can increase the electronic coupling between the donor and acceptor by highly efficient superexchange

interaction. Our experimental findings support the theoretical predictions of water effects on protein electron transfer.

We have explored the change in rate of a photoinduced electron transfer reaction when a molecular bridging unit that lies between the moieties is able to fluctuate. The strength of the electronic coupling between the donor and acceptor units depends strongly on the nature of the bridging unit and on its fluctuation. Our results show that the mechanism of the electron transfer changes with the strength of the electronic coupling and the response time of the solvent